VILNIUS GEDIMINAS TECHNICAL UNIVERSITY

Vitalij NOVICKIJ

DEVELOPMENT OF HIGH POWER SQUARE WAVE ELECTROPORATORS

DOCTORAL DISSERTATION

TECHNOLOGICAL SCIENCES,
ELECTRICAL AND ELECTRONIC ENGINEERING (01T)

VGTU
LEIDYKLA TECHNIKA
Vilnius 2015

Doctoral dissertation was prepared at Vilnius Gediminas Technical University in 2012–2015.

Supervisor

Dr Voitech STANKEVIČ (Vilnius Gediminas Technical University, Electrical and Electronic Engineering – 01T).

The Dissertation Defense Council of Scientific Field of Electrical and Electronic Engineering of Vilnius Gediminas Technical University:

Chairman

Prof Dr Vytautas URBANAVIČIUS (Vilnius Gediminas Technical University, Electrical and Electronic Engineering – 01T).

Members:

Dr Zigmas BALEVIČIUS (Vilnius Gediminas Technical University, Physics – 02P),

Prof Dr Georg MÜLLER (Karlsruhe Institute of Technology, Electrical and Electronic Engineering – 01T),

Habil Dr Arūnas Vytautas TAMAŠEVIČIUS (State Research Institute Center for Physical Sciences and Technology, Electrical and Electronic Engineering – 01T),

Prof Dr Algimantas VALINEVIČIUS (Kaunas University of Technology, Electrical and Electronic Engineering – 01T).

The dissertation will be defended at the public meeting of the Dissertation Defense Council of Electrical and Electronic Engineering in the Senate Hall of Vilnius Gediminas Technical University at **1 p. m. on 15 May 2015.**

Address: Saulėtekio al. 11, LT-10223 Vilnius, Lithuania.
Tel.: +370 5 274 4956; fax +370 5 270 0112; e-mail: doktor@vgtu.lt

The notification on the intend defending of the dissertation was sent on 14 April 2015.

A copy of the doctoral dissertation is available for review at the Internet website http://dspace.vgtu.lt/ and at the Library of Vilnius Gediminas Technical University (Saulėtekio al. 14, LT-10223 Vilnius, Lithuania).

VGTU leidyklos TECHNIKA 2313-M mokslo literatūros knyga

ISBN 978-609-457-789-5

vitalij.novickij@vgtu.lt

VILNIAUS GEDIMINO TECHNIKOS UNIVERSITETAS

Vitalij NOVICKIJ

DIDELĖS GALIOS STAČIAKAMPIŲ IMPULSŲ ELEKTROPORATORIŲ KŪRIMAS

DAKTARO DISERTACIJA

TECHNOLOGIJOS MOKSLAI,
ELEKTROS IR ELEKTRONIKOS INŽINERIJA (01T)

VGTU
LEIDYKLA TECHNIKA
Vilnius 2015

Disertacija rengta 2012–2015 metais Vilniaus Gedimino technikos universitete.

Vadovas

dr. Voitech STANKEVIČ (Vilniaus Gedimino technikos universitetas, elektros ir elektronikos inžinerija – 01T).

Vilniaus Gedimino technikos universiteto Elektros ir elektronikos inžinerijos mokslo krypties disertacijos gynimo taryba:

Pirmininkas

prof. dr. Vytautas URBANAVIČIUS (Vilniaus Gedimino technikos universitetas, elektros ir elektronikos inžinerija – 01T).

Nariai:

dr. Zigmas BALEVIČIUS (Vilniaus Gedimino technikos universitetas, fizika – 02P),

prof. dr. Georg MULLER (Karlsrūjės technologijos institutas, elektros ir elektronikos inžinerija – 01T),

habil. dr. Arūnas Vytautas TAMAŠEVIČIUS (Valstybinis mokslinių tyrimų institutas Fizinių ir technologijos mokslų centras, elektros ir elektronikos inžinerija – 01T),

prof. dr. Algimantas VALINEVIČIUS (Kauno technologijos universitetas, elektros ir elektronikos inžinerija – 01T).

Disertacija bus ginama viešame Elektros ir elektronikos mokslo krypties disertacijos gynimo tarybos posėdyje **2015 m. gegužės 15 d. 13 val.** Vilniaus Gedimino technikos universiteto senato posėdžių salėje.

Adresas: Saulėtekio al. 11, LT-10223 Vilnius, Lietuva.
Tel.: (8 5) 274 4956; faksas (8 5) 270 0112; el. paštas doktor@vgtu.lt

Pranešimai apie numatomą ginti disertaciją išsiųsti 2015 m. balandžio 14 d.

Disertaciją galima peržiūrėti interneto svetainėje http://dspace.vgtu.lt/ ir Vilniaus Gedimino technikos universiteto bibliotekoje (Saulėtekio al. 14, LT-10223 Vilnius, Lietuva).

Abstract

High power microsecond and submicrosecond electric pulse generation and the devices for pulse generation (electroporators) development and application problem is focused in the dissertation. The electric field technologies, pulse forming circuits and circuit transient process compensation methods are investigated.

The introduction presents the investigated problem, objects of research, importance of the dissertation, describes research methodology, scientific novelty and the defended statements.

In the first chapter the scientific publications in the area of the high power electric pulses generation and application for biological cell permeabilization are overviewed. The influence of the pulse parameters on the biological effects is analysed. The requirements for the electroporators are identified.

In the second chapter the prototypes of the high power square wave 5 μs – 10 ms up to 4 kV, 100 A and 200 ns – 5 μs up to 8 kV, 100 A electroporators are developed. The models for investigation of the transient processes in the circuits and the solutions for compensation are overviewed. The adequacy of the proposed models to the experimental results is analysed.

The interdigitated microelectrodes structure for planar electroporation is proposed. The resultant electric field distribution and the cell medium temperature rise due to the Joule heating are investigated.

The third chapter is focused on the experimental application of the developed high power microsecond and submicrosecond electroporators prototypes in biological experiments. The experimental results with different cell types are presented and conclusions are formed.

Research results on the dissertation subject are published in 5 scientific articles: 3 articles – Thomson Reuters ISI Web of Science database journals with impact factor, 2 – publications referenced and abstracted in other international databases, 4 presentations have been made in international conferences in Lithuania, Netherlands, Germany and Japan.

Reziumė

Disertacijoje nagrinėjama didelės galios plataus submikrosekundinio ir mikrosekundinio ruožo staciakampių elektrinių impulsų generavimo, didelės galios impulsų generatorių (elektroporatorių) kūrimo ir taikymo problema. Atliekama impulsų formavimo, elektrinio lauko generavimo technologijų ir pereinamųjų vyksmų kompensavimo analizė.

Įvadiniame skyriuje nagrinėjama disertacijos problema, tyrimo tikslai bei naujumas, aprašoma tyrimų metodologija ir ginamieji teiginiai.

Pirmame skyriuje pristatyta mokslinės literatūros apžvalga, atlikta elektrinių impulsų generavimo technologijų, jų taikymo ir impulso formos įtakos biologiniam poveikiui analizė. Nustatyti reikalavimai naujos kartos didelės galios elektroporatoriams.

Antrame skyriuje pateikti sukurti submikrosekundinio ir mikrosekundinio ruožo elekroporatorių modeliai. Atlikta elektroporatorių grandynų pereinamųjų vyksmų analizė, išnagrinėtos galimybės kompensuoti pereinamųjų vyksmų įtaką generuojamo impulso formai. Naudojant pasiūlytus modelius, sukurti didelės galios stačiakampių impulsų 5 μs – 10 ms iki 4 kV, 100 A ir 200 ns – 5 μs iki 8 kV, 100 A elektroporatorių prototipai. Eksperimentiškai įvertinta sukurtų modelių rezultatų atitiktis eksperimentiniams rezultatams.

Sukurti planarūs mikroelektrodai skirti elektroporacijos tyrimams. Išnagrinėtas elektrinio lauko pasiskirstymas ir ląstelių terpės įšilimo dinamika, panaudojant baigtinių elementų metodą.

Trečiame skyriuje atlikta mikrosekundinių ir submikrosekundinių didelės galios elektroporatorių eksperimentinė patikra, naudojant skirtingus biologinių ląstelių tipus.

Disertacijos tema paskelbti 5 straipsniai: 3 – Thomson Reuters ISI Web of Science duomenų bazėje referuojamuose moksliniuose žurnaluose su citavimo indeksu, 2 – kituose recenzuojamuose mokslo leidiniuose. Disertacijos tema perskaityti 4 pranešimai tarptautinėse konferencijose Lietuvoje, Olandijoje, Vokietijoje ir Japonijoje.

Notations

Symbols

a	–	electrode thickness;
C	–	capacitance;
E	–	electric field;
f	–	frequency;
g	–	gap between electrodes;
h	–	convective cooling coefficient;
I	–	electric current;
k	–	thermal conductivity;
L	–	inductance;
m	–	membrane thickness;
R	–	resistance;
r_{cell}	–	radius of the biological cell;
U	–	voltage;
V_{ef}	–	effective volume;
Z	–	impedance;
φ_m	–	transmembrane potential;
φ	–	angle between electric field and the point vector on membrane;
τ_p	–	cell polarization time;
σ	–	conductivity;

ε – permittivity;
Ω – ohm.

Abbreviations

ADC – analog to digital converter;
BJT – bipolar junction transistor;
BNC – Bayonet Neill–Concelman;
CFU – relative culture forming unit;
CFU_c – relative culture forming unit of the control;
CFU_t – relative culture forming unit after treatment;
DAC – digital to analog converter;
DC – direct current;
DNA – deoxyribonucleic acid;
EMR – electromechanical relay;
FEM – finite element method;
GTO – gate turn-off thyristor;
HV – high voltage;
IGBT – insulated-gate bipolar transistor;
IRE – irreversible electroporation;
LCD – liquid crystal display;
MMPG – micro-millisecond range pulse generator;
NMPG – nano-microsecond range pulse generator;
MOSFET – metal-oxide semiconductor field-effect transistor;
RPMI – Roswell Park Memorial Institute;
PEF – pulsed electric field
PCB – printed circuit board;
PDMS – polydimethylsiloxane;
SCR – silicon-controlled rectifier;
SSR – solid state relay;
TPP – tetraphenylphosphonium.

Contents

[1] Annexes are available in the CD attached to the dissertation.

Introduction

Problem Formulation

Generation of high power controlled shape electrical pulses is severely limited by the influence of the parasitic circuit elements, resultant oscillations, requirements for high current and voltage handling and the risks of damage of the pulse forming switches. However, high power electric pulse generators are in high demand. In the past decades pulsed power technology application in biological sciences showed a synergy, resulting in the development of new biomedical techniques such as electroporation, dielectrophoresis, inactivation or electrofusion of cells. The electroporation technique showed the highest potential for clinical applications and the generation of pulsed electric fields and investigation of the resultant biological effects became relevant for stimulation of drug delivery or suppression and treatment of tumors.

Currently, one of the major limitations in the field of electroporation are the limited pulse generation parameters of the available high power pulse generators (electroporators). In order to expand the research of the electroporation technique, the urge for development of high power square wave pulse electroporators, generating pulses in a wide range of durations and amplitudes has occurred. Therefore, research and development of the pulse forming, protection and compensation circuits is required.

Also, introduction of planar microelectrode structures allows minimizing the contamination and cell handling factors, which may distort the experimental results. For accurate interpretation of the cellular processes and biological object response to the high intensity electric field the investigation of the electric field distribution and the Joule heating influence during electroporation is required.

Relevance of the Thesis

Pulsed electric fields have a broad range of applications in biology. The parameters of the applied field influence the efficacy and the type of the biological effect. Due to this fact the experimental facilities are also application specific, however the urge for development of the devices, covering wide range of application is observed.

The complexity of such systems increases due to the higher requirements for pulse amplitude and duration ranges, higher power accumulation and safety requirements, inevitable system size issues and high voltage management. Therefore, the development of the compact pulsed electric field systems that could be successfully applied in a broad range of biological experiments requires new technological implementations, research and solutions.

Due to the inevitable influence of the parasitic circuit elements on the generated pulse shape, it is necessary to create simulation models for development of an efficient design for the new electroporators, introducing pulse forming, compensation and protection circuits.

For pulse delivery to biological cells the cuvettes or microelectrode arrays are required. It is necessary to investigate the electric field distribution and other factors that are influencing the treatment efficacy for accurate experimental results interpretation.

The development of the high power wide range electroporators can contribute for further investigation of a remarkable biomedical technique.

The Object of Research

The main objects of investigation are high power electroporators, circuit transient processes and the influence of the electrode parameters on the electric field distribution.

The Aim of the Thesis

The main aims of the thesis are the development of the high power electroporators, investigation of the transient processes in the electrical circuit of electroporators and the analysis of the electric field distribution in the planar microelectrode structures.

The Objectives of the Thesis

The following tasks have to be solved to achieve the aim of the work:

1. To develop the simulation model for square wave pulse generator, investigate the transient processes and possibilities for compensation of the parasitic elements influence on the generated pulse shape.
2. To develop the high power square wave pulse electroporators prototypes and investigate the applicability in biological cell permeabilization and absorption experiments.
3. To develop planar electroporation microelectrodes, investigate the distribution of the electric field and the Joule heating influence in the cell medium.

Research Methodology

The numerical and experimental methods were applied in this work. Transient processes were investigated using numerical methods by application of PSPICE program package. The electric field distribution and Joule heating analysis has been performed using COMSOL software package. Verification of the results has been performed experimentally.

Scientific Novelty of the Thesis

Research performed in this dissertation led to the following results, new in the scientific field of Electrical and electronic engineering:

1. The proposed simulation model is suitable for simulation of transient processes in high power electroporators.
2. The proposed transient process compensation circuit, consisting from double crowbar, double snubber diode, and RCD snubber circuit for

protection from overvoltage is effective for compensation of the transient processes in the submicrosecond and microsecond duration range.

3. Developed and investigated planar interdigitated microelectrodes structures for biological cell permeabilization experiments in electric fields up to 2 kV/cm with cell medium temperature rise limitation of 5 °C.

Practical Value of the Research Findings

The developed compact up to 4 kV, 5 μs – 10 ms and up to 8 kV, 200 ns – 5 μs square wave high power electroporators are suitable for electroporation experiments. Both prototypes were successfully applied in the project "Nanoelectroporator for biological cells" Nr. 31V–7 funded by Lithuanian Agency for Science, Innovation and Technology (MITA).

Developed electroporators were also applied in interdisciplinary experiments in Centre of Physical Science and Technology (Vilnius, Lithuania) and Nature Research Centre (Vilnius, Lithuania). The flexibility of the generated pulse parameters of the developed prototypes surpasses currently available commercial and non-commercial systems.

The Defended Statements

1. The developed simulation models results are in compliance with experimentally determined parameters of the electroporators and are suitable for simulation of the generated electric pulse parameters with uncertainty of ±5% for the microsecond and of ±10% for the submicrosecond pulse range.
2. The developed high power electroporator, which consists of the variable capacitance bank, IGBT switch and cuvette, ensures up to 4 kV with 550 ns rise time and 1.5 μs fall time pulse generation in a wide 5 μs – 10 ms range.
3. The developed high power electroporator, which consists of the capacitance bank, MOSFET switch and cuvette, ensures up to 8 kV with 40 ns rise time and 145 ns fall time pulse generation in a wide 200 ns – 5 μs range.

4. The developed planar microelectrode structures ensure generation of the electric field up to 2 kV/cm with low impedance cell medium temperature rise less than 5 °C in a 5–500 μs pulse range.

Approval of the Research Findings

Research results have been published in 5 scientific articles; 3 articles – in Thomson Reuters ISI Web of Science journals with impact factor, 2 – articles in journals referenced and abstracted in other international databases, 4 presentations on the subject have been made in the international conferences:

- International scientific conference *"IEEE Biomedical Systems and Circuits Conference – BIOCAS 2013"*. 2013. Rotterdam, Netherlands.
- International scientific conference *"5th Euro-Asian Pulsed Power Conference – EAPPC 2014"*. 2014. Kumamoto, Japan.
- International scientific conference *"IEEE International Magnetics Conference – INTERMAG 2014"*. 2014. Dresden. Germany.
- International scientific conference *"Electronics 2014"*. 2014. Palanga, Lithuania.

Dissertation Structure

Dissertation consists of introduction, three chapters, general conclusions, references, a list of the scientific publications by the author on the subject of the thesis and a summary in Lithuanian.

The volume of the dissertation is 112 pages excluding annexes. Dissertation contains 57 figures, 11 tables, 6 numbered formulas, 104 references are used.

Acknowledgements

I would like to thank my supervisor Dr Voitech Stankevič for his supervision during my PhD studies. I would also like to thank my internship supervisor Dr Stewart Smith for his supervision and collaboration.

I am grateful to all my colleagues in the Department of Electrical Engineering, Centre of Physical Science and Technology and Nature Research Centre for valuable discussion on topics related to my dissertation.

I am grateful to my family for support during these years.

1

Review of the Pulsed Electric Field Technology and Application

This chapter revises scientific literature related to the subject of the dissertation. Analysis of electroporation technique, the electric field generation technology, required pulse parameters, pulse shaping capabilities and devices used in pulsed electric field generators is performed. The biological objects response to high intensity pulsed electric field is described.

1.1. Electroporation

In the past decades the biomedical field is overcoming new frontiers of drug delivery for treatment of diseases on the cellular level (Lee *et al.* 2009; Kotnik *et al.* 2012; Haberl *et al.* 2013). Efficient and non-viral way of transfection of drugs, genes or other molecules is required in this field (Cathelin *et al.* 2013). Electroporation utilizes application of high intensity electric fields to create transient hydrophilic pores in the membrane structure and stimulates cell permeability, allowing transfection of drugs or other molecules (Potter 2003; Sardesai & Weiner 2011; Hargrave *et al.* 2012).

Schematic view of the reversible electroporation process in a biological cell is shown in Figure 1.1. As it can be seen in Figure 1.1 pores are formed in the

structure of the membrane, which allows transfer of ions or molecules inside and outside of the cell. The transient hydrophilic pores exist from several minutes to several hours, dependent on the treatment intensity without affection of the cell viability (Cahill 2010).

Very high intensity treatment results in irreversible electroporation (IRE) when the cell is damaged permanently, resulting in the necrosis of the biological object (Narayanan 2011). This feature is advantageous in oncology (Sundararajan *et al.* 2004). The treatment outcome depends on many physical and biological parameters (Zorec *et al.* 2013). However, the most crucial ones are the parameters of the applied electric field, which influence both the caused effect and the treatment efficacy, corresponding to the number of the affected cells (Chen *et al.* 2010; Pucihar *et al.* 2011). For example the same efficacy level of electroporation could be achieved with long medium voltage electrical pulses and shorter high voltage pulses, which implies that the total applied energy of the pulse should be always considered (Morshed *et al.* 2014). As a result development of generators for electroporation becomes the crucial factor influencing the success of the biomedical technique and introduces electronics and electrical engineering challenges, which have to be solved.

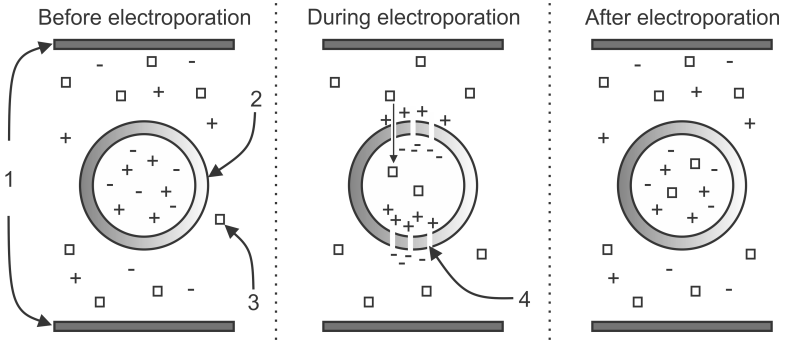

Fig. 1.1. Schematic view of the electroporation process, 1 – high voltage electrodes; 2 – biological cell membrane; 3 – drugs/DNA; 4 – nanometer temporary pores

In electroporation the amplitude of the pulses could vary from mV to kV, depending on the application and desired biological effect and pore size (Kotnik *et al.* 2012). The pulse width could also vary in a very broad range from nanoseconds to hundreds of milliseconds, which implies that the requirements for the pulsed electric field generator (electroporator) are application dependent (Chen *et al.* 2012; Kotnik *et al.* 2012). Typical applications of the electroporation technique are summarized in Table 1.1. From Table 1.1 it can be seen that there is a variety of biological effects induced by pulsed electric field.

However, the clinical procedures are usually limited to millisecond or microsecond pulses.

Table 1.1. Typical applications of the electroporation technique (Rebersek & Miklavcic 2011)

Electric pulse amplitude	Pulse width	Application
> kV	μs – ms	Tissue ablation
~ kV	μs	Electrofusion
mV – kV	ns – ms	Laboratory research
< kV	ms	Clinical transdermal drug delivery
~ kV	μs – ms	Gene transfection
~ kV	μs	Electrochemotherapy
>> kV	μs	Pasteurization
>> kV	ns	Inner organelles electroporation

It should be noted that application of mV range pulses requires very long duration pulses in the range of hundreds or thousands of milliseconds in order to deliver sufficient pulse energy (Rebersek & Miklavcic 2011). As a result use of long mV range pulse is very limited and rarely applied in the scientific works.

In every case electroporation effect is based on the polarisation processes happening inside the cell (Washizu & Techaumnat 2008; Suzuki *et al.* 2011; Das *et al.* 2014). When the biological cell is polarised and the threshold potential (transmembrane potential φ_m) between the inner cell structure and the outer cell medium is achieved, electroporation of the cell membrane could be observed (Kotnik *et al.* 2010; Hung & Chang 2012; Delemotte & Tarek 2012). Typically, it should be in 0.2–1 V range for the nanopores to appear and is dependent both on the electric field pulse parameters and biological cell type Equation (1.1) (Washizu & Techaumnat 2008; Kotnik *et al.* 2010).

$$\varphi_m = E\frac{1.5r_{cell}}{\sqrt{1+\left(2\pi f\tau_P\right)^2}}\cos\varphi, \tag{1.1}$$

where E – amplitude of the applied electric field, r_{cell} – the radius of the biological cell, τ_p – cell dependent polarization time, φ – the angle between the applied electric field and the point vector on the cell membrane, f is the frequency of the applied field.

The induced voltage causes the lipid bilayer molecules to rearrange themselves to form the nanometer pores for the drugs to enter the cytoplasm (Smith & Weaver 2008). As a result the technological implementations of the electroporators should allow controlling both the amplitude and the duration of

the pulses. The number of the affected cells is also dependent on the number of the delivered electrical pulses (Kandušer & Miklavčič 2008) (Figure 1.2).

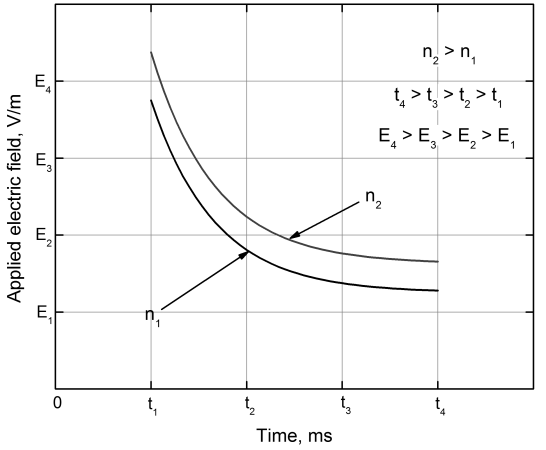

Fig. 1.2. Fraction of the affected cells during electroporation, n – number of pulses, t – pulse duration

As a result repetitive pulsing support should be introduced in the electroporator, which implies that the higher voltage supply power requirements will occur. The other important parameter that is influencing electroporation of the cell membrane is the repetition frequency of the pulses (Kandušer & Miklavčič 2008). If the frequency is in kHz range the delay between the pulses is too short for the cell to return to the pre-pulse state, resulting in a poor electroporation efficacy (Pavlin *et al.* 2005). Based on the experimental studies the optimal frequency for pulse delivery is in the 0.5–10 Hz range (Kandušer & Miklavčič 2008).

The rectangular and exponential decay pulses are more effective compared to triangular or sinusoidal ones (Miklavcic & Towhidi 2010). Subsequently, in the traditional electroporation square wave or exponentially decaying micro-millisecond pulses are typically used, while the electric field intensity is varied in the range of several kV/cm (Stroh *et al.* 2010). In this case the polarization time of the biological cells is shorter than the pulse duration and the field intensity is sufficient to cause transmembrane potential on the plasma membrane, while leaving the cell inner organelles shielded and unaffected (Stroh *et al.* 2010).

However, a new frontier of nanosecond electroporation is being researched (Weaver *et al.* 2012; Chen *et al.* 2012). In this case the biological cells are

subjected to high intensity (several 10 kV/cm) nanosecond pulses with rise times and the pulse duration shorter than the polarization time of the plasma membrane (Kolb *et al.* 2005; Smith & Weaver 2011; Beebe *et al.* 2013). The applied field is capable to pass the cytoplasm and induce voltage on the subcellular membranes (Chen *et al.* 2010). Transient permeabilization of interior organelles, mitochondrical membranes or nuclear envelopes becomes possible (Chen *et al.* 2010). Recent studies have shown that nanosecond pulses could exhibit necrosis and apoptosis of cell and tissue, while maintaining primarily non-thermal treatment due to limited energy of the pulse (Wang *et al.* 2012). The feasibility of the intracellular electroporation leads to the increased interest on the implementations of nanosecond electroporators.

1.2. Electrical Pulse Forming Concepts

Nanosecond, microsecond and millisecond high intensity electric field pulses are required for electroporation of biological cells. Basic concepts of the pulse forming technologies will be reviewed.

1.2.1. General Pulse Generation Concepts

Currently the pulse shaping for the electroporation technique falls into two major categories: exponential decay and the square-wave/rectangular pulses. The waveforms are presented in Figure 1.3.

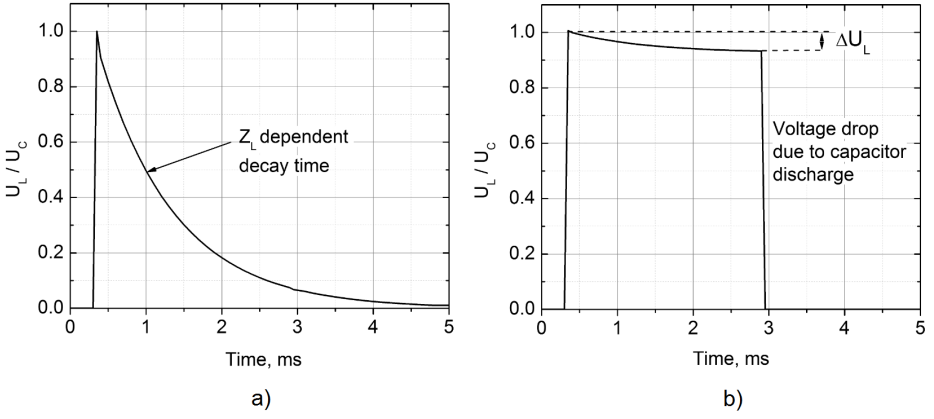

Fig. 1.3. Typical waveforms used for electroporation, a) exponential decay pulse; b) square wave pulse, where U_L – voltage on the load, U_C – charged voltage, Z_L – load impedance, ΔU_L – voltage drop during the pulse

In both of the cases the amplitude of the generated electric field, which depends on the applied voltage to the electrodes, should be high enough to exceed the threshold level, when the transmembrane potential is significant to cause the appearance of pores in the membrane.

The exponential decay fall time of the pulse depends on the load impedance Z_L as follows (Equation 1.2):

$$U_L = U_C e^{-t/Z_L C}, \tag{1.2}$$

where U_L – voltage on the load, U_C – charged voltage, C – total capacitance of the RC circuit.

The exponential decay pulse forming conceptual circuit is presented in Figure 1.4. This is one of the oldest and easily implemented electroporator concepts. It consists of the capacitor bank C_B, charging voltage supply, switch, load resistance R_L and the cuvette for biological cells with electrodes for pulse delivery.

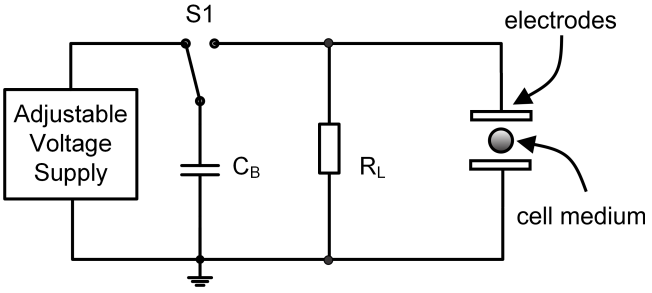

Fig. 1.4. The exponential decay pulse forming conceptual circuit

Such devices operate in two states: 1 – charging of the capacitor bank and 2 – full discharge of the accumulated energy through the electrolytic load. The impedance of the electrolyte is influenced by the concentration of the biological cells, used buffer, temperature and other cell parameters, which implies that the pulse waveform will be different each time (Gilboa *et al.* 2012; Moisescu *et al.* 2013). For this reason the R_L resistance is used, which is typically smaller by several orders compared to the minimum allowed impedance of the cell buffer (Rebersek & Miklavcic 2011). As a result it is easier to define the time constant for the experiments.

The exponential decay pulse generating facilities could be successfully applied for the majority of the electroporation applications including gene transfer to the biological cells (Jordan *et al.* 2008). However, due to the limited

pulse parameters regulation flexibility they are harder to apply in different experiments. The other disadvantage of such system is the charging time of the capacitor bank (Kalgren *et al.* 2007). During single pulse the capacitor is fully discharged through the load and must be charged again faster than the delay between two pulses. As a result faster degradation of the capacitor banks could be observed and a more complex high power voltage supplies must be implemented.

In order to introduce better flexibility of the treatment and improve the efficacy of the electroporation experiments square wave electric pulse generators have been developed (Sundararajan *et al.* 2004). The concept is also based on the capacitor discharge through the load, however in this case the switch is opened for a limited period of time, preventing full discharge of the capacitor. The conceptual circuit of a square wave electric pulse generating system is presented in Figure 1.5. During the pulse a voltage drop ΔU_L is experienced due to the capacitor discharge, resulting in the aberration from the ideal square wave pulse form (Figure 1.3 b). Same as in the exponentially decaying pulse concept the capacitor must be recharged to full between the pulses, however due to bigger capacitor bank the capacitor is not fully discharged each time, which positively affects the lifetime of the capacitor.

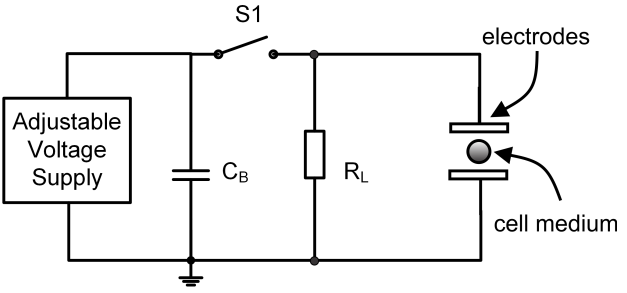

Fig. 1.5. The conceptual circuit of a square wave electric pulse generating system

The voltage drop during single pulse is dependent on the capacitor value, pulse duration and the impedance of the load (Equation 1.3)

$$\Delta U_C \sim \frac{t}{Z_L C}, \tag{1.3}$$

which implies that the concept has application limitations. In order to minimize the voltage drop, a balance between the cell buffer type, the capacitor value and the maximum supported pulse width must be found. Big capacitance arrays are

disadvantageous due to their size and high amount of accumulated energy, which may introduce safety issues during exploitation of the electroporation facility. Limitations of the biological cell buffers only to high impedance solutions also severely limit clinical application of such devices. Narrowing the generated pulse width range results in the limitations both for the clinical and the laboratory environment experiments. Nevertheless, application of square wave electroporators allows precise control of the electroporation process, therefore despite the experienced challenges they are preferable in this field (Rae 2002; MacQueen *et al.* 2008; Wallace *et al.* 2009).

Both of the concepts can deliver electrical pulses from sub-microsecond to millisecond range. In order to generate pulses in the range of several hundreds of nanoseconds other structures must be used (Merla *et al.* 2010; Nakagawa *et al.* 2010; Manabe *et al.* 2011).

1.2.2. Nanosecond Pulse Generation Concepts

One of the oldest concepts for nanosecond pulse generation is the Blumlein generator. The concept utilizes propagation of electrical pulses through the transmission line (Kolb *et al.* 2010; Soo Won *et al.* 2014). It consists of an adjustable voltage supply, current limiting resistor R1, switch S1 and two transmission lines T_{L1} and T_{L2}. The conceptual circuit of the Blumlein generator is presented in Figure 1.6.

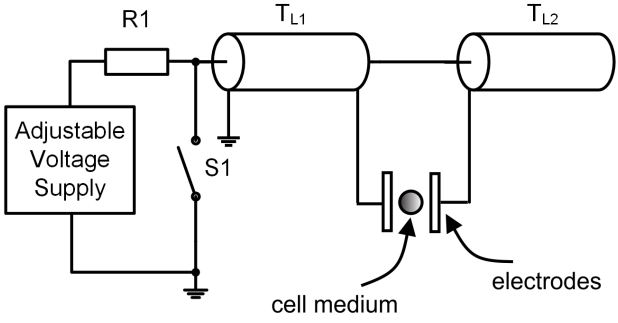

Fig. 1.6. The conceptual circuit of a Blumlein generator

The adjustable voltage supply charges both the transmission lines to the set voltage. When the switch is closed the transmission lines are discharged through the load (cuvette), which superimpose to a square-wave electrical pulse in the cell medium. The pulse duration is dependent on the velocity v of the electrical signal and the length l of the transmission lines. In order to generate the pulse

without reflections the impedance of the cuvette must be matched with the impedance of the transmission line. The rise times of the pulses are influenced by the switch S1 that is used in the circuit. Taking into account that the switch must withstand the high voltage and feature fast switching times such implementation of Blumlein generator sets high demands for the high power electronics components (Jin *et al.* 2012). Limited flexibility of the generated pulse parameters and requirement for load impedance match are considered as the main disadvantages of Blumlein generators in electroporation. Nevertheless Blumlein generators are frequently applied in electroporation for generation of short 10 – 400 ns square-wave pulses (Behrend *et al.* 2003; Scully *et al.* 2010).

As an alternative the diode opening switch generators could be used (Tang *et al.* 2005; Sanders *et al.* 2009; Kranjc *et al.* 2012). The concept is shown in Figure 1.7. The circuit working principle is based on the LC oscillators and the diode, which acts as an opening switch interrupting the current in the oscillation circuit and forming a pulse on the load R_L and the electroporation cuvette, respectively. In order to start the pulse generation cycle the switch S2 is closed and the S1 is opened, resulting in a charged capacitor C1 and empty capacitor C2.

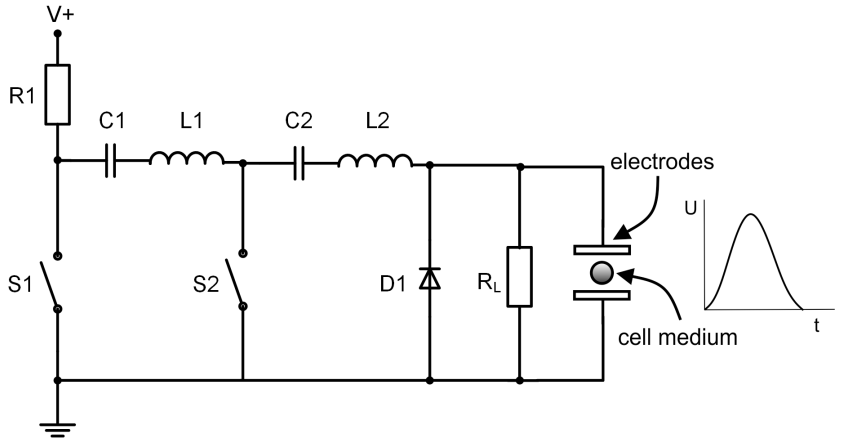

Fig. 1.7. The conceptual circuit of the nanosecond generator based on diode opening switch

Afterwards, the switch S2 is opened and the S1 is closed, resulting in the accumulation of charge in the diode depletion region and the capacitor C2, respectively, due to the half cycle of the forward-biased current. After half of the cycle the S2 is closed and a reverse-biased current due to inductance in the circuit starts to flow discharging the stored energy. A pulse similar to Gaussian

function is formed on the load. Later the switch S1 is opened in order to start charging the C1 again, thus the full pulse generation cycle is completed. Compared to Blumlein generators the diode opening switch based generators are much more complex, however lower demands are set for the switches. Diode opening switch based generators can generate voltages in the range of several kV and support current handling in the range of several A (Rebersek & Miklavcic 2011). The pulse form and the low current handling options make the diode opening switch based generators less applicable in the electroporation field compared to Blumlein generators.

An alternative to both topologies would be application of solid state switches according to concept that was presented in Figure 1.5. Introduction of solid state switches for nanosecond pulse forming is acceptable, however minimum pulse duration is limited in the range of several hundreds of nanoseconds. The maximum voltage handling capabilities of typical solid state switches are also restrained and the driving challenges occur.

1.3. Switches for Electrical Pulse Forming

One of the most important parts of the pulse shaping concepts is the switch. Based on the switch selection, the pulse form, peak current, maximum and minimum pulse widths and amplitudes will be defined (Deboy *et al.* 1998; Schamiloglu *et al.* 2004; Anderson *et al.* 2003). Therefore, analysis of possible switches must be performed. Certain switch technologies are more than hundred years old and are still viable nowadays, others such as semiconductor devices are being developed for several decades and are refined, however still having limitations (Grekhov *et al.* 2000). Choosing an appropriate switch and the pulse forming technology allows achieving the best flexibility and reliability of the device being developed, therefore increase the applicability and stimulate further research on the edge of technology (Weihua *et al.* 2004).

Both the square wave and the exponential decay pulse forming concepts require high current, high voltage handling switches with high reliability and simple driving circuit (Behrend *et al.* 2003; Xinjing *et al.* 2008; Sanders *et al.* 2009). Typically four switch implementations are used: 1) Thyristors; 2) Transistors; 3) Relays; 4) Spark gaps.

1.3.1. Thyristors

Thyristors or silicon controlled rectifiers (SCRs) are solid state switches consisting of several pn junctions. When they are triggered they act as a low-impedance open circuit, making a current path to the load. The distinguishing

features of these devices are the high current handling capability and the simple driving of the device (Watanabe *et al.* 1990; Podlesak *et al.* 1997). The trigger signal can be removed when the SCR is open and the device will remain open until the current reaches the low threshold level.

These features make the device highly applicable for exponentially decaying pulse forming, while the circuit remains simple and low cost. However certain limitations exist. Ones of the most crucial limitations for these devices are the *dI/dt* and *dV/dt* maximum ratings (Ramezani *et al.* 1993; Giorgi *et al.* 2004). Exceed of those rating results in permanent damage of the SCR. Also the driving pulse current must be sufficient for the avalanche breakdown of the blocking junction of the SCR.

Even though the SCRs can commutate currents in the range of kA, there are limitations for maximum allowed forward and reverse voltages. Typically the voltages range from hundreds of volts to 1.5 kV for discrete devices. Higher values are rare and the cost is increased dramatically, however thyristors are suitable for array applications both in series and parallel, therefore despite all those limitations they offer fast rise and fall times in sub-microsecond range (high frequency devices), reliable exploitation and high current handling capability (Podlesak *et al.* 2005).

Application of thyristors for square wave pulse forming is limited. Opposite to normal SCR in order to form a square wave pulse a fully controlled switch is required. Gate turn-off (GTO) thyristors could offer such versatility and high *dI/dt* (Podlesak *et al.* 1991; Temple 2004). Such devices are turned on by a positive gate signal and a negative signal is supplied for turn-off. It should be noted that typically GTO thyristors require higher driving current and are more susceptible to transient processes in the circuit, therefore overcurrent and overvoltage protection are implemented (Jae-Hyeong *et al.* 1997). The GTO thyristors typically are not used in electroporators for square wave pulse forming due to their price and susceptibility to transient processes.

1.3.2. Transistors

Transistors are fundamental parts of modern electronics, they are frequently used both for high power and low power applications as a switch for pulse forming. Electroporation wise certain requirements discussed above should be met, which limits applicable array of transistors to metal oxide semiconductor field effect transistors (MOSFETs) and insulated gate bipolar transistors (IGBTs).

Both of the transistor types are commonly used for electrical pulse forming in switching power supplies, electroporators and other pulse generators (Bortis *et al.* 2007; Dongdong *et al.* 2010).

The MOSFET's distinguishing features could be summarized as (Locher 1998; Jun *et al.* 2008):

Advantages:

- very fast switching times (rise and fall times in nanosecond range);
- low power dissipation;
- high input impedance;
- low gate signal power requirement;
- high frequency operation;
- less affected by temperature.

Disadvantages:

- high resistance channels;
- reduction of channel resistance results in parasitic capacitance increase;
- peak current is limited to hundreds of amperes;
- Can be easily destroyed by high voltages, susceptible to static electricity.

Taking into account all these features MOSFETs in electroporators are typically used for short microsecond square wave pulse forming into high impedance electrolytic loads. For generation of longer or exponentially decaying high current pulses the IGBTs are preferable. The IGBTs offer the output switching characteristics of a bipolar transistor, however same as MOSFETs, they are voltage controlled (Nawaz *et al.* 2013). The IGBT technology offers higher current and voltage handling capability compared to MOSFET, however slower switching times (Jong-Hyun *et al.* 2011). Also the IGBTs have the disadvantage of comparatively long current tail. Nevertheless due to higher power handling capability IGBTs are usually the device of choice for electroporators, which work in micro-millisecond range (Stirke *et al.* 2014).

In summary application of transistors is preferable for square wave pulse forming in electroporation. Precise control of the pulse width, easy driving of the switch, flexible peak current ranges define the superiority of these semiconductor technologies compared to other types of switches.

1.3.3. Modular High Voltage Semiconductor Switches

Modular switches consists of arrays of discrete switches connected in series or in parallel in order to expand the breakdown voltage and current handling ranges (Baek *et al.* 2005; Zorngiebel *et al.* 2011). Synchronization of the devices requires complex overvoltage protection circuits and increases both the switching times and the price of a single module (Jiannian *et al.* 2011). Therefore, modular switch implementations provide a solution for high voltage

and current handling, but still not commonly practiced due to the technological challenges (Zorngiebel *et al.* 2011).

Synchronization problems in such devices are ussually overcommen using trigger generators with multiple synchronized but galvanically decoupled channels. Inductive decoupling using a ferrite core can be used (Zorngiebel *et al.* 2011; Tao *et al.* 2014).

Despite the price and complexity of such modules, the synchronized modular switch based on MOSFETs or IGBTs can provide a solution for pulse forming in the kV range (Jong-Hyun *et al.* 2011). However, all the limitations applicable for transistors apply.

1.3.4. Relays

Relays could be also used as switch to form the electrical pulse for electroporation. There are two major relay types: 1) electromechanical; 2) solid state relays. Solid-state relays (SSRs) do not have moving parts and consist of the semiconductor switches (thyristors or transistors) and therefore all the limitations discussed above are also applicable for them (Fan & Liu 2014). The electromechanical relays (EMRs) have a moving contact, which is frequently operated using an electromagnet and the driving electrical signal (Turner 2014). As a result the SSRs have the size advantage over EMR's. Also since the SSRs have no magnetic interaction, moving parts and are immune to physical shock, they do not generate electrical noise and are not sensitive to electromagnetic interference.

Therefore, application of relays in electric pulse generators as a pulse forming switch is limited to SSRs. The EMR's relays are very rarely applied due to the contact bouncing, arcing, noise generation and other problems. However, the SSR's could provide sufficient pulse generation flexibility in micro-millisecond low voltage pulse range and feature a compact and easy to install design to simplify the circuit. For pulses shorter than hundreds of microseconds transistors and thyristors are preferable.

1.3.5. Spark Gap

Spark gaps typically consist of several conducting electrodes separated by gap filled with gas. High voltage applied to the electrodes creates high intensity electric field ionizing the gas and when the voltage exceeds the breakdown voltage, the low resistance path for the spark is formed (Deng *et al.* 2011; Mao *et al.* 2012; Saroj *et al.* 2014). Additional ionizing electrodes could be implemented for controlled switching.

Spark gaps are frequently applied for ultra short pulse generation, offering short rise and fall times and yet simple and cost-effective structure (Yi *et al.* 2013; Reddy *et al.* 2014). Nevertheless unlike solid state switches spark gaps have limited lifetime due to degradation of the electrodes. Also the limited breakdown voltage flexibility severely complexes application of spark gaps in electroporators. Therefore, as a rule spark gaps in electroporation are used for specific low frequency nanosecond range pulse forming (Balevicius *et al.* 2013). Transistors and thyristors are preferable for wide range pulse generation.

Based on the advantages and disadvantages of common switches used in the electrical high power pulse generators the diagram summarizing the features of these pulse forming devices is shown in Figure 1.8.

The pulse forming switch selection depends on the applications of the electroporator. The most universal types of switches are the transistors, which offer both simple driving and wide range of generated pulse durations. Also transistors are advantageous for generation of electrical pulses when low rise and fall times are a priority.

At the same time for high current handling and exponentially decaying pulse generation thyristors are preferable.

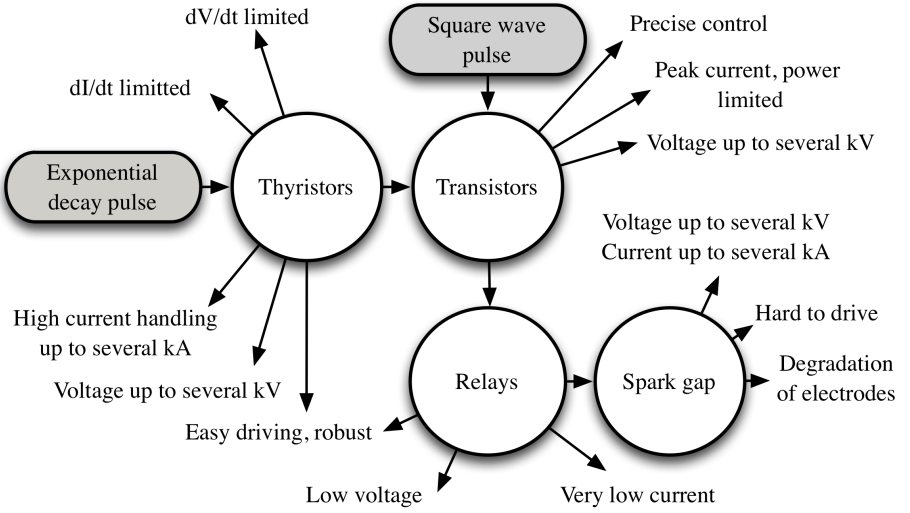

Fig. 1.8. Typical switches used for pulse forming in electroporators

Other switches such as relays or spark gaps are very application specific and as rule are inferior to transistors and thyristors when used for pulse forming.

It can be concluded that the discrete and modular transistor switches are the best choice for generation of pulses with controlled width and frequency, however consideration of the maximum breakdown voltage and current handling must be performed.

1.4. Present Status of Electroporation Technology

Electroporation is a widely applied biomedical technique that has already made a way to clinical application both *in vitro* and *in vivo*. Currently, a variety of different implementations of electroporators exists and an explicit analysis must be performed to overview the limitations, introduce the technological problems and determine the requirements for novel solutions on the edge of the current technology.

1.4.1. Available Electroporation Instruments

Since the electroporation is a profitable area having high demands for new technological implementations of electrical pulse generators, a variety of commercial and non-commercial scientific systems is available (Bradshaw *et al.* 1987; Sarkar *et al.* 2004; Rebersek *et al.* 2007). The square-wave pulse generators are better for pulse delivery in electroporation compared to the exponential decay wave generators and as a result in the past few years the square-wave pulse technology started to dominate both in scientific works and clinical applications. The direction for development of the commercially available pulsed generators has been confirmed. The typical commercially available square-wave electroporation systems are summarized in Table 1.2.

Table 1.2. Typical commercially available electroporation systems

Electroporator	Voltage range, kV	Pulse duration	Pulse series	Voltage drop during pulse	Maximum load	Dimensions
ECM 830 BTX	0–3	10 μs – 10 s	1–99	20%	20 Ω	32 x 31 x 14 cm^3
Bio Rad Pulse MxCell	0–3	50 μs – 0.1 s	1–3	–	10 Ω	31 x 30 x 14 cm^3
EPI 2500	0–2.5	20 μs – 0.1 s	1–99	–	25 Ω	30 x 24 x 13 cm^3
CUY-21	0.2–0.5	100 μs – 1 s	1–99	5%	25 Ω	39 x 45 x 25 cm^3

As it can be seen from Table 1.2 there is a tendency to cover a broad micro-millisecond pulse duration range with flexible voltage amplitude alteration capabilities. The ECM 830 BTX and Bio Rad pulsed systems are commonly used in research as a convenient scientific tool allowing research of electroporation process in a broad range of pulse parameters. The systems support high loads up to 10–20 Ω, which offers support of a wide array of cell buffers. All of the systems are based on the accumulation of energy in a capacitor with limited capacitance, therefore during discharge a voltage amplitude drop is observed. The voltage amplitude drop in the range of 20–25% is considered as acceptable and sufficient to provide decent repeatability of electroporation experiments. The physical size of the systems offers good transportation options, which is required in laboratory environment.

In all of the systems due to the limitations by the maximum current/voltage handling capabilities of the switches and capacitors the voltage range is limited by 3 kV. Implementation of even higher voltage pulse generators involves safety and transient processes compensation issues. Nevertheless, despite the offered pulse generation possibilities there is still a demand for new technological implementations, which will offer even better pulse flexibility. Higher voltage support is required when the volume of effect is an important factor like in *in vivo* applications. Also 0–3 kV voltage range electroporators are limited in variety of applicable electroporation cuvettes. Therefore, cuvettes with 5 mm or wider gap between the electrodes are rarely used.

1.4.2. State of Art Electroporation Instruments

The state of the art research of the electroporation technique investigates biological effects of high intensity electric fields generated by high voltage pulses, which are higher than several kV, while the pulse durations vary in the microsecond and sub-microsecond range. The nanosecond electroporation utilizes application of voltages higher than 5–7 kV, while the short microsecond pulse electroporation requires voltages in the range above 3 kV. In both of the cases complex solution must be provided in order to develop pulsed power systems with such parameters.

In both the nanosecond and micro-millisecond range there is a lack of prototypes, which could offer such parameter flexibility (Sanders *et al.* 2009; Li *et al.* 2011). The majority of scientific works focus on the generation of single high voltage fixed duration nanosecond or microsecond pulses, which severely limits the applicability of the prototypes for research of the electroporation technique (Napotnik *et al.* 2012).

In case of duration alteration capabilities as a trade-off the voltage range is dramatically reduced. Nevertheless, developments in this field are performed

very actively and in 2012 an adjustable nanosecond pulse duration concept based on solid state Marx generator has been proposed (Yao *et al.* 2012), which is shown in Figure 1.9.

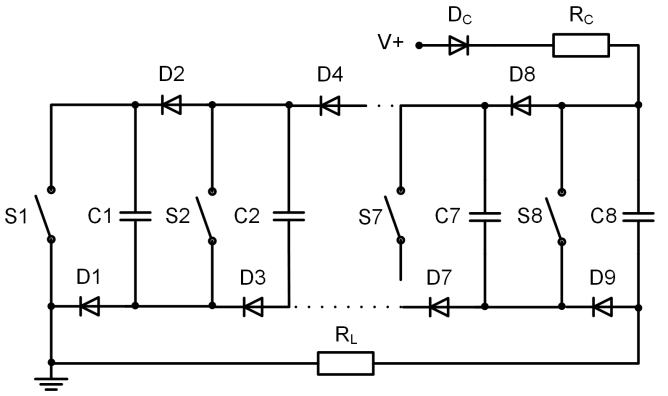

Fig. 1.9. Nanosecond electroporator concept based on solid state Marx generator (Yao *et al.* 2012)

The major advantage of such implementation is the low demands for the semiconductor switch voltage handling. However, IGBT synchronization and control requires complex driving pulse forming circuits.

Also load matching should be addressed. The prototype consists of the 8 stage solid state Marx generator capable of delivering 200–1000 ns electrical pulses up to 8 kV into loads up to 100 Ω (Yao *et al.* 2012). The power efficiency of 86.64% has been achieved. Implementation of more stages for the solid state Marx generator would increase the losses even further.

The development of the Blumlein type generators is also performed as an alternative. Recently the microstrip-line Blumlein concept has been proposed (Romeo 2013). An array of conductive meander strips realized to match specific electroporation cuvette loads has been used to form the Blumlein generator transmission line. The meander structures were implemented on the printing circuit boards featuring a non-conductive substrate covered with copper and later etched to form the meander. As a result up 100 ns pulses could be generated by the prototype (Romeo *et al.* 2013). The major advantage of the concept is the very simple structure and the low price of the system. However, the load matching issues and the poor pulse parameters flexibility still has to be addressed.

A variety of other implementations of nanosecond and microsecond electric pulse generators have been proposed in the recent years. However, the restrains

in the maximum delivered pulse amplitude or poor pulse duration flexibility makes them very specific for a certain experiment (Bertacchini *et al.* 2007). An explicit analysis of the electroporation technique in a broad range of pulse parameters is impossible.

1.5. Transient Process Compensation

Various technological implementations for connecting high power switches in series or in parallel, especially the MOSFETs and the IGBTs are usually the only solutions for generation of high voltage and high current pulses using the solid state switch technology. In such a case application of snubber, clipping, crowbar and clamping circuits is inevitable, which allows relieving the switching stress, diminish overvoltage and overcurrent issues and synchronize the semiconductor switch array. Analysis of possible transient process compensation circuits must be performed in order to prevent switching instability during transient turn-on and turn-off.

1.5.1. Snubber Circuits

The most frequent reasons for application of snubber circuits in high power electronics are to reduce the losses experienced during switching, limit the overvoltage on the switch due to the stray inductance in the circuit and improve the synchronization of the array of semiconductor devices (Austermann *et al.* 2014; Zhihao *et al.* 2014). Currently, many kinds of snubber circuits have been developed but the resistor-capacitor (RC) and the resistor-capacitor-diode (RCD) snubber circuits are the most commonly used.

The RC and RCD snubbers are usually used to limit overvoltage, overcurrent, switching losses and excessive *dI/dt* and *dV/dt* on the switch (Chen *et al.* 2011). Several snubbber topologies exist such as positively polarized, reverse polarized and non-polarized. The positively polarized RC snubber topology is shown in Figure 1.10.

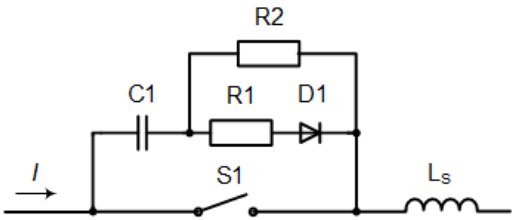

Fig. 1.10. Positively-polarised RC snubber topology

The R1 limits the forward *dV/dt,* while the R2 limits the current of the snubber capacitor C1. Additionally a high resistance resistor in the range of several MΩ is connected in parallel to the whole snubber topology, thus allowing equal DC voltage drop on the array-connected switches, when the switches are closed. The *dV/dt* and *dI/dt* limitation is required due to the presence of stray inductance L_S in the circuit, which leads to submicrosecond high voltage spikes on the switch. Additional fast recovery snubber diode could be implemented parallel to the switch to restrain the influence of the reverse biased current from the stray inductance.

The reverse polarised topology is used to limit the reverse *dV/dt*. The principle of operation is the same, however the RCD snubber topology is connected with reversed polarity. The non-polarized snubber is the simplest topology, which consists of the RC circuit connected in parallel to switch. Depending on the time constant of the snubber the *dV/dt* and *dI/dt* are restrained.

1.5.2. Clipping and Clamping Circuits

Wave-shaping could be used as method to restrain all the aberrations from the required pulse form due to the transient processes occurring in the circuit. Removing (clipping) a part of the wave allows controlling the maximum or the minimum pulse amplitude, thus the clipping circuits are frequently refereed as voltage limiters (Pierco *et al.* 2012; Wolfus *et al.* 2014). Clipping technique could be successfully applied for IGBT or MOSFET driver pulse forming. Identical and synchronized driving pulse waveforms are crucial in switch array applications. A common Zener diode clipping circuit is shown in Figure 1.11.

The R1 limits the current of the pulse, while two Zener diodes conducting in the reverse breakdown region form the clipped shape of the output pulse.

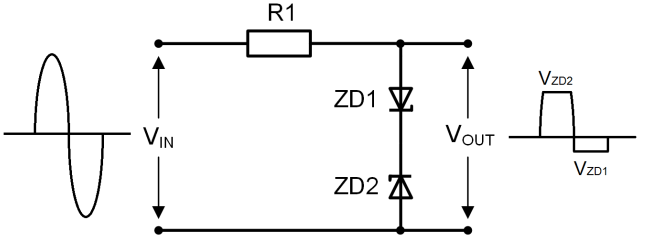

Fig. 1.11. Clipping circuit based on Zener diodes

The amplitudes are equal to applied Zener diode voltage +0.7 V voltage drop. The circuit could be successfully applied to form required amplitude and

reduced level of distortions switch driving pulses. The clamping circuit is also a convenient tool for driving pulse forming. It is usually used to move the positive or negative signal to another level by the means of adding a positive or negative DC component to the input. As a rule a combination of a voltage source and a diode in parallel to the load is applied. Clamper circuits do not help transient process compensation, however combined with clipping circuits offer better pulse forming flexibility.

1.5.3. Crowbar Circuits

In pulsed power technology the crowbar circuit is used for pulse fall time forming purposes and as a tool to limit overvoltage on the switch due to the inductive loads and reverse-biased currents (Dongdong *et al.* 2010; Sun *et al.* 2011). The typical passive crowbar circuit is shown in Figure 1.12.

The passive crowbar circuit consists of a high power diode D1 and a current limiting resistor R1. Due to the parasitic inductances in the circuit or the inductive nature of the load during the pulse fall time a reverse biased current is induced.

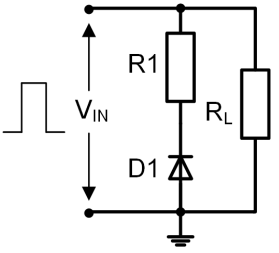

Fig. 1.12. Crowbar circuit

As a result voltage spikes can occur on the semiconductor switch and the capacitor bank is negatively charged. Both of these factors influence the durability decrease of the circuit components and issues in pulse shaping. Implementation of a crowbar circuit introduces a low-conducting pass for the forward-biased current and high-conducting contour for the reverse-biased signal. As a consequence the overvoltage problem is solved, however as a trade-off the fall time of the pulse is increased.

1.6. Scientific Demands for the Electroporation Setup

The square-wave pulse electroporation systems are more advanced for transfection of drugs or other molecules inside the biological cell. Steep rise and fall times of the electrical pulse ensure better control over the treatment intensity and therefore have higher clinical and scientific application potentials and demands. The aim of this section is to investigate and determine the parameters of the electroporation systems for transfection of impermeable molecules, tissue ablation and permeabilization of inner cell organelles.

1.6.1. Evaluation of the System Parameters

The molecule transfection system should cover the whole range of currently known electroporation stimulated transfection applications and have a reserve in flexibility to be used as a novel biomedical scientific tool for further research of the electroporation technique.

The electroporation stimulated transfection methodology could be applied both *in vivo* and *in vitro* and utilizes pulses in the micro-millisecond range. The electric field strength that is applicable for transfection is ranging from 0.1 kV/cm to 10 kV/cm. For *in vitro* applications cuvettes with integrated electrodes are introduced. The typical gap between the electrodes is ranging from 0.5 mm to 5 mm, which implies that voltages in the range of 0.5–1 kV are sufficient to cover the whole array of applications, offering electric field intensities up to 20 kV/cm in a 5 mm cuvette.

In vivo procedures are more complex and the electric field intensity is dependent on the structure of the electrodes and the effective volume of the tissue that is under the treatment. The tissue ablation or irreversible electroporation methodology utilizes pulses up to 100 kV/cm. As a result voltages up to 4 kV must be supported, which will allow covering the whole array of possible applications and perform electroporation research on the edge of technology. Subsequently the pulse duration range must be defined. Currently the 1 μs – 100 μs pulse duration range is less studied due to higher voltages and currents required for achievement of the permeabilization phenomena. The absolute majority of the protocols use the 0.1–10 ms repetitive pulsing procedures, when the voltage could be significantly reduced. However, there is a clear tendency in the research works to reduce the pulse duration and increase the electric field intensity. Consequently, the nanosecond range frontier must be addressed.

As it has been mentioned in previous chapters the total energy of the pulse plays a crucial role in the outcome of the treatment. Therefore, if for the 1 μs – 10 ms pulse duration range the 0–4 kV voltage range is sufficient, for the

nanosecond pulse treatment the voltage range must be further expanded. Voltages up to 6–8 kV should be supported, which will offer treatment intensities up to 160 kV/cm with 5 mm gap cuvettes. Further increase of voltage introduces safety issues. Pulse duration flexibility wise the nanosecond range is poorly studied. The prototype should cover at least several hundreds of nanoseconds at maximum 6–8 kV voltage in order to introduce novelty and high potential of application of the device.

1.6.2. Evaluation of the Scientific Novelty and Practical Value

In order to evaluate the novelty and the practical value of the electroporation system with the pulse parameters described in previous chapter, the comparison analysis with the most advanced and successful prototypes was performed. As it has been shown previously, currently, one of the most advanced scientific instruments for electroporation is the ECM 830 BTX Harvard Apparatus (Kim *et al.* 2012; Zeng *et al.* 2012; Cathelin *et al.* 2013; Meng *et al.* 2014).

The summary of the ECM 830 BTX pulse parameters and the pulse parameters that should be introduced in the next generation electroporation facilities is presented in Table 1.3.

Table 1.3. Summary of the ECM 830 BTX pulse parameters and the pulse parameters that should be introduced in the next generation electroporation facilities

Status	ECM 830 BTX		Required parameters	
	Supported voltage, kV	Pulse duration range	Supported voltage, kV	Pulse duration range
Not supported	–	–	7–8	0.4–0.6 μs
Not supported	–	–	5–6	0.6–1 μs
Not sufficient	0–3	10 μs – 0.1 ms	3.5–4	1 μs – 0.1 ms
Not sufficient	0–2.5	0.1–0.3 ms	3	0.1–0.3 ms
Not sufficient	0–0.75	0.3–3 ms	1.5–2	0.3–3 ms
Acceptable	0.5	0.4 ms – 1 s	0.5–1	3–10 ms

As it can be seen from Table 1.3 almost all of the pulse parameters should be improved in order to address the scientific problems in a poorly studied electroporation pulse ranges. The respective improvement demands in comparison to the one of the most advanced commercially available scientific instruments ECM 830 BTX for the nano-microsecond pulse duration range are presented in Figure 1.13.

The minimum duration of the pulse generated by the BTX system is 10 μs with the peak amplitude of 3 kV. Due to this factor such applications as

sterilization, food preservation, inner cell organelle permeabilization, partly tissue ablation are not accessible, when the required volume of effect is high.

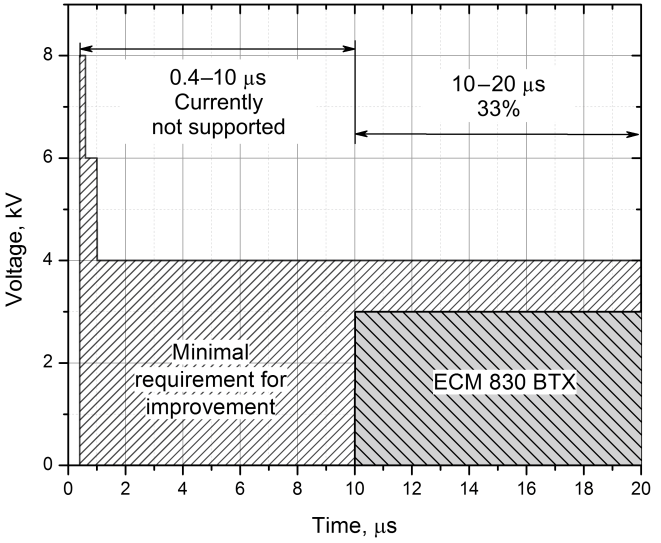

Fig. 1.13. Requirement of pulse parameter improvement compared to the ECM 830 BTX

In order to support high volume cuvettes with electrode gap size of 5 mm or more, in the short 10–100 μs pulse duration range the voltage amplitude should be expanded to 4 kV (33% required increase) to allow all possible microsecond range transfection experiments. The short microsecond and submicrosecond pulse up to 8 kV generation capabilities should be introduced, which will significantly burst the novelty and practical application of the setup. Currently there are no commercially available systems offering such parameters and the non-commercial scientific prototypes lack flexibility.

The micro-millisecond electroporation range is well studied compared to the short microsecond or submicrosecond pulse electroporation. However, introduction of the expanded peak voltage support and improvement of the flexibility independent from the cuvette type and gap between the electrodes is required.

The summary of required pulse parameter improvement in the micro-millisecond electroporation range in respect to the ECM 830 BTX device is presented in Figure 1.14.

As it can be seen in Figure 1.14 the 100 μs – 3 ms pulse duration range requires major improvements up to 260 % compared to the BTX device. The

long millisecond pulse diapason is acceptable offering up to 10 kV/cm electric fields in a 5 mm gap cuvette (0.5 kV charging voltage).

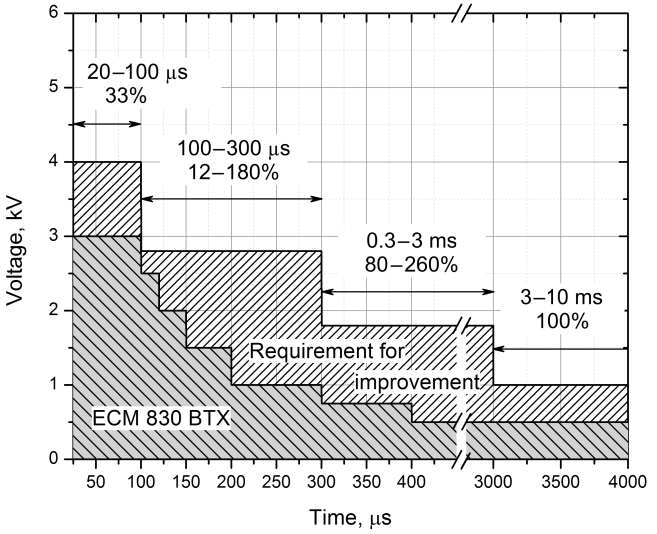

Fig. 1.14. Requirement of pulse parameter improvement in the micro-millisecond range compared to the ECM 830 BTX

However, for *in vivo* experiments the supported voltage should be improved up to 1 kV at least.

The development of an electroporation system offering the flexibility of parameters discussed above will significantly contribute to the electroporation field as a unique scientific instrument. Research of the whole spectrum of the electroporation applications will be achievable. Introduction of short microsecond and submicrosecond pulse support will inevitably contribute to the acquisition of new novel experimental data, which is scientifically significant.

Based on these considerations the thesis tasks have been formed and the scientific problem that requires solution was determined.

1.7. Chapter 1 Conclusions. Thesis Tasks

1. Application of electrical pulses in biology has a high potential as a remarkable biomedical technique known as electroporation, which is used as a cellular level drug delivery stimulation tool. In the last decades

the relevancy of the electroporation technique increased both in clinical and laboratory environment.

2. The biological effects of the electrical pulses depend on the shape, amplitude, duration and other pulse parameters. As a result development of pulsed systems capable of delivering electrical pulses with high parameter flexibility is required.
3. Electroporation efficacy depends on the parameters of the electric field. The cell medium temperature rise due to the high current flow may distort the experimental results. Development of applicators with high electric field homogeneity and limited Joule heating influence is required for study of electroporation phenomenon.
4. The square-wave electrical pulse shape is the most convenient waveform for the electroporation technique due to the possibilities for precise control of the delivered pulse energy and the voltage threshold based electroporation mechanism.
5. The prototypes of the electrical pulse generators capable of forming square-wave pulses above 3 kV for research of electroporation technique in microsecond range are in high demand.
6. The submicrosecond electroporation range is poorly studied due to the lack of the flexible high voltage submicrosecond duration pulse generation systems, which are in high demand.
7. Development of high voltage short microsecond and submicrosecond electrical pulse generation systems capable of delivering repetitive pulses with high pulse parameter alteration flexibility is a complex and relevant electronics and electrical engineering task. Compensation of the transient processes due to the influence of the parasitic circuit elements is required in order to generate high precision high voltage pulses.

The following tasks have to be solved in order to achieve the aim of the thesis:

1. Develop the simulation model for square wave pulse electroporators, investigate the transient processes and possibilities for compensation of the parasitic elements influence on the generated pulse shape.
2. Develop the high power square wave pulse electroporators prototypes and investigate the applicability in biological cell permeabilization and absorption experiments.
3. Develop electroporation electrodes, investigate the distribution of the electric field and the Joule heating influence in the cell medium.

2

Development and Research of the Square Wave Pulse Electroporators

The nanosecond-microsecond and micro-millisecond square wave pulse electroporators are investigated in this section. The PSPICE and COMSOL models of the generators and the microelectrodes for the electroporation technique are overviewed. The analysis and the corresponding compensation procedures of the transient processes in the high power circuits are performed. The prototype of the electroporators are investigated and compared to the simulation model results. Based on the results the adequacy of the prototype to the goals of the dissertation is studied.

Four scientific publications were published on the section topic (Stankevič, Novickij *et al.* 2013; Novickij *et al.* 2014a; Novickij *et al.* 2014b; Novickij *et al.* 2015b).

2.1. Micro-millisecond Range Electroporators for Transfection of Impermeable Molecules

In this section the research of the electroporator, which will allow coverage of the micro-millisecond electroporation range experiments, is performed. Based on the results the circuit for the electroporator is developed and the PSPICE simulation model for the compensation of the transient processes and selection of optimal components is developed.

2.1.1. The Model of the Micro-Millisecond Pulse Generator

The most convenient way of generation of the square-wave electrical pulse is the discharge of the capacitor array through the load using a controlled opening time switch. In order to determine the optimal components, structure and compensate the transient processes of the MMPG, the PSPICE simulation model of the generator was developed. The simulation circuit of the MMPG is presented in Figure 2.1.

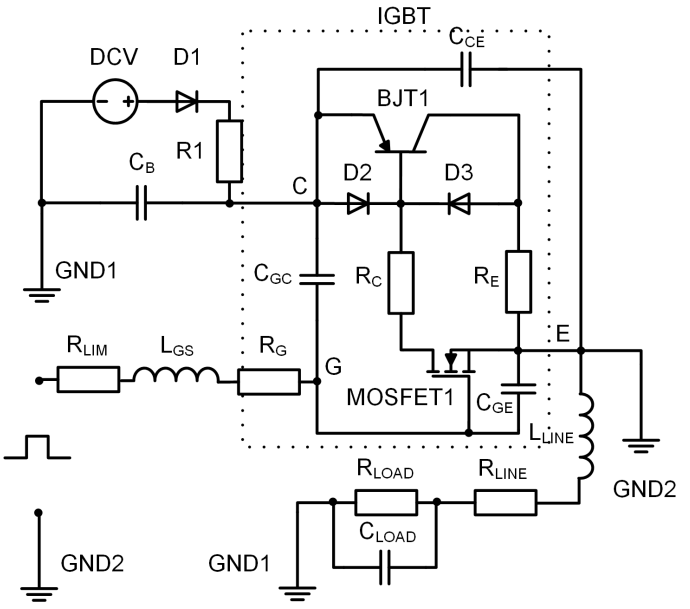

Fig. 2.1. Simulation circuit of the micro-millisecond pulse range electrical pulse generator

The switch plays the crucial role in the circuit of the MMPG. The IGBT is the best choice in the micro-millisecond diapason due to the relatively fast rise and fall times and the high power handling capability compared to the MOSFET. Essentially the IGBT switch is a MOSFET with additional layer in series with the collector, which implies that it could be simulated as a power MOSFET1 and a bipolar PNP transistor BJT1. In order to introduce the voltage breakdown features of the simulated switch the diodes D2 and D3 have been introduced. The stray capacitance and the inevitable resistance of the collector-emitter channels have been simulated using capacitors C_{GC}, C_{GE}, C_{CE} and the R_C, R_E, respectively. The inner gate resistance R_G has been introduced. Driving of the IGBT is performed by an external signal, while the resistor R_{LIM} limits the driving signal power. The L_{GS} is implemented to introduce the influence of stray inductance of the driver circuit.

The capacitor array for pulse power accumulation has been simulated as C_B. The charging has been implemented as a DC voltage source in series with the charging resistor R1. The diode D1 has been introduced to minimize the ripples of the charging circuit.

The load of the generator has been simulated as a resistor R_{LOAD}. The influence of the parasitic components of the load and the transmission line has been implemented as C_{LOAD}, R_{LINE}, L_{LINE}, respectively.

The required output parameters of the circuit are summarized in Table 2.1.

Table 2.1. Summary of required output parameters for the micro-millisecond pulse range electrical pulse generator

Voltage range	Pulse duration range	Load	Voltage drop during pulse
0–4 kV	1 μs – 0.1 ms	40 Ω – 2 kΩ	< 25%
0–3 kV	0.1–0.3 ms		
0–2 kV	0.3–3 ms		
0–1 kV	3–10 ms		

Taking into account the requirements for the MMPG the optimal IGBT switch must be chosen. Four switches have been considered in this work: IXEL40N400, IXGK75N250, IXBH20N300 (Ixys, Switzerland) and QID4515001 (Powerex, USA). The summary of the main switching characteristics of these IGBTs is presented in Table 2.2. All of the switches support high current handling capability sufficient for required application. High voltage handling wise only the QID4515001 and IXEL40N400 are acceptable without series connection topology. Naturally, implementation of a series connected topology of the IXGK75N250 or IXBH20N300 is possible and

acceptable, however stray capacitance and inductance of the circuit will be increased. Also synchronization and precise voltage distribution issues during switching will have to be addressed. All of these factors will increase the complexity of the circuit and worsen the switching parameters of the system.

Table 2.2. Summary of required output parameters for the micro-millisecond pulse range electrical pulse generator

IGBT	Peak voltage	Current	Rise, fall times	Turn off delay time
IXEL40N400	4000 V	400 A	100 ns / 425 ns	630 ns
IXGK75N250	2500 V	530 A	225 ns / 455 ns	270 ns
IXBH20N300	3000 V	140 A	210 ns / 504 ns	300 ns
QID4515001	4500 V	300 A	500 ns / 1.2 µs	3.5 µs

It was concluded that using a single IGBT module is advantageous. However the QID4515001 IGBT is inferior to the IXEL40N400 due to the slower switching characteristics. Based on these considerations the IXEL40N400 IGBT has been selected as optimal choice for the micro-millisecond pulse electroporator. The parameters of the IGBT model presented in the simulation circuit (Figure 2.1) have been adjusted to match the switching characteristics of the IXEL40N400.

The simulation parameters are summarized in Table 2.3.

Table 2.3. Micro-millisecond pulse range electrical pulse generator simulation parameters

Parameter	Value	Denotation	Determined values
Power supply capacitance	1 µF – 1 mF	C_B	–
Power supply limiting resistance	20–80 kΩ	R1	–
Collector-emitter capacitance	200–300 pF	C_{CE}	280 pF
Gate-collector capacitance	50–200 pF	C_{GC}	120 pF
Gate-emitter capacitance	1–10 nF	C_{GE}	6 nF
Inner gate resistance	1–10 Ω	R_G	5 Ω
Driving signal power limiting resistance	1–40 Ω	R_{GS}	–
Driver circuit stray inductance	0.5–2 µH	L_{GS}	0.8 µH
Transmission line stray inductance	2–10 µH	L_{LINE}	–
Load resistance	40 Ω – 2 kΩ	R_{LOAD}	–
Parasitic load capacitance	1–800 pF	C_{CAP}	–

The pulse forming capabilities of the simulation circuit have been evaluated. In order to determine the required compensation for the transient processes during switching the influence of the parasitic circuit parameters L_{LINE} and C_{LOAD} has been analysed. The dependence of the generated 2 μs pulse waveform on the stray inductance L_{LINE} is shown in Figure 2.2.

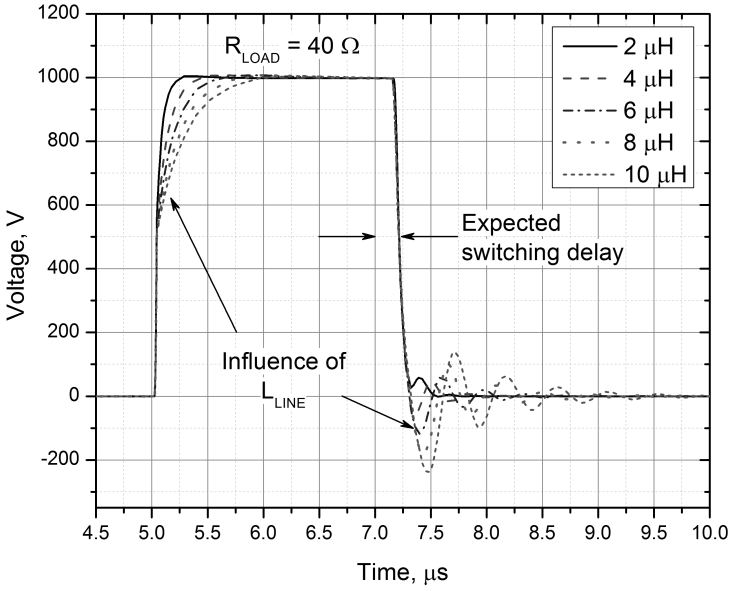

Fig. 2.2. The dependence of the generated pulse waveform on the stray inductance L_{LINE}

As it is seen in Figure 2.2 due to the parasitic inductance in the circuit the aberration from the square waveform is observed. The maximum allowed load of 40 Ω has been used in the model to maximize the current and therefore the loop effect, which may appear in the prototype circuit. The rise time of the pulse is increased dramatically to 0.5–0.7 μs dependent on the stray inductance value. The switching delay of 200–500 ns that is introduced in the simulation is typical for IGBTs, therefore was also implemented in the model to improve the adequacy of results. The voltage spikes and oscillations during turn-off of the IGBT are proportional to the total loop inductance of the MMPG, which in the real prototype comes from PCB tracks, terminal leads, inner electronic component inductance and wire-bond connections. Obviously, minimization of the total system inductance is a priority during development of a square wave pulse generator, however the loop effect due to the stray inductance is still inevitable. Taking into account that the oscillations amplitude could exceed 20%

of the total pulse amplitude (10 μH stray inductance), at 4 kV up to 0.6–1 kV amplitude oscillations are expected, thus compensation of the transient processes will be required. Independent from the stray inductance coming from electronic components such as resistors, IGBTs, capacitor, etc., the self-inductance of the wire connections contributes to the total loop effect.

The self-inductance of a wire with rectangular cross-section can be estimated as (Piatek *et al.* 2012):

$$L_{\text{wire}} = \frac{\mu_0 l_{\text{w}}}{2\pi}\left(\ln\frac{2l_{\text{w}}}{a_{\text{w}}+h_{\text{w}}} + 0.5 + 0.22\left(\frac{a_{\text{w}}+h_{\text{w}}}{l_{\text{w}}}\right)\right), \tag{1.4}$$

where μ_0 is the magnetic constant, l_{w} is the length of the wire, a_{w} and h_{w} are the width and the thickness of the wire, respectively. The mutual inductance can be approximated as (Piatek *et al.* 2012):

$$L_{\text{M}} = \frac{\mu_0 l_{\text{w}}}{2\pi}\left(\ln\frac{2l_{\text{w}}}{b_{\text{w}}} - 1 + \frac{b_{\text{w}}}{l_{\text{w}}}\right), \tag{1.5}$$

where b is the distance between two wires. As a result the total inductance of the circuit could be evaluated as (Piatek *et al.* 2012):

$$L_{\text{T}} = \frac{L_{\text{wire}} + L_{\text{M}}}{2} + L_{\text{ec}}, \tag{1.6}$$

where L_{ec} is the self-inductance of used electronic components. According to Equations (2.1–2.2) the minimal self-inductance of the MMPG wire/PCB track connections is expected to be in the range of 0.3–0.5 μH. Combined with the high power electronic components self-inductance the minimum total expected value of L_{T} is expected to be in the 2–7 μH range. The wire connections contribute as much as < 10% of the total expected circuit inductance, however minimizing this value is still advantageous. According to Equation (2.1) implementation of shorter wire routing and higher cross-sectional area wires is preferable.

Another non-desired parameter influencing the output pulse shape is the parasitic capacitance that is also present in the circuit. This parameter mainly impacts the rise time of the pulse during turn on of the high voltage IGBT. During turn-on there is a risk of high inrush current forming due to the charging of the stray capacitance, however it can be diminished by a ballast resistor in series with the load. In order to estimate the effect of the stray capacitance on the output pulse of the generator without compensation circuit the C_{LOAD} parameter influence has been investigated in the proposed MMPG model. The results are presented in Figure 2.3.

During the simulation the self-inductance of the circuit has been selected to be the lowest expected value of 2 μH. The load of the system is the maximum of 40 Ω.

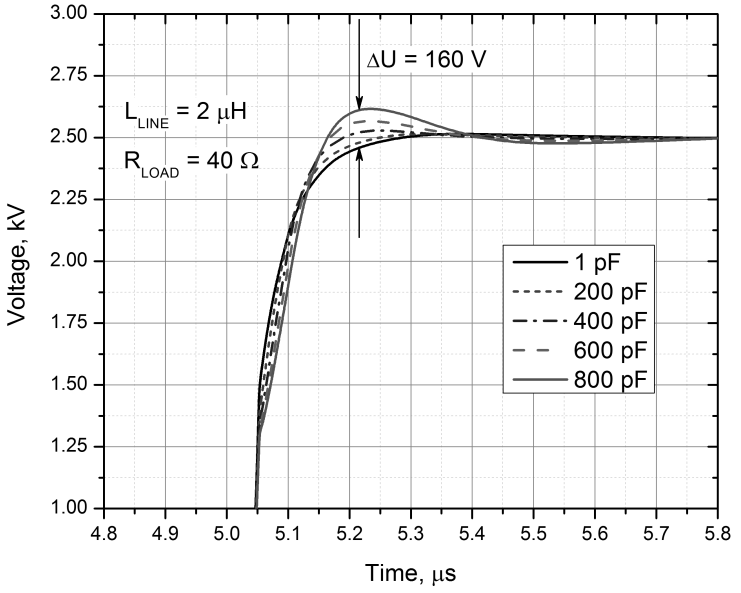

Fig. 2.3. The dependence of the generated pulse rise time on the stray capacitance C_{LOAD}

A voltage spike below 10% of the total pulse amplitude could be acquired when the 800 pF stray capacitance is present in the circuit. However, if the total stray inductance of the circuit will be higher than 2 μH or a series to the load ballast resistor is implemented, the effect of stray capacitance according to the proposed MMPG model is not significant and could be neglected.

The IGBTs have a significantly lower on state voltage compared to the MOSFETs. Also the high current and power handling capability and the high breakdown voltage limit makes IGBT a better fit for the MMPG compared to the MOSFET. However, one of disadvantages of the IGBT that will influence the output pulse of the generator is the tail current during turn off, until the charge carriers are swept out and recombined in the semiconductor structure of the switch. The influence of the tail current could be minimized by increase of the gate current, however the risk of the IGBT latchup increases. If the driving signal power is outside of the datasheet rating the IGBT can fail and no longer be controlled by the transistors gate. According to the specifications of the IXEL40N400, the optimal R_{GS} for the IGBT is in the range of 30 Ω.

The current tail of the IGBT has been evaluated using the MMPG model at maximum load and in the 0–4 kV voltage range. The results of the simulation are presented in Figure 2.4.

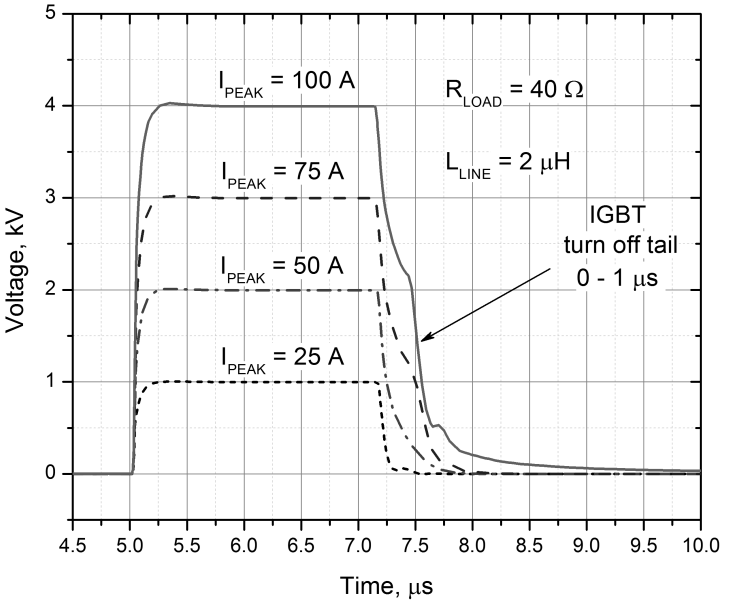

Fig. 2.4. The evaluated tail current of the insulated gate bipolar transistor

As it can be seen in Figure 2.4 up to 0.5–1 μs increase of the fall time could be observed due to the tail current of the IGBT. Decrease if the gate resistance below the recommended value may involve safety issues due to the possible IGBT failure, therefore the minimum value of 30 Ω has been selected.

In order to ensure the safe operation of the MMPG the IGBT overvoltage protection requirements must be investigated. It has been pointed out that the stray inductance present in the circuit influences the pulse waveform on the load. The oscillations occur due to the reverse biased voltage generated in the circuit by the parasitic inductive loop. Especially, the voltage spikes are experienced on the IGBT switch during transient state of turn-off. In order to prevent overvoltage issues on the IGBT the switch, the transient processes dependence on the stray inductance of the circuit was investigated. The developed MMPG model was used to simulate the potential difference on the IGBT during turn off with the maximum load of 40 Ω. The results of the simulation are presented in Figure 2.5.

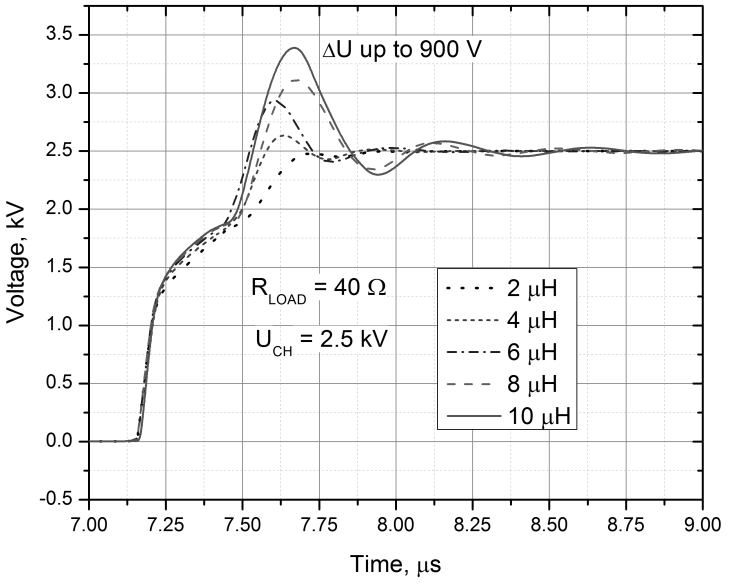

Fig. 2.5. Transient processes in the insulated gate bipolar transistor switch during turn-off

As it can be seen in Figure 2.5 the overvoltage protection circuit will be required in the prototype of the MMPG. The reverse biased voltage can reach up to 36% of the total pulse amplitude if the stray inductance is in the 10 μH range. In the proposed application of the IXEL40N400 no reserve in voltage is made, which implies that the generated voltage during transient processes is outside the applicable ratings of the switch if a 4 kV pulse is formed. Also reverse-biased voltage will discharge the capacitor bank C_B more rapidly, which is not desirable for repetitive pulsing procedures. Since the load of the MMPG is a cuvette with electrolyte, there is a risk of voltage breakdown between the electrodes, which implies that a *dV/dt* and *dI/dt* protection due to the rapid load resistance change must be implemented.

In order to compensate the transient processes, improve the generated pulse shape and the overall safety of the system an overvoltage protection circuit was developed. In this work a double crowbar diode, RCD snubber topology is proposed. The model of the MMPG has been improved with the overvoltage protection circuit and the resultant structure is presented in Figure 2.6.

The double snubber diode D_{S1} and D_{S2} topology prevents reverse biased current flow to discharge the capacitor bank C_B. Also the D_{S2} prevents the

reverse biased voltage occurrence on the IGBT, however transient processes faster than the recovery time of the diode are still possible.

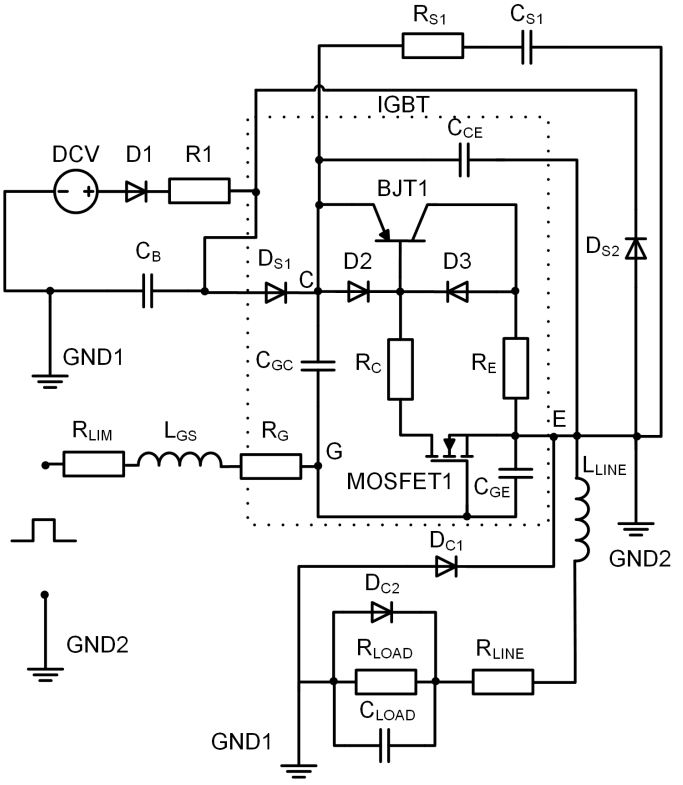

Fig. 2.6. Improved model of the micro-milisecond pulse generator with the overvoltage protection circuit

In order to address this issue an RC snubber and the double crowbar diode circuit have been implemented. The crowbar diodes circuit is used to make the path for the reverse biased current induced due to the stray inductance of the system. Combined with the RC snubber circuit the *dV/dt* and *dI/dt* are limited. The R_{S1} has been selected to be 1 Ω to limit the current and ensure low inductance. In order to determine the optimal value of the C_{S1} the dependence of the pulse shape on the C_{S1} value has been simulated. The results of the simulation are presented in Figure 2.7.

As it can be seen in Figure 2.7 the reverse biased voltage during transient processes due to the parasitic parameters of the circuit has been completely compensated even when the high inductance value of 10 μH is used.

Both the switching dynamics of the IGBT and the shape of the output pulse have no oscillations or voltage spikes.

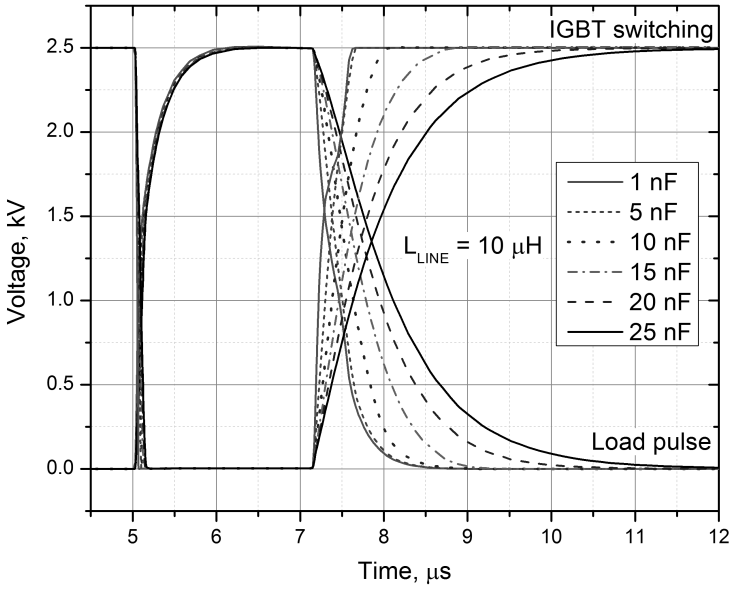

Fig. 2.7. Switching dynamics and the output pulse shape dependence on C_{S1}

However, there is still a risk of a spark occurring in the cuvette during electroporation, which implies that the value of C_{S1} equal to 5–10 nF is preferable, ensuring a considerable reserve of *dV/dt* limitation. As a trade-off a 100–200 ns increase of the fall time will be experienced.

The pulse forming unit of the MMPG has been developed, however certain trade-offs on the rise and fall times have been made, which negatively affected the minimum generated square wave pulse duration. It has been decided that the transition times due to the turn-on and turn-off of the IGBT should not exceed 50% of the total pulse duration (time gap between 50% of the peak amplitude). The simulated output pulses of different duration are presented in Figure 2.8.

From Figure 2.8 it can be seen that the typical rise time (10–90% of the pulse amplitude) is in the range of 0.5 μs, while the fall time (90–10% of the pulse amplitude) is in the range of 1 μs – 1.5 μs. During the maximum pulse amplitude of 4 kV the turn-off dynamics of the IGBT are slightly altered due to the RC snubber and crowbar circuits present in the MMPG. However, the reverse biased voltage is fully compensated, which was the major goal of the transient process compensation circuit development.

Taking into account the transition time of 1.5–2 μs the minimum acceptable pulse duration has been limited to 3–4 μs according to the simulation results with minimum inductance of 2 μH.

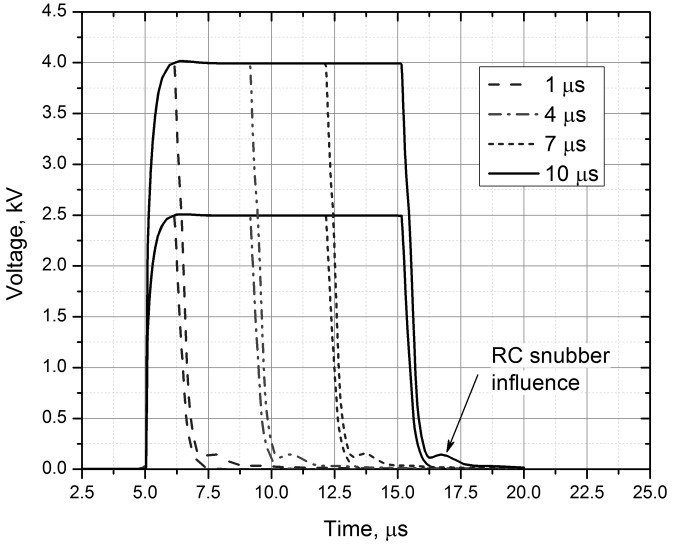

Fig. 2.8. Output pulses of the micro-millisecond pulse generator according to the developed simulation model

In order to ensure generation of the longer micro-millesecond pulses a proper value capacitor array C_B must be chosen. The discharge of the capacitor bank during single pulse must not exceed 25%. In order to meet the requirements summarized in Table 1.4 evaluation of the simulation model results with varied capacitor bank value has been performed. The results are presented in Figure 2.9.

In Figure 2.9a the amplitude decrease during the maximum 100 μs pulse due to the discharge of the capacitor bank is shown. According to the simulation results the 10 μF capacitor is discharged from 4 kV to 3.1 kV at maximum load, which is equal to a 23% decrease. It implies that the 10 μF capacitor bank is sufficient for the 5 μs – 100 μs region. In the Figure 2.9b similar analysis for the 5–300 μs, 0–3 kV region has been performed. Based on the simulation results a capacitor bank in the 30–50 μF region was determined to be acceptable. The 0–2 kV, 0 μs – 3 ms diapason is presented in Figure 2.9c. The capacitor bank in the 300–500 μF range is suitable to ensure sufficient amount of energy. The longest 0–10 ms, 0–1 kV diapason has been investigated and the results are presented in Figure 2.9d.

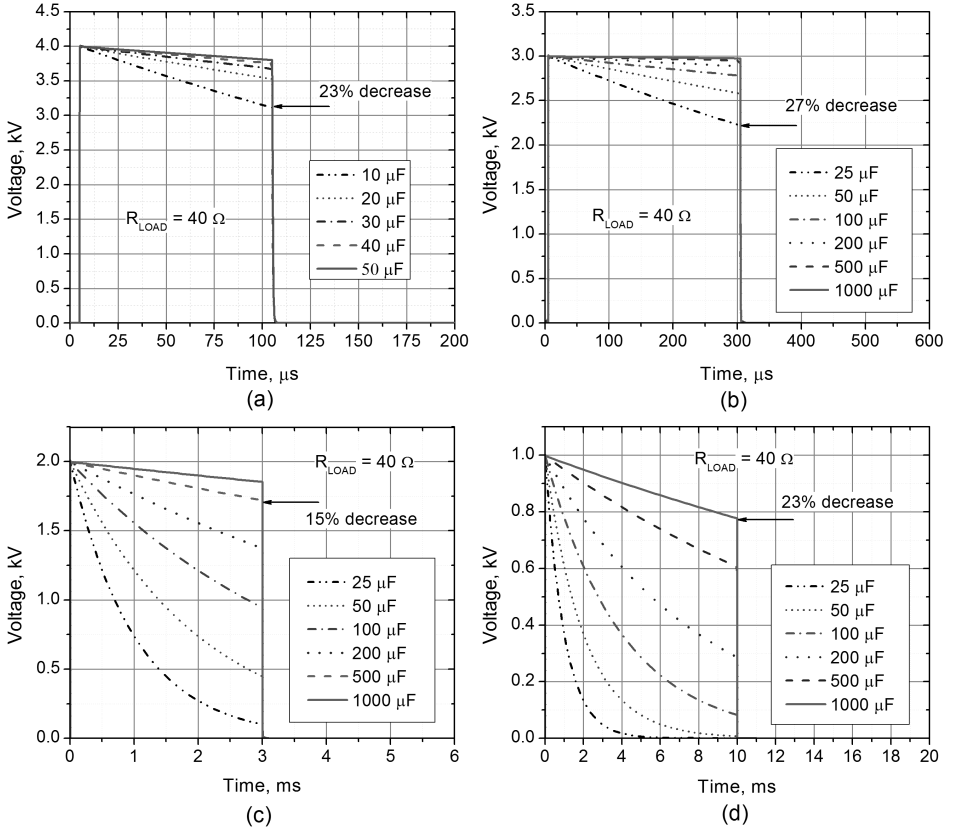

Fig. 2.9. Applicability of different capacitor values for the micro-millisecond pulse generator

The capacitor bank in the range of 1 mF ensures voltage amplitude fluctuations during the pulse below 25%. Based on the results it could be noted that in order to cover all of the electroporation ranges the capacitor bank of 4 kV, 1 mF is required (accumulated energy of 8 kJ). However, accumulation of high amount of energy involves safety issues. Also the size and weight of such capacitor bank exceeds expectations for a compact electroporation device.

As a result a variable capacitor bank circuit topology has been developed, which allowed covering all of the required electroporation ranges with minimum stored energy. The developed variable capacitor bank circuit is shown in Figure 2.10.

Switching of the capacitors in parallel or/and in series allows coverage of all of the ranges of pulse widths and operating voltages corresponding to the mentioned conditions.

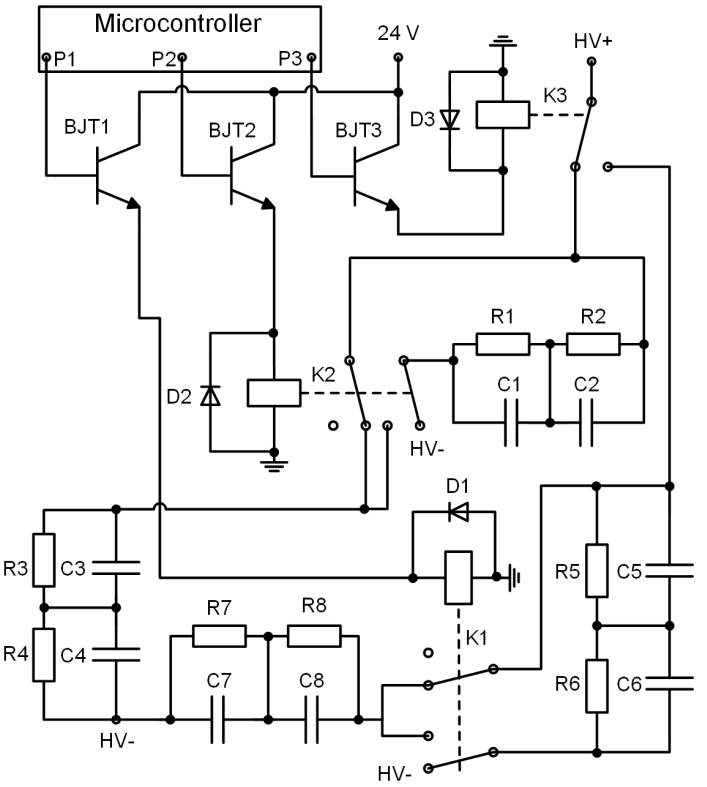

Fig. 2.10. Variable capacitance bank circuit

The switching of the capacitors is implemented by using of 3 high voltage relays. Each relay is controlled by the low power transistor (BJT1–BJT3), which is driven by a respective microcontroller port pin, resulting in a 3-transistor/relay structure. Opening one or several transistors at the same time allows covering all of the capacitor commutation variations required for the setup. Four possible connections were realized: 1) four capacitors (C_1–C_4) are connected in series; 2) two by two capacitors (C_1, C_2 and C_3, C_4) connected in series and then interconnected in parallel; 3) four capacitors (C_5–C_8) are connected in series; 4) two by two capacitors are connected in series (C_5, C_6 and C_7, C_8) and then interconnected in parallel. Optimally, the two types of capacitors with different

operating voltages and different capacity (four high voltage capacitors C_{HV} 50 μF x 1500 V and four low voltage C_{LV} 1000 μF x 500 V) are suitable. The C_{HV} capacitors were connected to the C_1 – C_4 and the C_{LV} capacitor to the C_5–C_8, respectively. As a result the proposed circuit allowed to change the total capacity and the operating voltage of the capacitive storage unit as follows: 1) 12.5 μF x 6000 V, 2) 50 μF x 3000 V, 3) 500 μF x 2000 V and 4) 1000 μF x 1000 V, respectively.

2.1.2. The Prototype of Square Wave Micro-Millisecond Pulse Electroporator

Based on the simulation model results the prototype of the MMPG has been developed.

The resultant simplified block diagram of the electroporator is shown in Figure 2.11 (Stankevič, Novickij *et al.* 2013).

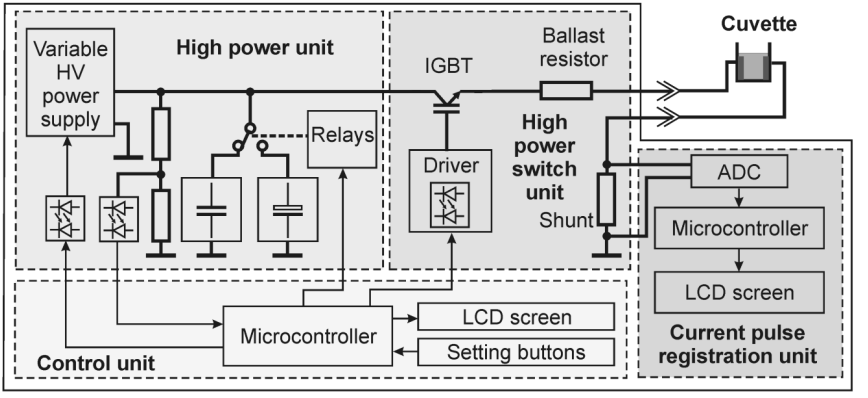

Fig. 2.11. Simplified block diagram of the developed micro-millisecond pulse generator (Stankevič, Novickij *et al.* 2013)

It includes a high power unit, a control unit, a high power switch, a pulse registration unit and a load (electroporation cuvette). The variable high voltage power supply ISEG EPX40406, the capacitors (four C_{HV} and four C_{LV}) and the high voltage relays form the high power unit. The output voltage and the current of the variable power supply can be controlled by analog signal 0–5 V, corresponding to 0–4 kV output. The high power switch unit consists of the insulated-gate bipolar transistor (IGBT) IXEL40N400, snubber diode, driver circuit, ballast resistor and the precision shunt (0.1 Ω) connected in series with the cuvette.

The photograph of the resulting prototype is shown in Figure 2.12.

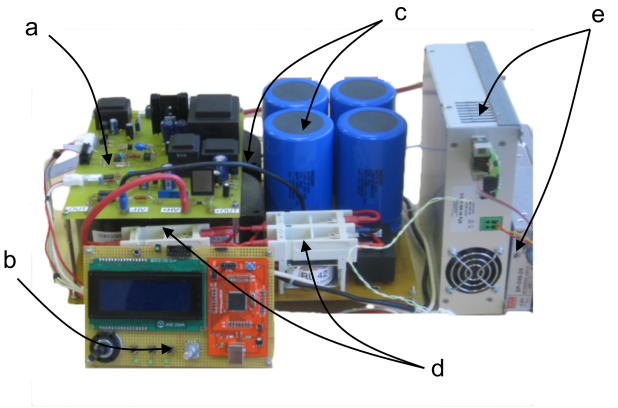

Fig. 2.12. Photograph of the developed micro-millisecond pulse generator prototype, where a – pulse forming circuit; b – control circuit; c – capacitor array; d – relays; e – power supply

The prototype features a compact design both for mobility and for reduction of the total parasitic inductance of the pulse forming circuit.

For pulse control, registration and visualization, two XMEGA 128A3U microcontrollers have been used. The first microcontroller produces square-wave pulses ranging from 5 μs to 10 ms, controls the voltage of power supply, measures voltage across the capacitors and controls the configuration of the capacitors connections. The second microcontroller controls the analog-digital converter, which allows measurement of the voltage drop across the precision shunt. The measured signal is displayed on the graphic display. For a more precise measurement of signals, a BNC connector is provided allowing connection of an external oscilloscope. The square-wave electrical pulses are generated by switching on-off of the IXEL40N400 IGBT transistor. The power consumption of the proposed generator for cell electroporation is 240 W. The rise time and fall time of generated pulse depend on the shape of the driver pulse, the load type and the initial parameters of the transistor. For this purpose a high-speed optically decoupled driver HCPL3180 (Fairchild Semiconductors) has been chosen. In order to acquire a steep fall time of the generated high voltage output pulse the negative voltage bias driving circuit has been implemented.

The algorithm of the control of the MMPG is shown in Figure 2.13. The operation of the system can be divided into three regimes: 1) Data input mode; 2) Pulse generation; 3) Pulse visualization. During the first regime the

microcontroller monitors the input and updates the parameters on the LCD screen.

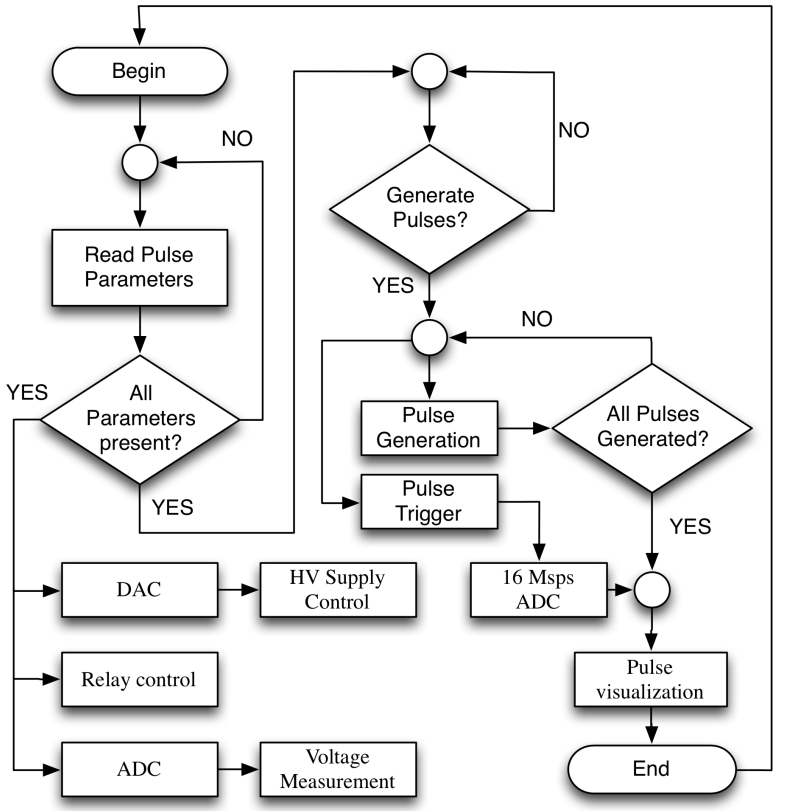

Fig. 2.13. Control algorithm of the micro-millisecond pulse generator

There are four main parameters that are altered: charging voltage, pulse width, the number of pulses and the manual relay commutation mode. By default the relay commutation is based on the continuous check of the two input parameters: voltage and pulse width, between which the voltage has a higher priority. Therefore, based on the voltage setting entered by the user, the microcontroller identifies the applicable operation modes, following by the pulse width check that is used to select the optimal operation range ensuring that the decrease of the pulse amplitude is no more than 25% for selected pulses. In order to implement all of the requirements the cycled algorithm based on interrupt events with different timings has been developed. The first interrupt

event is responsible for the synchronization between microcontrollers and the square pulse generation based on the input parameters supplied by the user. When the user via button sends and interrupting event to generate a pulse or pulse sequence two different timers are started. One is responsible for pulse width determination and is adjustable and the other for the delay between the pulses, which is fixed and equal to 0.1 s (10 Hz). The timers responsible for pulse width and delay are started as follow-up tasks.

When the first timer reaches an overflow (depends on the selected pulse width) the second interrupt is generated, which sets both pins to low state (end of pulse) and the parameter corresponding to the number of pulses is reduced by one. The system waits for the second timer to overflow (delay of 0.1 s). When it reaches an overflow the timer is stopped and the third interrupt is generated. During the interrupt the parameter responsible for the number of pulses is checked and compared to zero. If the true value is returned the algorithm is stopped and waits for the next pulse generation trigger from the user. Otherwise, the trigger is sent automatically resulting in a cycled algorithm. One of the biggest advantages of such implementation is ability for task prioritization and multitasking. Therefore, during pulsing all other system functions are maintained like DAC control, relay control, LCD control and high voltage supply control. The microcontroller processor does not have unnecessary idle times due to task prioritization. The pulse width corresponds to the pulse settings selected by the user allowing precise control of the transistor opening time and, therefore, accurate pulse forming across the load. The resulting pulse generator can output either single short pulses or series of pulses with predefined frequency of 10 Hz.

As it has been mentioned above pulse waveform acquisition and visualization is performed by the second XMEGA128A3U microcontroller. For pulse acquisition an external 16 MSps ADC is used, which reads voltage from the 0.1 Ohm shunt resistor. The shunt resistor is connected in series with the load cuvette. The ADC is triggered by the synchronization pulse from the first microcontroller. The data is accumulated in the XMEGA128A3U memory.

The proposed control algorithm and the driving circuit based on the XMEGA128A3U microcontroller can be successfully applied for pulse generators featuring single switch or array of switches.

Also in the proposed system the ADC readings have been calibrated in the program code by introducing proportionality coefficients. Conversion to the corresponding current value is performed according to the Ohm's law. When the pulse acquisition is complete the ADC is stopped and the data is displayed on the graphical 128 x 64 display. The scaling and the step size on the X and Y axis are selected manually by the user with respective adjusting knobs.

The photograph of the developed electroporator are presented in Figure 2.14.

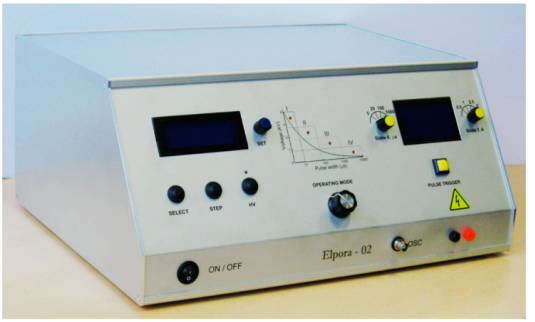

Fig. 2.14. The photograph of the developed electroporator (Stankevič, Novickij *et al.* 2013)

The designed device is build into the 45x37x20 cm^3 aluminium case (Richard Wöhr GmbH). The control of the system is performed via 4 buttons and 4 knobs. Manual relay commutation mode selection has been implemented in the device. Each electroporation system operation mode is highlighted by the red photodiode on the voltage vs. pulse width graph when selected. Manual high voltage on/off switch has been also implemented in the design.

2.1.3. The Output Pulse Adequacy to the Micro-Millisecond Pulse Generator Model

In order to estimate the adequacy of the MMPG model to simulate the experimental output pulse parameters the simulation data has been compared to the measurement results in the 5–35 μs pulse range, when the duration of the rise and fall time is considerable compared to the total pulse width (Novickij *et al.* 2014a)[*].

The typical simulated and measured output pulses are presented in Figure 2.15. The highest variance between the experimental and simulation results is during the switch state transient. The pulse has been divided into three regions: turn on transient (10–90% pulse amplitude), turn off transient (90–10% pulse amplitude) and the pulse plateau (90–100% pulse amplitude). Due to high inductance value of 6.5 μH of the experimental setup and thus increased transient time, the minimum pulse width has been limited to 5 μs.

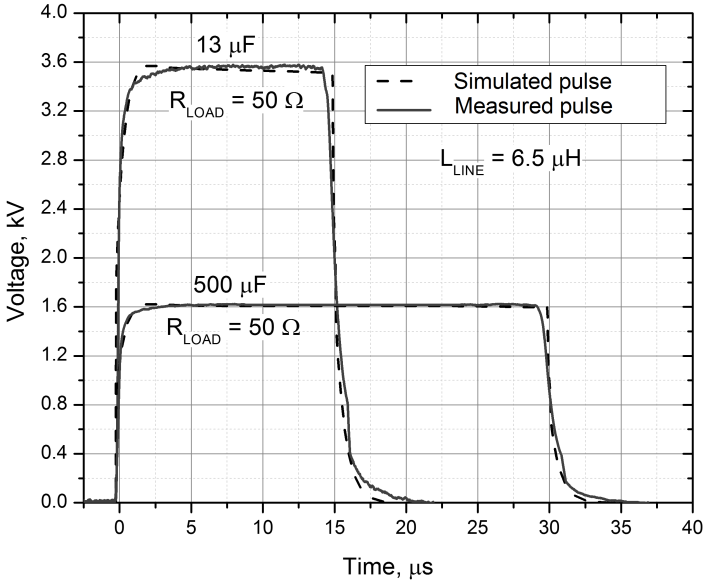

Fig. 2.15. The typical simulated and measured micro-millisecond pulse generator output pulses

For model adequacy evaluation the 5 μs, 15 μs, 25 μs and 35 μs pulses have been selected. The simulation uncertainties for the turn on and the turn off transients were evaluated on the time scale, while in the plateau case the difference in amplitude was investigated.

Taking into account the 1.5% DC accuracy variations of the oscilloscope and the 1% resistance value uncertainty, the simulation model uncertainty in the plateau region was <±3%. On the time scale due to the high accuracy of the oscilloscope (±0.4 ns), the influence of the measurement equipment has been neglected. The time scale uncertainties of ±1.2% for the turn on and the ±5% for the turn off transients have been ensured. The percentile values have been evaluated in respect to the shortest MMPG generated pulse of 5 μs.

The proposed simulation model was successfully used for estimation of the pulse power generator's parameters and compensation of the influence of the parasitic elements (Novickij *et al.* 2014a).

2.2. Nano-Microsecond Range Electroporator for Biological Cell Permeabilization

In this section the development and research of the nano-microsecond pulse electroporation system is performed. The developed PSPICE simulation model is applied for the compensation of the transient processes and selection of optimal circuit components. The prototype of the nano-microsecond pulse range electroporation system that will be applicable for permeabilization of inner cell organelles is overviewed and investigated.

2.2.1. The Model of the Nano-Microsecond Pulse Generator

The nano-microsecond pulse generator (NMPG) model has been developed on the basis of the MMPG model presented in previous chapter. The simulation circuit of the NMPG is presented in Figure 2.16.

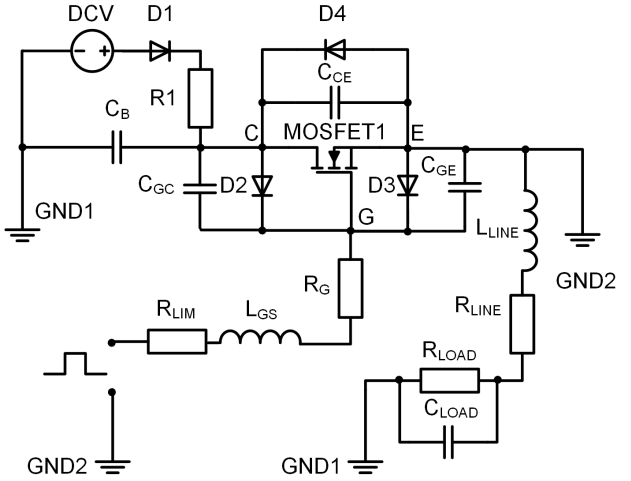

Fig. 2.16. Simulation circuit of the nano-microsecond pulse generator (Novickij *et al.* 2014b)

As it can be seen in Figure 2.16 the model consists of a power source, switch and the load. The power source and the load have been approximated in a similar manner as in the MMPG model (Figure 2.1). The MOSFET model consists of the switch and an array of diodes (D2–D4) and the corresponding capacitances (C_{GC}, C_{GE}, C_{CE}). The diode array introduces the capability to simulate the breakdown parameters of the MOSFET. The MOSFET has been

used as a switch to ensure fastest rise and fall times. Since the maximum duration of the system is <10 μs, the advantages of the IGBTs are not significant, making this switching technology inferior to the MOSFET in the nanosecond range.

The required output parameters of the circuit are summarized in Table 2.4.

Table 2.4. Summary of output parameters for the nano-microsecond pulse generator

Voltage range	Pulse duration range	Load	Voltage drop during pulse
0–8 kV	300–500 ns	0.1–2 kΩ	<5%
0–6 kV	500 ns – 1 μs		
0–4 kV	1–5 μs		

Taking into account the required parameters the only way to introduce the high voltage support is to use multiple MOSFET switches connected in series. However, such implementation is highly disadvantageous. Multiple switches will involve additional parasitic parameters to the circuits. Also synchronized driving will be highly challenging due to the nanosecond duration of the pulses.

Recent developments in the area of semiconductor doping, photoresist development and nanostructured oxide deposition have led to the production of the new generation of metal oxide semiconductor field effect transistors, which can reach a high level of synchronization. As a result the combined MOSFET array topologies allow generation of nanosecond electrical pulses, while featuring low inner resistance and parasitic capacitance. Such implementations positively influence the complexity of the circuits, while introducing the capability to switch voltages in the range of several kV. In this work the HTS 91-12 MOSFET switch by Behlke Power Electronics (Germany) is applied. The switch is capable of commutating voltages up to 9 kV and has a pulsed current support up to 120 A. Nevertheless, generation of nanosecond pulses with flexible pulse parameters is complicated by the pulse distortion, ringing effects, overvoltage and overcurrent transient processes due to the parasitic reactive and non-matched loads. Special efforts should be made to reduce the stray inductance of the circuit and maintain sufficient insulation for the high voltage contacts.

The NMPG model according to the datasheet has been adjusted to match the switching characteristics of the HTS 91-12 MOSFET. The maximum load of the system has been selected to be 100 Ω. The load has been limited due to the limited power and current handling capability of the switch. In order to evaluate the influence of the stray inductance the L_{LINE} has been varied in the 1–6 μH. The range of inductance variance has been reduced compared to the MMPG

(Table 1.4) based on the lower expectation of the stray inductance and final system size of the prototype because of the simplified design of the circuit.

The simulation results of the influence of the L_{LINE} on the output pulse waveform are presented in Figure 2.17.

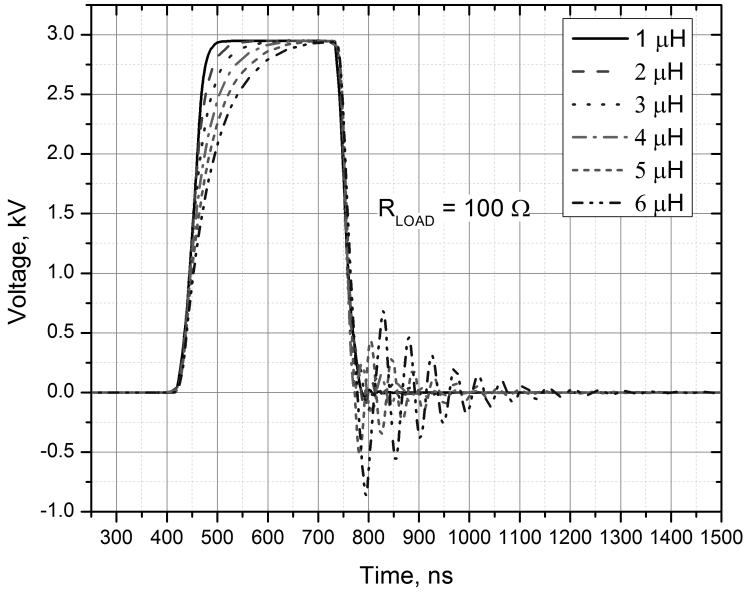

Fig. 2.17. Influence of L_{LINE} on the output pulse of the nano-microsecond pulse generator (Novickij *et al.* 2014b)

As it can be seen in Figure 2.17 a 300 ns 3 kV pulse has been simulated. The stray inductance has a dramatic influence on the shape of the pulse. Due to high *dV/dt* the oscillations during transient process have high amplitude up to 28% of the pulse. The transient time is similar to the pulse duration, which is unacceptable for electroporation experiments. Also if for the microsecond pulses the rise time decrease was not so critical with increase of the stray inductance, for the nanosecond range the stray inductance <4 μH must be ensured in the prototype, which will allow to acquire a rise time <100 ns. The stray capacitance influence has been also investigated. The results featuring the influence of the C_{LOAD} on the final waveform of the NMPG are presented in Figure 2.18.

As it can be seen in Figure 2.18 the influence of the C_{LOAD} on the form of the pulse is also increased compared to the micro-millisecond pulse generator. During simulation the C_{LOAD} has been varied in the 50–200 pF region. Similar to the MMPG the expected valued was in the 50–100 pF range. From the results it

can be seen that both the rise and fall times area increased with the increase of the load capacitance. A considerable voltage spike up to 20% of the total pulse amplitude could be experienced during transient turn on of the MOSFET.

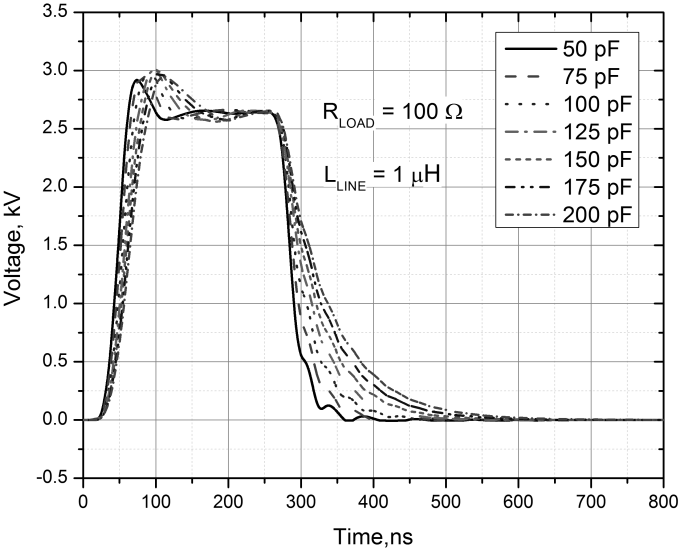

Fig. 2.18. Influence of C_{LOAD} on the output pulse of the nano-microsecond pulse generator (Novickij *et al.* 2014b)

The voltage spike during turn on occurs due to the parasitic RLC circuit and the inrush current. Combined with the increased pulse width, the C_{LOAD} will negatively affect the quality of electroporation experiments, therefore should be minimized as much as possible.

Same as the IGBTs the MOSFETs are sensitive to the overvoltage and high *dV/dt* during turn on/off transient. In order to estimate the required transient process compensation procedures, the transient processes on the MOSFET during the nanosecond range pulse have been simulated. The results are presented in Figure 2.19.

Naturally, the stray inductance negatively affects the load pulse shape and is responsible for high voltage oscillations due to the generated reverse-biased currents. In the nanosecond pulse duration range the influence is increased even more. The voltage spikes amplitude is proportional to the *dV/dt* of the pulse.

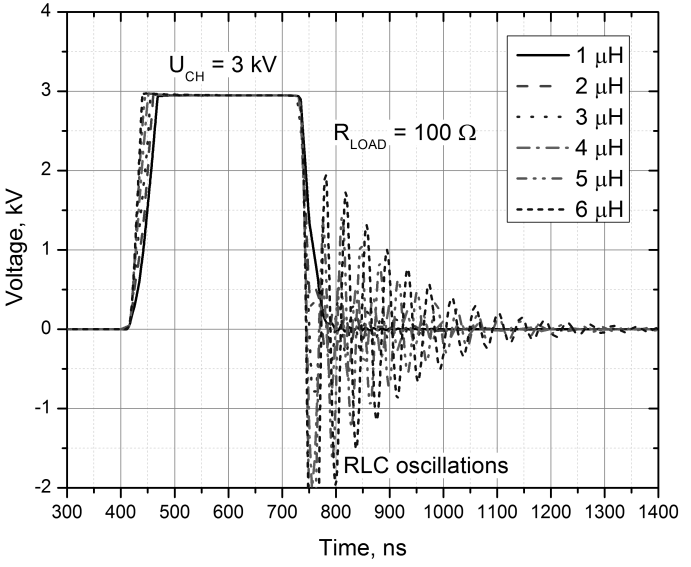

Fig. 2.19. Transient processes on the metal-oxide-semiconductor field-effect transistor dependence on the L_{LINE}

Combined with parasitic capacitance C_{LOAD} and the high current due to high voltages and high resistive loads, the induced oscillations on the MOSFET because of the RLC contour are almost of the same amplitude as the generated pulse. Without compensation a huge reserve on the breakdown voltage of the switch will have to be made. Since the duration of the transient processes are comparable to the generated square wave pulse, the power losses will be increased dramatically, which will limit the high frequency pulse generation capabilities.

Also same as in the MMPG case the reverse-biased voltage will discharge the capacitor bank C_B more rapidly, which is not desirable for repetitive pulsing procedures. Therefore, in order to compensate the transient processes, improve the generated pulse shape and the overall safety of the system an overvoltage protection circuit was developed (Novickij *et al.* 2014b).

The earlier proposed circuit consisting of the double crowbar diode and the RCD snubber topology was applied. As a result the model of the NMPG has been improved with the overvoltage protection circuit and the resultant structure is presented in Figure 2.20.

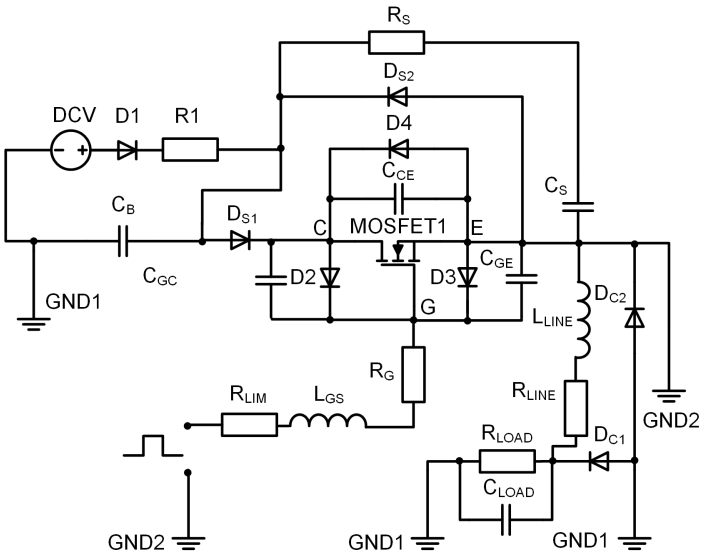

Fig. 2.20. Improved nano-microsecond pulse generator model with transient process compensation circuit (Novickij *et al.* 2014b)

Same as in the MMPG case the crowbar diodes circuit is used to make the path for the reverse biased current induced due to the stray inductance of the system. Combined with the RC snubber circuit the *dV/dt* and *dI/dt* are limited. The R_S has been selected to be 1 Ω to limit the current and ensure low inductance. In order to determine the optimal value of C_S the dependence of the pulse shape on the C_S value has been simulated and is presented in Figure 2.21.

According to the simulation results and as it can be seen in Figure 2.21 the double diode crowbar circuit is very efficient for compensation of the induced reverse-biased current. Even with maximum expected inductance value of 6 μH there are no any significant voltage spikes during turn off transient. Combined with RCD snubber circuit both the switch and the load are protected from overvoltage and overcurrent.

Compensation of the voltage spike during turn on due to the capacitive load was not performed. In order to address this issue the clipping techniques must be used or either shunting of the load with low resistance should be performed. In both cases it is disadvantageous. The output signal clipping circuit will be too complex to clip >8 kV pulse, while load shunting will limit the reserve in pulsed current, which will introduce safety issues and risks of the MOSFET failure.

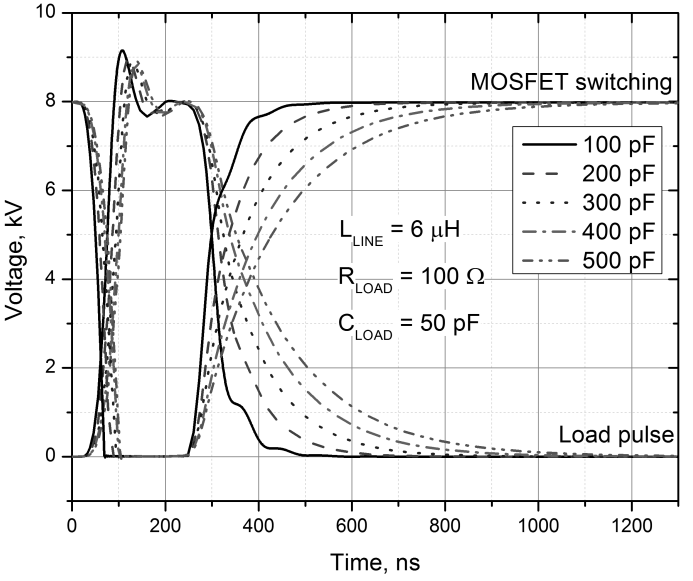

Fig. 2.21. Switching dynamics of the metal-oxide-semiconductor field-effect transistor and output pulse dependence on C_S (Novickij *et al.* 2014b)

The pulse shape that could be acquired using the proposed circuit is presented in Figure 2.22. Electroporation wise the power of the spike during turn on transient is not significant compared to the total power of the minimum pulse duration. Therefore, for the specific application of nanosecond electroporation, the stray capacitance compensation could be minimized to fit the parameters of the switch with a 1–1.5 kV reserve of the breakdown voltage.

As it can be seen from Figure 2.21 and Figure 2.22 after compensation the pulse shape almost does not depend on the stray inductance of the circuit. The turn on transient is proportional to the charging voltage and does not exceed 10%. Due to the limited duration of the spike (40–50 ns) the influence of the voltage spike on the electroporation experiment could be neglected.

Same as in the MMPG case a proper C_B capacitor bank value must be selected for the nanosecond electroporation system. However, since the maximum pulse duration is only 5 μs, the energy of single pulse is comparably low.

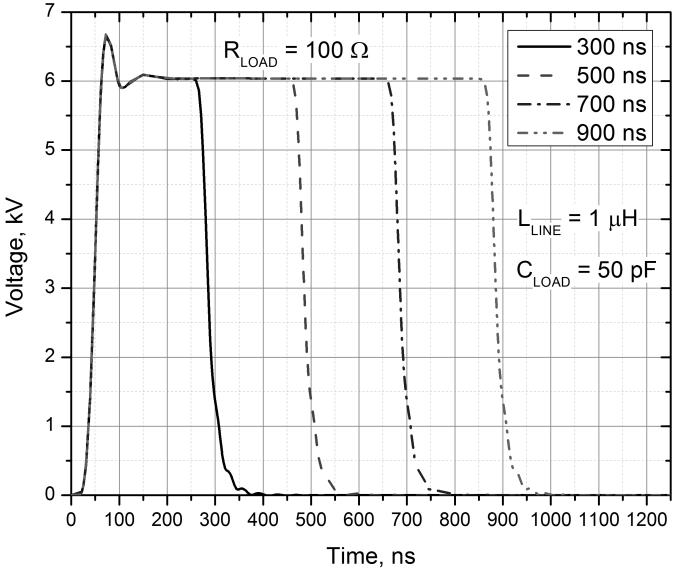

Fig. 2.22. Expected output pulse of the nano-microsecond pulse generator with minimum stray inductance of 1 μH

A capacitor bank in the 1–5 μF range is sufficient to ensure <5% voltage drop during single 5 μs pulse with maximum load.

2.2.2. The Prototype of Nano-Microsecond Pulse Generator

Based on the PSPICE model the prototype of the NMPG has been developed. The block diagram of the prototype is shown in Figure 2.23.

The capacitor bank consists of eight 70 μF, 1200 V polypropylene low inductance capacitors connected in series (total capacitance of 8.75 μF, 9.6 kV) (Novickij *et al.* 2014b).

The cuvette is connected using a high voltage coaxial cable. An external oscilloscope is used for output signal measurement and storage. The 8 kV, 7 mA adjustable power source ISEG EPP80705245 is used to charge the capacitor bank.

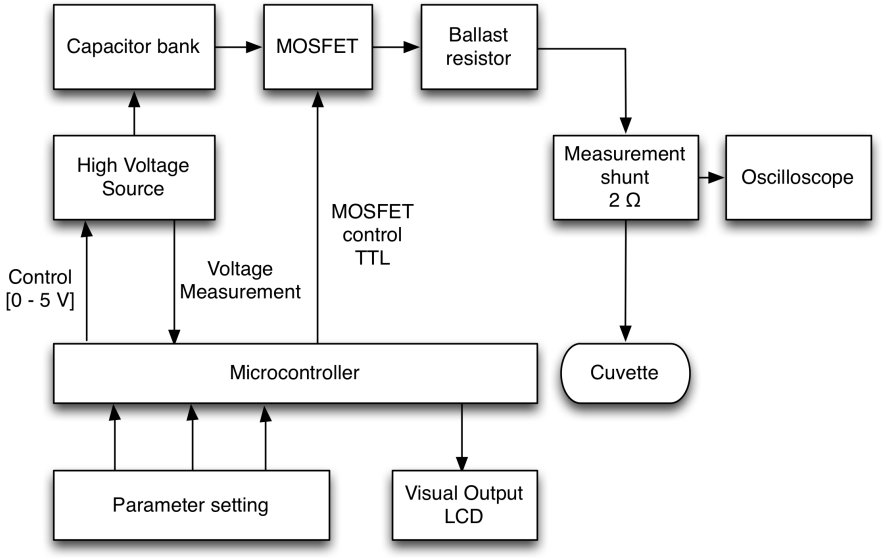

Fig. 2.23. Simplified block diagram of the nano-microsecond pulse generator prototype (Novickij *et al.* 2014b)

The photograph of the pulse forming circuit is shown in Figure 2.24. The control algorithm is simplified compared to the MMPG (Figure 2.13). The pulse generation does not involve multiple timers and interrupt implementation.

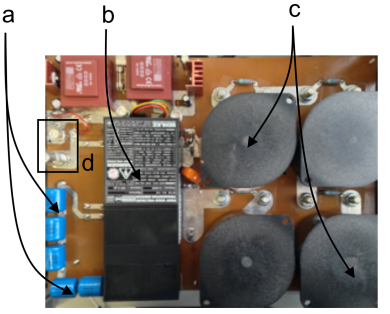

Fig. 2.24. Photograph of the pulse forming circuit, where a – ballast resistors; b – pulse forming switch; c – capacitor array; d – load connector

The microcontroller stores an array of delay functions, which correspond to the discrete values of pulse duration with a step of 33 ns for the nanosecond range. In the microsecond range pulsing with a step of 1 μs is implemented using the MMPG control algorithm.

The photograph of the NMPG is presented in Figure 2.25. The device features a compact size of 43 x 35 x 25 cm^3.

Fig. 2.25. Photograph of the nano-microsecond pulse generator prototype (Novickij *et al.* 2014b)

The control of the NMPG has been also simplified compared to the MMPG. Three buttons are used for parameter input. For safety a high voltage turn-off switch and a LED as an indicator have been implemented.

2.2.3. The Output Pulse Adequacy to the Nano-Microsecond Pulse Generator Model

In order to estimate the adequacy of the NMPG model to simulate the experimental output pulse parameters the simulation data has been compared to the measurement results in the nanosecond pulse range. The shortest electrical pulse generated by the prototype and the corresponding simulation model results are presented in Figure 2.26. The load of the system is a 50 μl cuvette with a cell buffer (total impedance of 315 Ω). The model parameters have been adjusted to maximally match the output pulse of the NMPG.

As it can be seen in Figure 2.26 the L_{LINE} has been selected to be 3 μH and the C_{LOAD} equal to 75 pF. In order to estimate the accuracy of the model the pulse same as in the MMPG case has been divided into three regions: turn on transient, pulse plateau and turn-off transient.

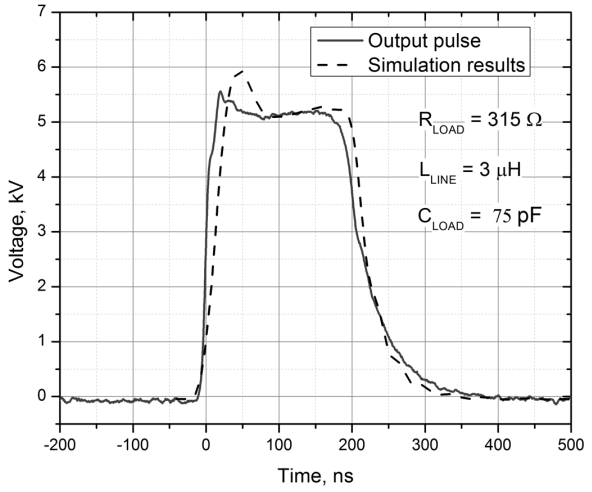

Fig. 2.26. Simulated and measured pulse of the nano-microsecond pulse generator (Novickij *et al.* 2014b)

The simulation uncertainties for the turn on and the turn off transients were evaluated on the time scale, while in the plateau case the difference in amplitude was investigated. As a result in the simulation model uncertainty in the plateau region was <±8.5%. The time scale uncertainties of ±5.4% for the turn on transient and the ±9.6% for the turn off transient have been ensured. The percentile values have been evaluated in respect to the shortest NMPG generated pulse of 200 ns. It was concluded that the results of the proposed NMPG simulation model are in acceptable compliance with the experimental data, ensuring value uncertainty of ±10%.

2.3. Development of Planar Microelectrodes for Electroporation

The electroporation cuvette is the load of the electric pulse generator. Depending on the cuvette structure the intensity of the electric field and the homogeneity of the distribution are influenced. As a result the treatment efficacy and intensity also depend on the cuvette structure. By alteration of the gap between the electrodes, the volume for the cell buffer and the effective contact area of the electrodes the impedance of the load cuvette is determined. Consequently, the load of the pulse generator is altered.

Currently many commercial and non-commercial designs of electroporation cuvettes exist. Most of the cuvettes feature a 20–200 µl effective volume for *in vitro* electroporation studies. One of the major issues using this method is the post-electroporation state observation due to the required cell handling from the cuvette to the microscope slide. Observation of the dye release dynamics is not possible during pulsing procedures. However, introduction of planar electroporation electrode structures, which can be fitted directly under the microscope provide a solution for real time electroporation process observation.

In this chapter the development of the planar microelectrodes for electroporation will be overviewed. The distribution of the generated electric field and the influence of Joule heating will be evaluated using finite element method analysis.

Electroporation technique requires high intensity electric field to alter the permeability of biological cells. As a result for traditional electroporation the implementation of electrode arrays is inevitable. Depending on the structure and superposition of the electrodes the intensity and homogeneity of the electric field will be influenced.

In order to estimate the required parameters for the microelectrode array the spherical model of the Jurkat T biological cell has been used (Lučinskis, Novickij *et al.* 2014). The cell was approximated as a conducting sphere where the membrane thickness is much smaller than the cell radius. The model allowed evaluation of the polarization effects happening during electrical pulses and estimation of the resultant transmembrane potential. The parameters of the Jurkat T cell are summarized in Table 2.5.

Table 2.5. Used Jurkat T cell parameters (Lučinskis, Novickij *et al.* 2014)

Parameter	Value	Denotation
Radius	8 µm	r_{cell}
Membrane thickness	10 nm	m
Membrane conductivity	50 µS/m	σ_{mem}
Inner cell volume conductivity	1 S/m	σ_i
Outer medium conductivity	1.2 S/m	σ_m

It has been determined that electric field strength in the range of 0–2 kV/cm is sufficient to induce transmembrane potential of 0.2–1 V. Even lower field intensity is required for larger cells, therefore it has been decided to limit the generated electric field in the 0–2 kV/cm range, which is suitable for permeabilization and transfection experiments in the micro-millisecond pulse

duration range. The summary of required electrodes parameters is presented in Table 2.6.

Table 2.6. Summary of required parameters for the electrodes

Parameter	Value	Denotation
Electric field strength	0–2 kV/cm	E
Effective volume	<3 µl	V_{ef}
Minimum electrode gap	>50 µm	g_{min}

The effective volume of the cell medium that is required for each experiment should be as low as possible, which is advantageous for cell morphological analysis. Taking into account that the target cells are not limited to Jurkat T, and the size of the cells may be in the range of tens of micrometers (*Saprolegnia*, *Achlya* species), thus the minimum allowed gap between the electrodes has been selected to be in the range of 50 µm.

Also during experiments it is convenient to have several identical experimental instances for low results uncertainty, thus the final electrode structure should involve separate identical experimental chambers or areas for the cells.

Based on these requirements the interdigitated electrode structure has been developed. The proposed structure is shown in Figure 2.27.

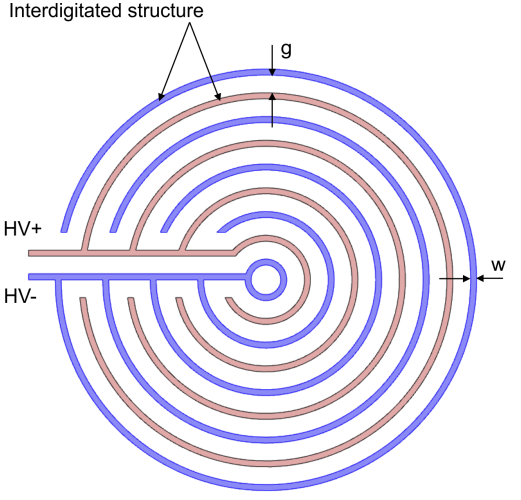

Fig. 2.27. Proposed microelectrode structure

The proposed structure features eight separate experimental instances. In order to investigate the electric field distribution and the Joule heating influence the finite element method analysis has been applied. The FEM analysis has been performed using COMSOL Multiphysics software during doctoral student internship in the University of Edinburgh (Scotland, UK).

The free triangular mesh has been applied in the simulation. The minimum and maximum finite element size of 0.5 μm and 0.37 mm were selected, respectively.

The mesh of the resultant model is shown in Figure 2.28. The thickness of the electrodes in the simulation is 7 μm.

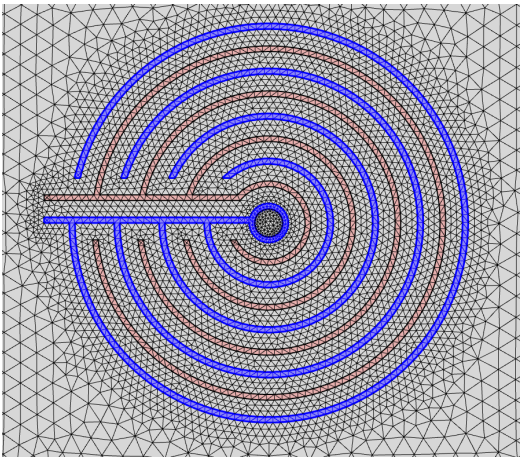

Fig. 2.28. Microelectrode mesh

The minimum size of the finite element was influenced by the geometry of the proposed microelectrodes. The maximum element growth rate of 1.2 has been selected. The investigated electrode structure has been divided into a total of 8918 finite elements.

The model includes a surrounding air container (4 mm x 10 mm), where the electrode structure is placed (copper electrodes on FR-4 substrate). The thickness of FR-4 substrate is 1 mm. The 0.1 mm (thickness) glass coverslip is applied to cover the electrodes and the cell medium.

Application of glass or PDMS slides as a substrate is also possible and does not influence the result of the simulation significantly due to the similar dielectric constants in the 3.5–6 range.

The summary of simulation parameters is presented in Table 2.6.

Table 2.6. Summary of simulation parameters (Novickij *et al.* 2015b)

Parameter	Value	Denotation
Electrode width	20–200 μm	w
Electrode gap	50–500 μm	g
Electrode thickness	200 nm – 10 μm	a
Applied voltage	100–300 V	U_{ap}
Medium permittivity	70–80	ε_m
FR-4/Glass permittivity	3.5–6	ε_G
Medium conductivity	0.1–2 S/m	σ_m
FR-4/Glass conductivity	1 x 10^{-14} S/m	σ_G
Copper conductivity	6 x 10^{7} S/m	σ_C
Copper thermal conductivity	400 $Wm^{-1}K^{-1}$	k_C
FR-4/Glass thermal conductivity	0.9 $Wm^{-1}K^{-1}$	k_G
Medium thermal conductivity	0.596 $Wm^{-1}K^{-1}$	k_M
Convective cooling coefficient	13.51	h

The resultant configuration of the electrodes and the respective voltage potential distributions that are acquired in x0y and y0z planes are shown in Figure 2.29.

In the proposed simulation the 100 V voltage potential has been applied. The resultant distribution of the electric potentials across the microelectrode structure is identical between separate electrode fingers or mirrored with a respective mirror plane in the centre of the array. Therefore, it is convenient to analyse the distribution between two fingers only. Eight separate experimental instances are formed. However, it will be crucial to ensure the whole structure encapsulation with the cell medium. Otherwise, voltage breakdown issues may arise due to the air presence between a pair of electrodes.

Also as it can be seen in Figure 2.29 in the z plane the distribution of voltage potentials is not symmetrical. It is due to the differences in the permittivity between the "sandwich" structure of FR4/cell medium/glass coverslip and air.

Taking into account that the cells dependent on the type, vary on size, the z plane electric field homogeneity should be ensured at least in the 50 μm region.

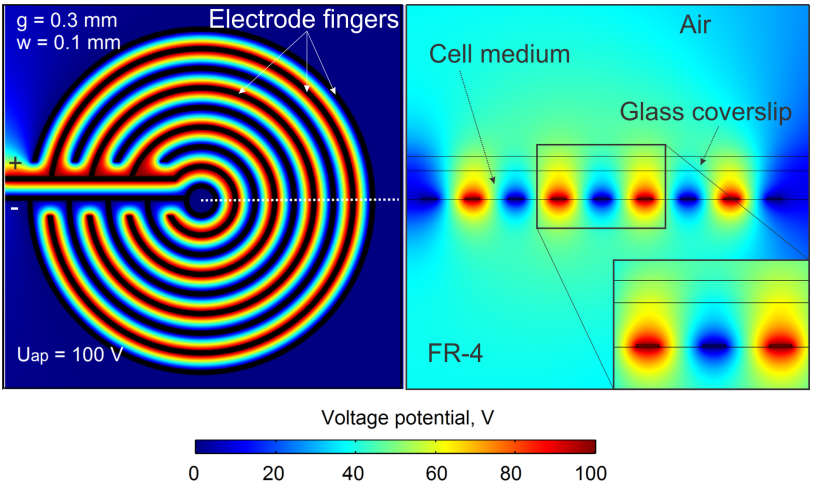

Fig. 2.29. Voltage potential distribution in x0y plane (Left) and y0z plane (Right) (Novickij *et al.* 2015b)

The electric field distribution between two electrode fingers when the 100 V voltage potential is applied has been evaluated. The results are presented in Figure 2.30.

The region with high electric field homogeneity (557–650 μm) is suitable for planar electroporation (E = 2 kV/cm), however it is convenient to increase the segment. The nonhomogeneous regions can be also successfully used in electroporation for irreversible treatment, DNA or fluorescent marker transfection experiments, however, analysis of cell permeabilization thresholds is hardly achievable due to inevitable uncertainty in results. For accurate estimation of the treatment efficacy or analysis of the biophysical processes the cells should be subjected to highly homogeneous electric field. Therefore, the defined 50 μm region of homogeneous electric field in multiple experimental instances is required.

In order to address this issue the influence of electrode gap on the electric field distribution was studied.

The homogeneous segment has been evaluated as the distance between two points in the same plane, where the amplitude of the electric field does not vary more than 20%, 5% and 1% from the minimal value. The results are presented in Figure 2.31.

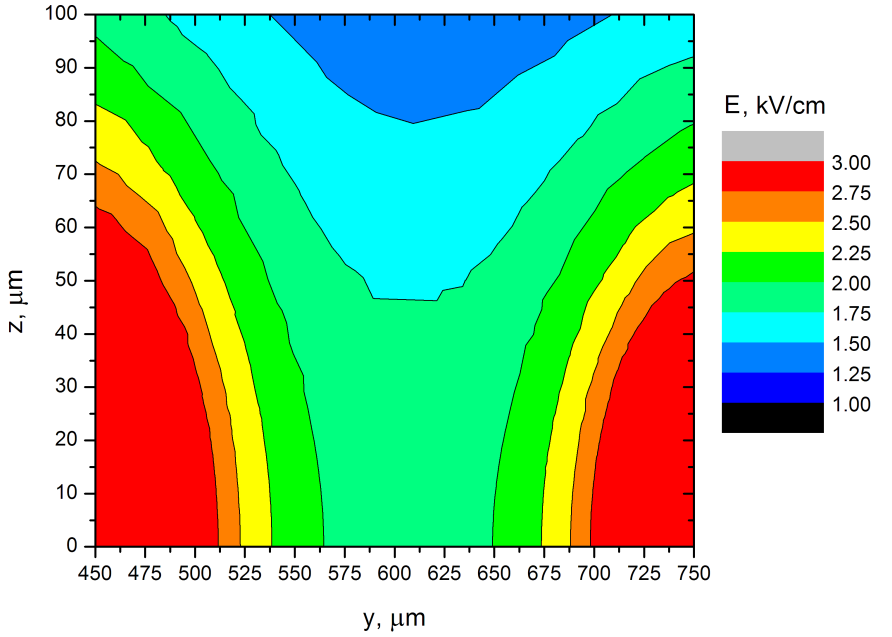

Fig. 2.30. Electric field distribution (y0z), when w = 0.1 mm, g = 0.3 mm, V_{ap} = 100 V (Novickij *et al.* 2015b)

The acceptable size of the required homogeneous region is limited by the size of the cells. Therefore the electrodes with the 50 µm gap are not applicable. In opposite, the 500 µm gap electrodes offer the widest homogeneity region, however as a trade-off the voltage applied is significantly higher to achieve the same magnitude of electric field.

If a <20% non-homogeneity rate is acceptable, the 250–350 µm gap electrodes are optimal for cells <50 µm, providing a sufficient reserve in area for cell movement during pulsing.

Apart from the electric field generation the Joule heating management problems arise when the current is flowing through the cell medium. A simulation of the temperature rise has been performed when a 100 V, 500 µs duration pulse was applied. The results are shown in Figure 2.32.

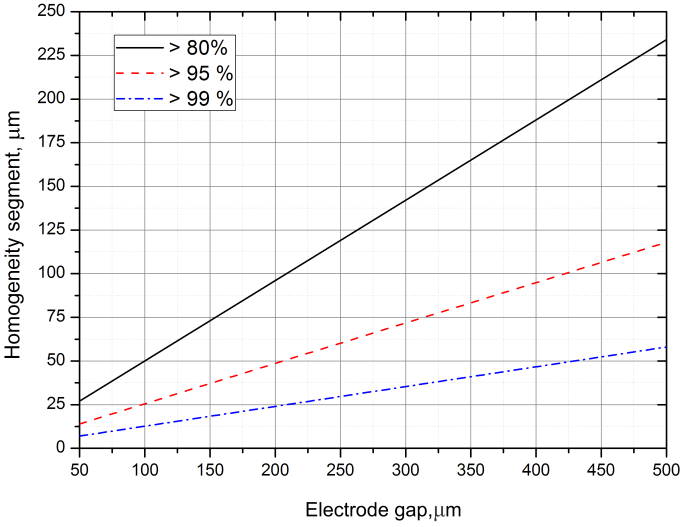

Fig. 2.31. The influence of the electrode gap on the homogeneity region (Novickij *et al.* 2015b)

As it can be seen in Figure 2.32 the 4.7 °C transient temperature rise is expected. Taking into account that most of the cell tolerate up 10 °C short-term temperature fluctuations it has been assumed that there is no significant Joule heating influence on the results of the electroporation (Pavlin *et al.* 2005; Heng *et al.* 2006; Zutta *et al.* 2011). Based on the simulation results it was confirmed that the circular interdigitated electrodes configuration is suitable for the electroporation studies.

It was decided that the electrode geometry with 300 µm gap is optimal due to the relatively wide >130 µm homogeneity region (>80%, Figure 2.33). The final design and photograph of the circular interdigitated microelectrode array with a set of 6 electrodes is shown in Figure 2.33.

The electrodes have been fabricated on a PCB copper board using laser etching (facilities of the Scottish Microelectronics Centre, University of Edinburgh, Scotland, UK).

The copper layer thickness is equal to 7 µm. The dimensions of the final chip are 5.5 cm x 3.3 cm.

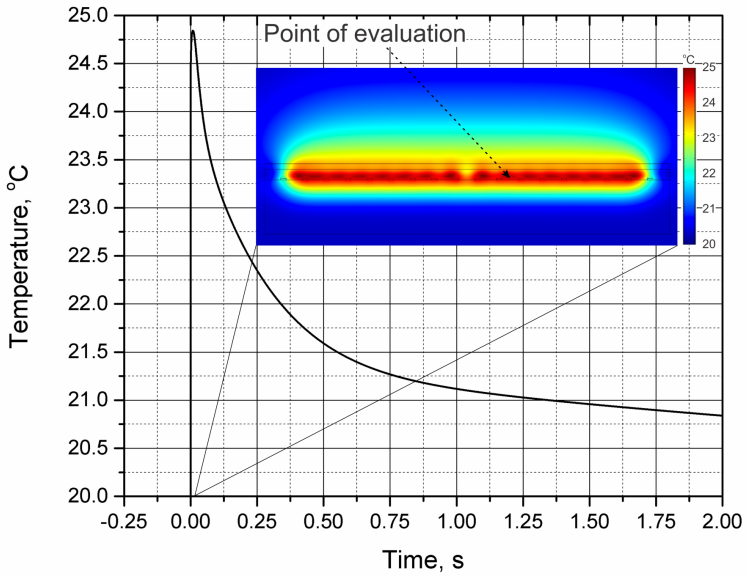

Fig. 2.32. The resultant temperature rise in the cell medium after 0.5 ms, 100 V pulse (Novickij *et al.* 2015b)

The temperature rise due to Joule heating has been also evaluated experimentally using indirect method of conductance change measurement (Hayashi, 2004; Pavlin *et al.* 2005; Suzuki *et al.* 2011). The microelectrodes have been used as a load of the microsecond electroporator and the changes in the conductivity during the pulse have been evaluated (Novickij *et al.* 2015b). As a medium distilled water (high impedance) and 0.9% NaCl solution (low impedance) were selected. Since the load of the electroporator are the selected electrolytes, the pulsed current value is also proportional to the conductivity of the medium (Novickij *et al.* 2014a; Novickij *et al*. 2015b).

Based on the difference in the pulsed current during the pulse the conductivity change and the respective temperature rise can be evaluated. For the experiments the 100 µs and 500 µs pulses were applied. The experimental results are presented in Figure 2.34. In the distilled water case the pulsed current is in the mA range, resulting in absence of significant thermal effects due to Joule heating (no change in the voltage drop during the pulse).

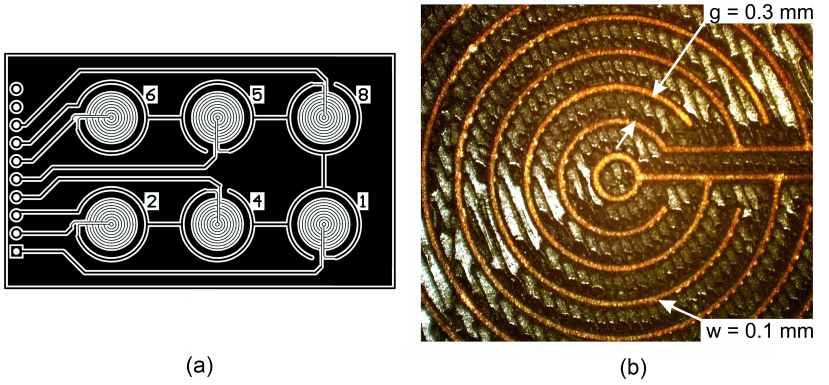

Fig. 2.33. Microelectrodes structure, where a) the resultant chip with electrodes; b) the photograph of interdigitated laser etched microelectrodes on FR-4 epoxy laminate (Novickij *et al.* 2015b)

As it can be seen in Figure 2.34 for both the 100 μs and 500 μs pulses there is no difference in the voltage during the pulse, therefore the Joule heating influence can be neglected.

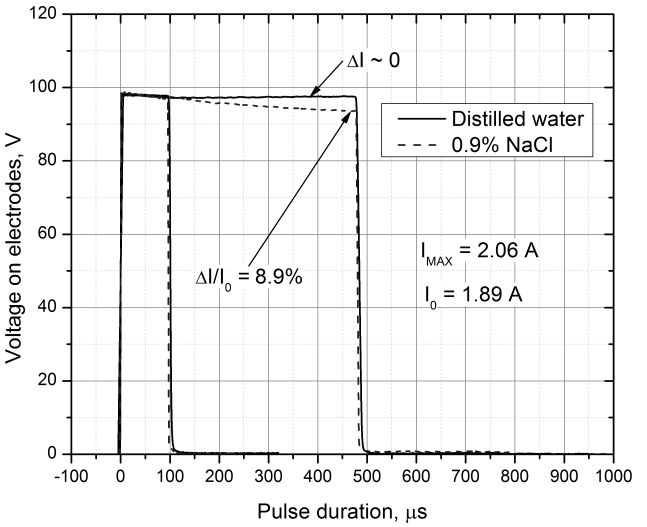

Fig. 2.34. Change of the voltage drop on the electrodes due to increasing cell medium conductivity, where I_0 is the current in the beginning of the pulse (Novickij *et al.* 2015b)

On the opposite side the highly conductive medium of 0.9% NaCl results up to 8.9% voltage drop and therefore pulsed current value change during the 500 μs pulse and less than 1% for the 100 μs pulse. The recalculation of the conductivity change to temperature difference has been performed in accordance to the temperature-electrical conductivity relation (Hayashi 2004). The conductivity change in the 500 μs pulse case corresponds to 3–4 °C temperature rise. The experimental data is in acceptable compliance with the simulation results.

The developed electrodes are suitable for electroporation in the microsecond range, however, certain limitations for fluorescence study will apply, such as a requirement of a direct light source for fluorescence excitation.

2.4. Conclusions for the Chapter 2

1. The developed microsecond square wave electroporator PSPICE simulation model has been used to estimate and compensate transient processes in the generator circuit based on IGBT switch. The model has results uncertainty of ±5%.
2. The developed submicrosecond square wave electroporator PSPICE simulation model has been used to estimate and compensate transient processes in the generator circuit based on MOSFET switch. The model has results uncertainty of ±10%.
3. The developed microsecond square wave pulse electroporator can deliver up to 4 kV, 5 μs – 10 ms electric pulses into loads up to 40 Ω.
4. The developed submicrosecond square wave pulse electroporator can deliver up to 8 kV, 200 ns – 5 μs electric pulses into loads up to 100 Ω.
5. The double crowbar, double snubber diode, RCD overvoltage circuit topology is effective for compensation of the transient processes in the submicrosecond and microsecond duration ranges.
6. The developed planar microelectrodes ensure generation of the electric field up to 2 kV/cm with the cell medium temperature rise less than 5 °C in the 5–500 μs pulse duration range.

3

Application of the Square Wave Pulse Electroporators

In this chapter the developed electroporators are experimentally applied. Based on the experimental data the adequacy of the developed systems to the thesis tasks is analysed. The experiments with pathogenic fungi are performed and the influence of the pulsed electric field treatment is investigated. The buffer conductivity change dynamics during electroporation are overviewed.

Four scientific publications were published on the section topic (Stankevič, Novickij *et al.* 2013; Novickij *et al.* 2014a; Novickij *et al.* 2014b; Novickij *et al.* 2015a)

3.1. Electroporation of Jurkat T

Human lymphoma Jurkat T cell line is frequently used to study cell leukemia, determine the mechanisms and efficacy of drugs and exposure to pulsed treatment such as pulsed electric or magnetic fields.

For the experiments the Jurkat T lymphoblasts have been grown in RPMI-1640 medium (Lonza, Germany), which contained 10% fetal bovine serum, 50 units/ml penicillin and 50 mg/ml streptomycin. The cells were cultured at 37 °C in humidified 5% CO_2 atmosphere. After centrifugation and re-suspension procedures the final concentration of 1 million cells/ml has been ensured.

The experiments have been performed at room temperature and the changes in medium conductivity have been measured throughout the treatment. As a cuvette a circular electrode structure with 1 mm gap and 50 µl volume was used. Since the used cell buffer has low impedance a 40 Ω ballast resistor in series with the cuvette was used. The waveform of the generated 1 ms electric pulse across the total load of 67 Ω (40 Ω ballast resistor and 27 Ω cell buffer) is presented in Figure 3.1.

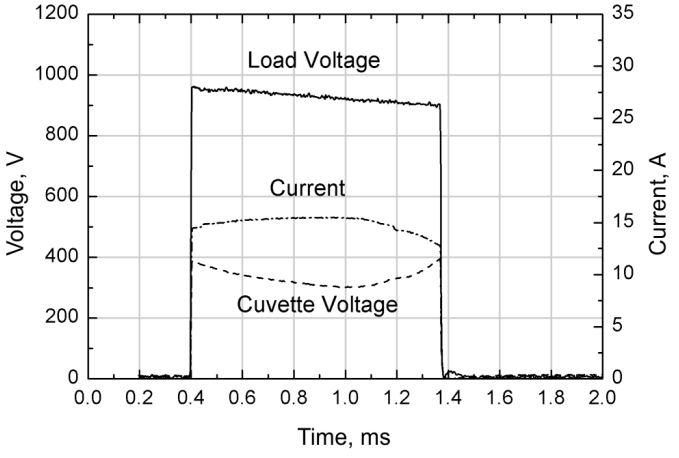

Fig. 3.1. Generated pulse across the load of 67 Ω (solid line), across the cuvette with cell buffer (27 Ω) (dash line) and the current through the cuvette (dash dot line) (Stankevič, Novickij *et al.* 2013)

The MMFG was switched to the third operation region of 500 µF, 2000 V, supporting pulses up to 3 ms. As it can be seen from Figure 3.1 the voltage drop during the pulse is equal to 8.1%. The voltage on the cuvette drops up to 25% during the pulse from 400 V to 300 V. The current through the cuvette is

changed in the opposite direction. The phenomenon could be explained by the cell buffer resistance change during electroporation. The cell buffer resistance change dynamics during pulses of different voltage and duration are presented in Figure 3.2.

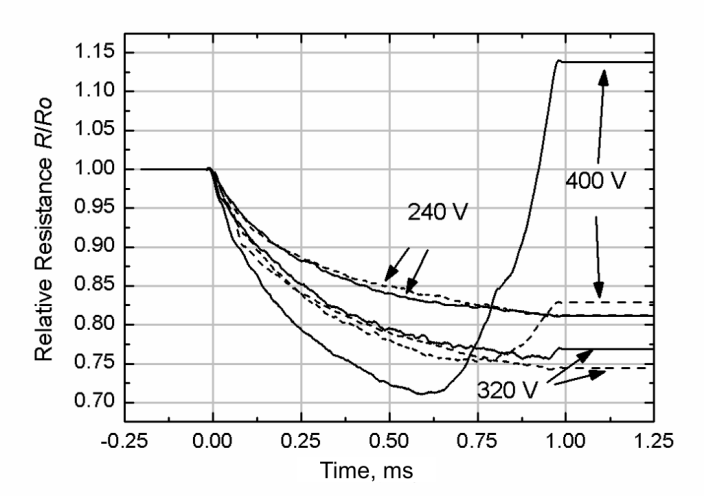

Fig. 3.2. Resistance change dynamics of buffer with cells (solid line) and buffer without cells (dash line) during electric pulses (Stankevič, Novickij *et al.* 2013)

As it can be seen in Figure 3.2 higher applied voltage results in a bigger drop of resistance during electroporation, which implies that the amount of the electroporated cells is increased. During 400 V a rapid decrease of resistance is observed after 0.6 ms, which was influenced by the appearance of bubbles between the cuvette electrodes. Further increase of the voltage or pulse duration results in the voltage breakdown in the cuvette. Similar tendency is observed in experiments with medium without the cells. It implies that during electroporation due to Joule heating there is a change in the cell buffer temperature. A significant variance of resistance between the cell buffer with cells and without ones was observed, when the 400 V pulses up to 0.6 ms were applied.

Additional experiments with pulse sequences have been performed. The same load was subjected to five subsequent 400 V, 1 ms electric pulses at a repetition frequency of 10 Hz. The results overviewing the voltage drops experienced during pulsing are presented in Figure 3.3.

As it can be seen from Figure 3.3a the power 40 W supply has enough time to re-charge the capacitor array during the delay between the pulses.

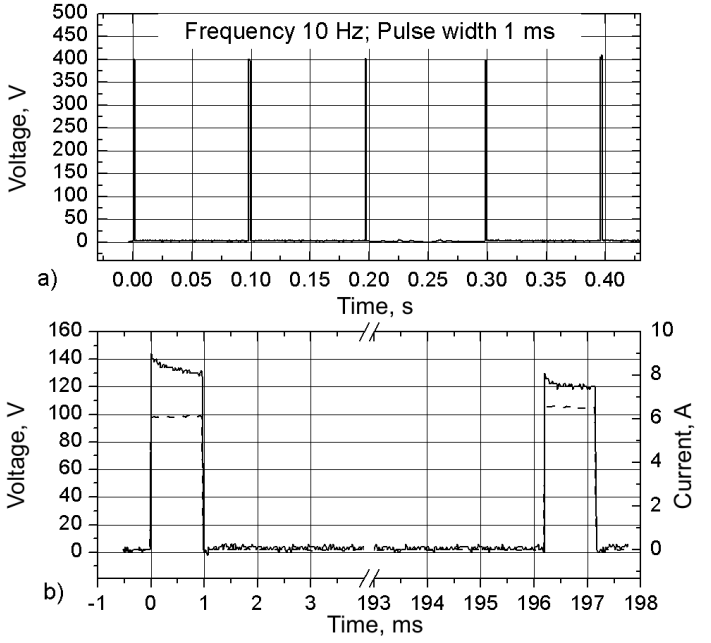

Fig. 3.3. Output pulses of the electroporator: a) Pulse sequence across the load; b) voltage drop (solid line) and current (dash line) in the cuvette during electroporation first and third pulses are shown (Stankevič, Novickij *et al.* 2013)

As it can be seen in Figure 3.3b the same tendency of current increase (resistance decrease) is observed during multiple pulsing procedures. For comparison only the first and the third pulses are shown. It was concluded that the result is due to synergistic effect of ion release during electroporation and the Joule heating, resulting in the increase of medium temperature up to 3 °C.

It was concluded that the developed high voltage square wave micro-millisecond electroporation system is suitable for electroporation research. The accuracy of pulse delivery and the quality of experiments are in good compliance with the thesis tasks. The Jurkat T cells respond to the pulsed electric field treatment and further studies of the temporary and irreversible permeabilization could be performed. The drug delivery stimulation dynamics and the pulsed electric field effects on the intracellular ion transfer mechanisms could be successfully addressed.

3.2. Irreversible Electroporation of Pathogenic Fungi

The irreversible electroporation experiments have been performed with pathogenic fungi *Saprolegnia parasitica*. These fungi species are one of the causes of cellular necrosis or epidermal damage in fish or freshwater organisms.

The *Saprolegnia parasitica* species have been subjected to 4 kV/cm (U_{CH} = 400 V) and 7 kV/cm (U_{CH} = 700 V) 1 ms repetitive pulsed electric field. The repetitive frequency of the pulses was 10 Hz. The electrical conductivity of the medium with fungi has been measured throughout the experiment. The results are presented in Figure 3.4.

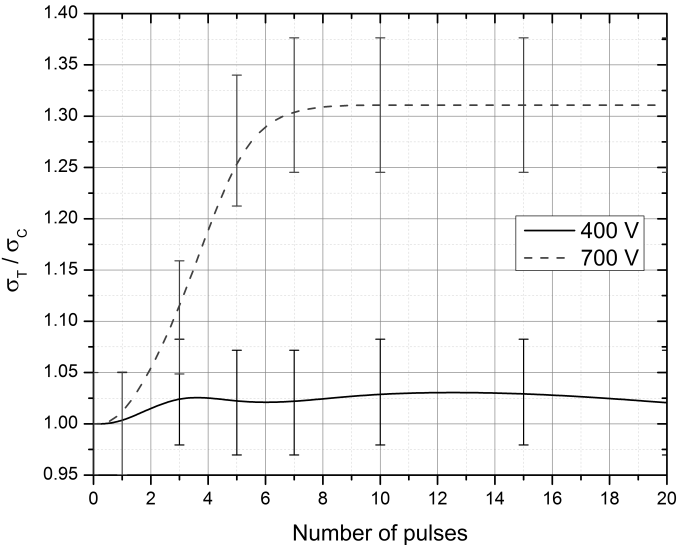

Fig. 3.4. Conductivity change of the electrolyte during pulsed electric field treatment, where σ_T is the conductivity of the treated sample, and the σ_C is the conductivity of the control sample without treatment (Novickij *et al.* 2014a)

As it can be seen in Figure 3.4 the 4 kV/cm (U_{CH} = 400 V) electric field has no significant effect on the *Saprolegnia parasitica*. The change of concentration of the ions in the cell medium is insignificant, which implies that the electroporation was not achieved. This could be explained by the strong cell wall composed of the β-1.3 and β-1.6 glucans, which implies that the treatment intensity must be increased to penetrate this barrier.

When the treatment intensity was increased to 7 kV/cm (U_{CH} = 700 V) the cytoskeleton of the *Saprolegnia parasitica* was permeabilized. As it can be seen

in Figure 3.4 up to 30% increase in the conductivity was observed when 8 or more 1 ms electric pulses were applied. The morphological analysis of the species after the treatment showed irreversible changes in the structure of the cell membrane. The microphotographs of the *Saprolegnia parasitica* after the treatment are presented in Figure 3.5.

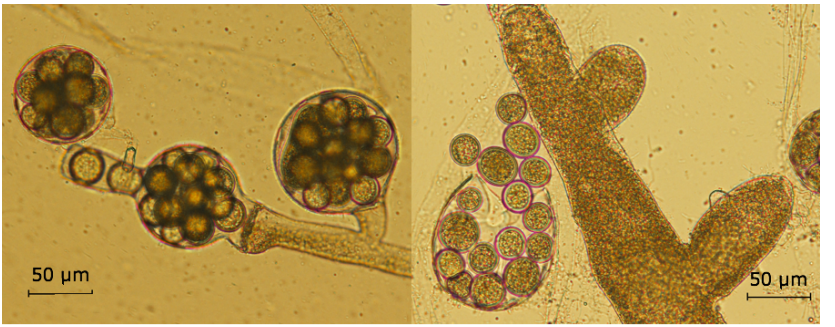

Fig. 3.5. Microphotographs of the *Saprolegnia parasitica* after pulsed electric field treatment, where a) treatment intensity of 4 kV/cm, 20 x 1 ms pulses; b) treatment intensity of 7 kV/cm, 20 x 1 ms pulses (Novickij *et al.* 2014a)

The fungi species show no morphological changes (Figure 3.5a) from the control sample, which is also in compliance with the conductivity change results presented in Figure 3.4. However, in the 7 kV/cm case (Figure 3.5b) the membrane is heavily lacerated. The spores freely leave the inner structure of the fungi cell. The hyphae are also lacerated and the morphological structure is altered. Due to heavily lacerated membrane additional charge carriers were introduced into the electrolyte, resulting in the total conductivity increase of the medium.

However, even though the outer membrane of the fungi cell was damaged the colony still will be viable if the oospores are not destroyed. When the pulsed electric field treatment intensity is further increased by increase of the total number of pulses the colony could be completely destroyed.

The microphotograph of the effect of irreversible electroporation on the morphological structure of the *Saprolegnia parasitica* is shown in Figure 3.6.

During experiments the 7 kV/cm 60 x 1 ms pulse sequence was applied. The treatment intensity was sufficient to destroy the species.

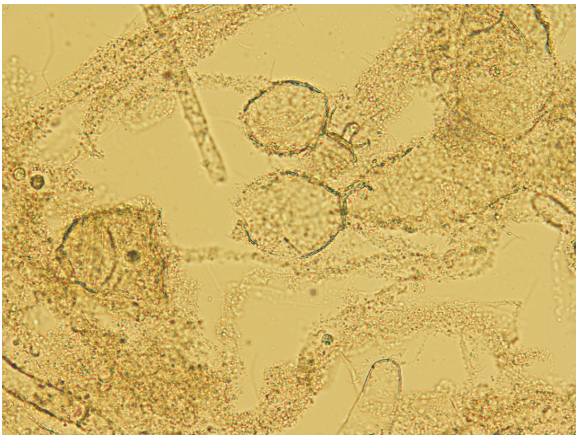

Fig. 3.6. Microphotograph of the fungal colony after high intensity 7 kV/cm 60 x 1 ms pulsed electric field treatment

It was concluded that the micro-millisecond square wave pulse electroporation system has been successfully applied for irreversible electroporation experiments of the pathogenic fungus-like water molds *Saprolegnia parasitica*.

The system offers a broad array of applications, covering the majority of currently known electroporation procedures. The flexibility of the load handling and high voltage and current support ensures the applicability of the developed square wave pulsed system as powerful scientific tool in the biotechnological and biomedical research.

3.3. Drug and Pulsed Electric Field Treatment Experiments

Pathogenic fungus such as *Candida albicans* is frequently responsible for diseases with lethal outcome in individuals with immune system deficit. Ones of the most commonly used antifungal drugs are Amphotericin B and Naftifine HCl. However, application of pulsed electric field in this field potentially may result in a more effective antifungal treatment due to the increased permeability of the fungi cells. Therefore, the developed prototypes have been applied in drug and PEF treatment experiments.

The clinical strain of *C. albicans* was grown on Sabourad dextrose agar (SDA) medium at 28 °C. For *in vitro* electroporation experiments the cells were

suspended in distilled water, and 1% naftifine hydrochloride ($C_{21}H_{21}N{\cdot}HCl$) at 5 mg/ml. For investigation of the Amphotericin B and PEF treatment efficacy the cells were suspended in distilled water and Amphotericn B 5 mg/l medium. The turbidity of the cell suspension was ensured with a spectrometer.

The influence of repetitive 5 μs 1 kV/cm and 2.5 kV/cm pulses on the antifungal treatment efficacy has been evaluated. In order to estimate the impact of the PEF treatment on the outcome of the synergistic treatment, the fungi have been subjected to pulsed electric field without antifungal agents. The results are presented in Figure 3.7.

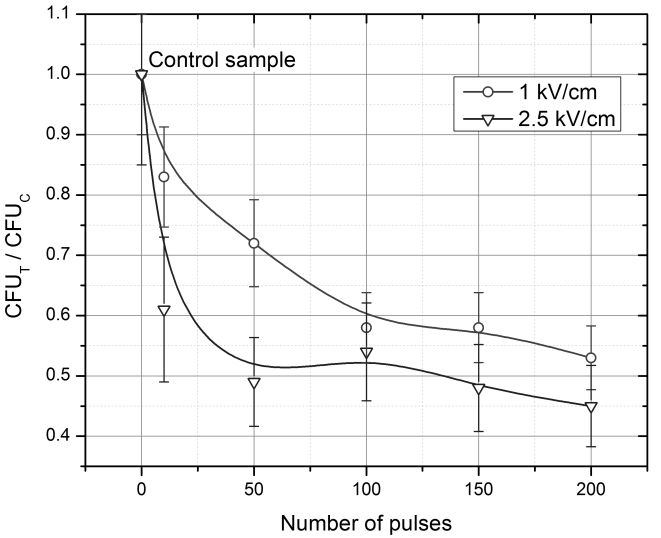

Fig. 3.7. Dependence of the vitality of the *Candida albicans* colony on the short microsecond pulsed electric field treatment (Novickij *et al.* 2015a)

During the experiments the colony forming units (CFU) have been evaluated, where CFU_T is the number of colony forming units after the treatment and the CFU_C is the colony forming units of the control sample without treatment. As it can be seen in Figure 3.7 the *C. albicans* is susceptible to the pulsed electric field treatment. Up to 65% decrease in the viability of the colony was observed when 200 x 5 μs 2.5 kV/cm pulses have been delivered to the cuvette.

In order to estimate the synergistic effect of antifungal treatment the antifungal drugs efficacy with PEF exposure and without the exposure has been evaluated. The results are presented in Figure 3.8.

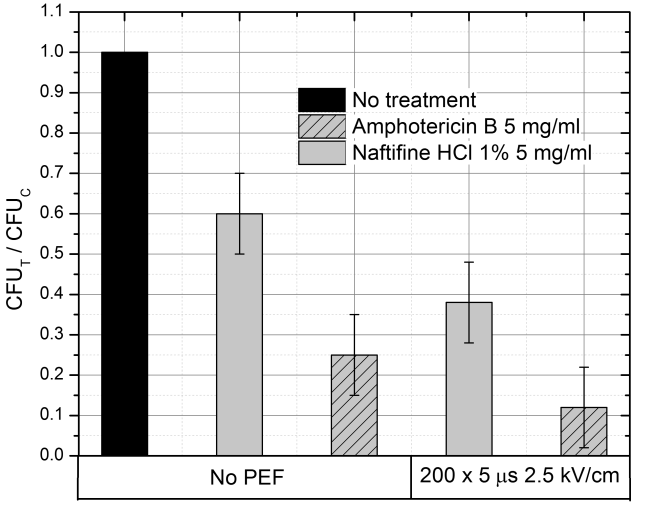

Fig. 3.8. Dependence of the colony vitality on the pulsed electric field and antifungal drugs treatment intensity (Novickij *et al.* 2015a)

As it can be seen in Figure 3.8 the antifungal drugs are effective against the *C. albicans*. Both the Amphoteric B treatment and Naftifine HCl treatment resulted in the decrease of the vitality of the colony to 40% and 65%, respectively. Co-applying drugs and the PEF treatment showed even better efficacy. The Amphotericin B treatment combined with pulsed electric field exposure resulted in the decrease of vitality up to 62%, which is 55% efficacy increase compared to the treatment with the drug only. The Naftifine HCl synergistic treatment showed similar tendency. The combined treatment efficacy was 88%, which is a 35% efficacy increase compared to the drug only procedure. It was concluded that the developed square wave pulsed electric field system are suitable for drug and PEF treatment experiments in order to improve treatment efficacy and offer high flexibility of the experiments.

3.4. Submicrosecond Range Electroporation

The developed submicrosecond range electroporator was tested on budding yeast *Saccharomyces cerevisiae* cells suspension using 13 kV/cm pulses which duration was varied from 250 ns to 860 ns.

The effectiveness of the electroporation was estimated using the indirect tetraphenylphosphonium (TPP+)-selective probe-based method to quantify the acceleration of TPP+ absorption by yeast cells.

The results demonstrating how the electric field induces acceleration of TPP^+ adsorption by yeast cells are presented in Figure 3.9. As a parameter, which enables estimation this acceleration, the ratio (k) between maximal possible TPP+ accumulation obtained without treatment of the cells and TPP+ accumulated during 3 min after cells exposure by pulsed electric field was used. It was shown that depending on the duration and number of pulses it is possible to achieve different TPP^+ absorption rates.

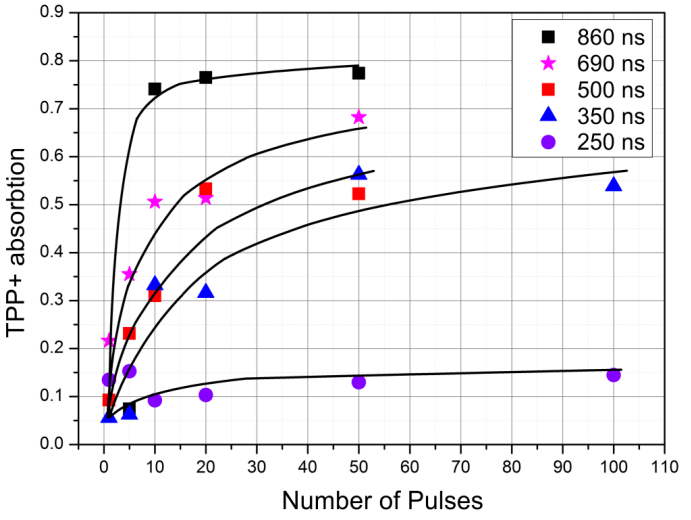

Fig. 3.9. Electropermeabilization influence on TPP+ absorption rate: k vs. pulse number dependence at different duration of electric pulses generating the same electric field strength (13 kV/cm)

3.5. Evaluation of the Developed Systems Parameters Adequacy to the Demands of the Research Field

This work was focused on the development of the electroporation system that could cover all of the major electroporation ranges. The proposed setup consists of two electric pulse generators: 1) micro-millisecond square wave pulse generator; 2) nano-microsecond square wave pulse generator. The summary of the parameters of the developed system is presented in Table 3.1.

Table 3.1. Summary of parameters of the developed electroporators

Developed electroporators		Required parameters	
Supported voltage, kV	Pulse duration range	Supported voltage, kV	Pulse duration range
0–8	200 ns – 5 μs	0–8	200 ns – 0.6 μs
		0–6	0.6–1 μs
0–4	5 μs – 0.1 ms	0–4	1 μs – 0.1 ms
0–2.8	0.1–0.3 ms	0–3	0.1–0.3 ms
0–2	0.3–3 ms	0–2	0.3–3 ms
0–0.9	3–10 ms	0–1	3–10 ms

As it can be seen in Table 3.1 the developed MMPG and NMPG allow coverage almost all of the required electroporation ranges. The 0.1–0.3 ms up to 3 kV voltage range was limited to 2.8 kV based on economical considerations during selection of high voltage capacitors. Due to the same considerations the 3–10 ms range was limited to 0.9 kV. If required the capacitors could be changed and the whole range would be covered.

It was concluded that the developed electroporation system consisting of MMPG and NMPG allowed achieving the aims of the work and is suitable for application in electroporation as a novel scientific tool.

3.6. Conclusions for the Chapter 3

1. The developed electroporators have been successfully applied in electroporation experiments. It has been determined that the proposed setups are suitable for application in transient permeabilization electroporation experiments, irreversible electroporation experiments and stimulation of drug efficacy procedures using pulsed electric field.
2. The proposed electroporators can be successfully applied for *in vitro* electroporation experiments. The introduced flexibility of pulse parameters allows inducing different biological effects in biological cells.

General Conclusions

1. The developed simulation model of the up to 4 kV electroporator ensures results uncertainty in the ±5% range. The model is suitable for estimation of the transient processes in the electrical circuits of micro-millisecond range pulsed power generators and can be used for development of high power systems.
2. The developed simulation model of the up to 8 kV electroporator ensures results uncertainty in the ±10% range. The model is suitable for development of transient process compensation circuits for submicrosecond range pulsed power generators and can be used for development of high power systems.
3. The proposed overvoltage and overcurrent protection and compensation scheme, consisting from RC circuit, snubber diodes and crowbar circuit is suitable for transient process compensation in pulse forming circuits for pulse generation in the 200 ns – 10 ms range.
4. The developed prototype of the high power up to 4 kV electroporator covers 5 μs – 10 ms range with 550 ns rise time and 1.5 μs fall time pulse generation and is suitable for application in the cell permeabilization experiments.

5. The developed prototype of the high power up to 8 kV electroporator covers 200 ns – 5 μs range with 40 ns rise time and 145 ns fall time pulse generation and is suitable for application in the absorption experiments triggered by electroporation.
6. The developed planar microelectrode structures ensure electric field generation up to 2 kV/cm with cell medium limited temperature rise of 5 °C in the 5–500 μs pulse range. The developed electrodes are suitable for electroporation in the microsecond range, however, limitations for fluorescence study apply, such as a requirement of a direct light source for fluorescence excitation.

References

Anderson, D.E.; Ridge, O. 2003. Recent developments in pulsed high power systems. *Proceedings of LINAC*; Knoxville, Tennessee USA. 541–545.

Austermann, J. *et al*. 2014. Indirect Current Source Inverter with Regenerative Snubber Circuit. *PCIM Europe 2014; International Exhibition and Conference for Power Electronics, Intelligent Motion, Renewable Energy and Energy Management; Proceedings of*; 20–22 May 2014. 1–8.

Baek, D.J.W. *et al.* 2005. Solid state Marx generator using series-connected IGBTs. *Plasma Science, IEEE Transactions on* 33(4): 1198-1204.

Balevicius, S. *et al*. 2013. System for the Nanoporation of Biological Cells Based on an Optically-Triggered High-Voltage Spark-Gap Switch. *Plasma Science, IEEE Transactions on* 41(10): 2706–2711.

Beebe, S.J. *et al*. 2013. Induction of Cell Death Mechanisms and Apoptosis by Nanosecond Pulsed Electric Fields (nsPEFs). *Cells* 2(1): 136–162.

Behrend, M. *et al*. 2003. Pulse generators for pulse electric field exposure of biological cells and tissues. *Dielectrics and Electrical Insulation, IEEE Transactions on* 10(5): 820–825.

Bertacchini, C. *et al*. 2007. Design of an irreversible electroporation system for clinical use. *Technology in cancer research & treatment* 6(4): 313–320.

Bortis, D. *et al*. 2007. Active gate control for current balancing in parallel connected IGBT modules in solid state modulators. *Pulsed Power Conference, 2007 16th IEEE International*; 17–22 June 2007. 1323–1326.

Bradshaw, H.D.; Jr. *et al*. 1987. Design, construction, and use of an electroporator for plant protoplasts and animal cells. *Analytical biochemistry* 166(2): 342–348.

Cahill, K. 2010. Cell-penetrating peptides, electroporation and drug delivery. *IET systems biology* 4(6): 367–378.

Cathelin, D. *et al*. 2013. Silencing of the glucocorticoid-induced leucine zipper improves the immunogenicity of clinical-grade dendritic cells. *Cytotherapy* 15(6): 740–749.

Chen, C. *et al*. 2011. The loss calculation of RCD snubber with forward and reverse recovery effects considerations. *Power Electronics and ECCE Asia (ICPE & ECCE), 2011 IEEE 8th International Conference on*; May 30 2011 – June 3 2011. 3005–3012.

Chen, X. *et al*. 2010. Apoptosis initiation and angiogenesis inhibition: melanoma targets for nanosecond pulsed electric fields. *Pigment Cell & Melanoma Research* 23(4): 554–563.

Chen, X. *et al*. 2012. Long term survival of mice with hepatocellular carcinoma after pulse power ablation with nanosecond pulsed electric fields. *Technology in cancer research & treatment* 11(1): 83-93.

Deboy, G. *et al*. 1998. A new generation of high voltage MOSFETs breaks the limit line of silicon. *Electron Devices Meeting, 1998 IEDM '98 Technical Digest, International*; 6–9 Dec. 1998. 683–685.

Delemotte, L.; Tarek, M. 2012. Molecular Dynamics Simulations of Lipid Membrane Electroporation. *The Journal of membrane biology* 245(9): 531–543.

Deng, G. *et al*. 2011. A pulsed power generator with a 20 stage transmission-line-transformer and 20 spark-gap switches. *Pulsed Power Conference (PPC), 2011 IEEE*; 19–23 June 2011. 602–605.

Dongdong, W. *et al*. 2010. All-Solid-State Repetitive Pulsed-Power Generator Using IGBT and Magnetic Compression Switches. *Plasma Science, IEEE Transactions on* 38(10): 2633–2638.

Fan, X.; Liu, J. 2014. A 70 kV solid-state high voltage pulse generator based on saturable pulse transformer. *The Review of scientific instruments* 85(2): 024708.

Gilboa, E. *et al*. 2012. Estimating Electrical Conductivity Tensors of Biological Tissues Using Microelectrode Arrays. *Annals of biomedical engineering* 40(10): 2140–2155.

Giorgi, D.M. *et al*. 2004. A high current, high dI/dt, light activated thyristor. *Electromagnetic Launch Technology, 12th Symposium on*; 25–28 May 2005. 186–190.

Grekhov, I.V.; Mesyats, G.A. 2000. Physical basis for high-power semiconductor nanosecond opening switches. *Plasma Science, IEEE Transactions on* 28(5): 1540–1544.

Haberl, S. *et al*. 2013. Cell membrane electroporation-Part 2: the applications. *IEEE Electrical Insulation Magazine* 29(1): 29–37.

Hargrave, B. *et al*. 2012. Electroporation-mediated gene transfer directly to the swine heart. *Gene Therapy* 20(2): 151–157.

Hayashi, M. 2004. Temperature-electrical conductivity relation of water for environmental monitoring and geophysical data inversion. *Environ Monit Assess* 96: 119–128.

Heng, B.C. *et al.* 2006. Low temperature tolerance of human embryonic stem cells. *Int J Med Sci* 3(4): 124–129.

Hung, M.-S.; Chang, Y.-T. 2012. Single cell lysis and DNA extending using electroporation microfluidic device. *BioChip Journal* 6(1): 84–90.

Jae-Hyeong, S. *et al*. 1997. A new snubber circuit for high efficiency and overvoltage limitation in three-level GTO inverters. *Industrial Electronics, IEEE Transactions on* 44(2): 145–156.

Jiannian, D. *et al*. 2011. The 100-kJ Modular Pulsed Power Units for Railgun. *Plasma Science, IEEE Transactions on* 39(1): 275–278.

Jin, Y.S. *et al*. 2012. High voltage ultrawide band pulse generator using Blumlein pulse forming line. *The Review of scientific instruments* 83(4): 044704.

Jong-Hyun, K. *et al*. 2007. High Voltage Marx Generator Implementation using IGBT Stacks. *Dielectrics and Electrical Insulation, IEEE Transactions on* 14(4): 931–936.

Jordan, E.T. *et al*. 2008. Optimizing electroporation conditions in primary and other difficult-to-transfect cells. *Journal of biomolecular techniques : JBT* 19(5): 328–334.

Jun, W. *et al*. 2008. Characterization, Modeling, and Application of 10-kV SiC MOSFET. *Electron Devices, IEEE Transactions on* 55(8): 1798–1806.

Kalgren, P.W. *et al*. 2007. Application of Prognostic Health Management in Digital Electronic Systems. *Aerospace Conference, 2007 IEEE*; 3–10 March 2007. 1–9.

Kandušer, M.; Miklavčič, D. 2008. Electroporation in Biological Cell and Tissue: An Overview. In: Electrotechnologies for Extraction from Food Plants and Biomaterials. Edited by Food Engineering Series. New York: Springer; p. 1–37.

Kim, D. *et al*. 2012. MicroRNA-34a modulates cytoskeletal dynamics through regulating RhoA/Rac1 cross-talk in chondroblasts. *The Journal of biological chemistry* 287(15): 12501–12509.

Kolb, J. *et al*. 2005. Measurements of the Transmembrane Voltage in Biological Cells for Nanosecond Pulsed Electric Field Exposures. *Pulsed Power Conference, 2005 IEEE*; 13–17 June 2005. 1286–1289.

Kolb, J.F. *et al*. 2010. Sub-nanosecond electrical pulses for medical therapies and imaging. *Antennas and Propagation (EuCAP), 2010 Proceedings of the Fourth European Conference on*; 12–16 April 2010. 1–5.

Kotnik, T. *et al*. 2012. Cell membrane electroporation- Part 1: The phenomenon. *IEEE Electrical Insulation Magazine* 28(5): 14–23.

Kotnik, T. *et al*. 2010. Induced Transmembrane Voltage and Its Correlation with Electroporation-Mediated Molecular Transport. *The Journal of membrane biology* 236(1): 3–13.

Kranjc, M. *et al*. 2012. Numerical simulations aided development of nanosecond pulse electroporators. *Antennas and Propagation (EUCAP), 2012 6th European Conference on*; 26–30 March 2012. 344–347.

Lee, W.G. *et al*. 2009. Microscale electroporation: challenges and perspectives for clinical applications. *Integrative Biology* 1(3): 242.

Li, C. *et al*. 2011. Dependence on electric field intensities of cell biological effects induced by microsecond pulsed electric fields. *IEEE Transactions on Dielectrics and Electrical Insulation* 18(6): 2083–2088.

Locher, R. 1998. Introduction to Power MOSFETs and Their Applications. Fairchild Semiconductor. Ap. Note 558.

Lucinskis, A. *et al*. 2014. Modelling the Cell Transmembrane Potential Dependence on the Structure of the Pulsed Magnetic Field Coils. *Elektronika ir Elektrotechnika* 20(8): 9–12.

MacQueen, L.A. *et al*. 2008. Gene delivery by electroporation after dielectrophoretic positioning of cells in a non-uniform electric field. *Bioelectrochemistry* 72(2): 141–148.

Manabe, Y. *et al*. 2011. Influences of pulsed electric fields on the gene expression of pathogenic bacteria. *Pulsed Power Conference (PPC), 2011 IEEE*; 19-23 June 2011. 1242–1246.

Mao, J. *et al*. 2012. A compact, low jitter, nanosecond rise time, high voltage pulse generator with variable amplitude. *Review of Scientific Instruments* 83(7): 075112–075116.

Meng, X.W. *et al*. 2014. Poly(ADP-ribose) polymerase inhibitors sensitize cancer cells to death receptor-mediated apoptosis by enhancing death receptor expression. *The Journal of biological chemistry* 289(30): 20543–20558.

Merla, C. *et al*. 2010. A 10- Ω High-Voltage Nanosecond Pulse Generator. *Microwave Theory and Techniques, IEEE Transactions on* 58(12): 4079–4085.

Miklavcic, D.; Towhidi, L. 2010. Numerical study of the electroporation pulse shape effect on molecular uptake of biological cells. *Radiology and oncology* 44(1): 34–41.

Moisescu, M.G. *et al*. 2013. Changes of cell electrical parameters induced by electroporation. A dielectrophoresis study. *Biochimica et biophysica acta* 1828(2): 365–372.

Morshed, B.I. *et al*. 2014. Investigation of Low-Voltage Pulse Parameters on Electroporation and Electrical Lysis Using a Microfluidic Device With Interdigitated Electrodes. *IEEE Transactions on Biomedical Engineering* 61(3): 871–882.

Nakagawa, R. *et al*. 2010. Effects of pulse electric fields to the pathogenic bacteria. *Power Modulator and High Voltage Conference (IPMHVC), 2010 IEEE International*; 23–27 May 2010. 686–689.

Napotnik, T.B. *et al*. 2012. Nanosecond electric pulses cause mitochondrial membrane permeabilization in Jurkat cells. *Bioelectromagnetics* 33(3): 257–264.

Narayanan, G. 2011. Irreversible electroporation for treatment of liver cancer. *Gastroenterology & hepatology* 7(5): 313–316.

Nawaz, M. *et al*. 2013. Dynamic Characterization of Parallel-Connected High-Power IGBT Modules. *IEEE Energy Conversion Congress and Exposition (ECCE), Denver, Colorado, US,* 15–19 September 2013. 4263–4269.

Pavlin, M. *et al*. 2005. Effect of cell electroporation on the conductivity of a cell suspension. *Biophysical journal* 88(6): 4378–4390.

Piatek, Z. *et al.* 2012. Self inductance of long conductor of rectangular cross section. *Przeglad Elektrotechniczny* 88(8): 323–326.

Pierco, R. *et al*. 2012. Diode string with reduced clamping-voltage for ESD-protection of RF-circuits. *Electronics Letters* 48(6): 317–318.

Podlesak, T.F. *et al*. 1997. Solid state switches for electric gun applications. *Magnetics, IEEE Transactions on* 33(1): 490–494.

Podlesak, T.F. *et al*. 1991. Demonstration of compact solid-state opening and closing switch utilizing GTOs in series. *Electron Devices, IEEE Transactions on* 38(4): 706–711.

Podlesak, T.F. *et al*. 2005. Preliminary Evaluation of Super GTOS in Pulse Application. *Plasma Science, IEEE Transactions on* 33(4): 1235–1239.

Potter, H. 2003. Transfection by electroporation. *Curr Protoc Mol Biol* 9(3): 1–13.

Pucihar, G. *et al*. 2011. Equivalent pulse parameters for electroporation. *IEEE transactions on bio-medical engineering* 58(11): 3279–3288.

Rae, J. 2002. Electroporation of Single Cells in Natural Lens and Cornea Preparations. *Investigative Ophtalmology and Visual Science* 43(12): 458.

Ramezani, E. *et al*. 1993. High peak current, high di/dt thyristors for closing Switch Applications. *Pulsed Power Conference, 1993 Digest of Technical Papers, Ninth IEEE International*; 21–23 June 1993. 680–683.

Rebersek, M. *et al*. 2007. Electroporator with automatic change of electric field direction improves gene electrotransfer in-vitro. *Biomedical engineering online* 6: 25.

Rebersek, M.; Miklavcic, D. 2011. Advantages and Disadvantages of Different Concepts of Electroporation Pulse Generation. *Automatika* 52(1): 12–19.

Reddy, C.S. *et al*. 2014. Experimental investigations of argon spark gap recovery times by developing a high voltage double pulse generator. *Review of Scientific Instruments* 85(6): 064703–064709.

Romeo, S. *et al.* 2013. A Blumlein-type, nanosecond pulse generator with interchangeable transmission lines for bioelectrical applications. *Dielectrics and Electrical Insulation, IEEE Transactions on* 20(4): 1224–1230.

Sanders, J.M. *et al*. 2009. A linear, single-stage, nanosecond pulse generator for delivering intense electric fields to biological loads. *Dielectrics and Electrical Insulation, IEEE Transactions on* 16(4): 1048–1054.

Sardesai, N.Y.; Weiner, D.B. 2011. Electroporation delivery of DNA vaccines: prospects for success. *Current opinion in immunology* 23(3): 421–429.

Sarkar, A. *et al*. 2004. A low voltage single cell electroporator with a microfabricated sense-porate aperture. *Micro Electro Mechanical Systems, 2004 17th IEEE International Conference on (MEMS)*; 2004. 375–378.

Saroj, P.C. *et al*. 2014. Synchronization and reliable operation of triggered spark gap switches in 40 kJ, 20 kV EMM system. *Discharges and Electrical Insulation in Vacuum (ISDEIV), 2014 International Symposium on*; Sept. 28 2014 – Oct. 3 2014. 353–355.

Schamiloglu, E. *et al*. 2004. Modern Pulsed Power: Charlie Martin and Beyond. *Proceedings of the IEEE* 92(7): 1014–1020.

Scully, N. *et al*. 2010. Pulsed discharges for medical applications. *Plasma Science, 2010 Abstracts IEEE International Conference on*; 20–24 June 2010. 1–1.

Smith, K.C.; Weaver, J.C. 2008. Active Mechanisms Are Needed to Describe Cell Responses to Submicrosecond, Megavolt-per-Meter Pulses: Cell Models for Ultrashort Pulses. *Biophysical journal* 95(4): 1547–1563.

Smith, K.C.; Weaver, J.C. 2011. Transmembrane molecular transport during versus after extremely large, nanosecond electric pulses. *Biochemical and biophysical research communications* 412(1): 8–12.

Soo Won, L. *et al*. 2014. Nanosecond High-Voltage Pulse Generator Using a Spiral Blumlein PFL for Electromagnetic Interference Test. *Plasma Science, IEEE Transactions on* 42(10): 2909–2912.

Stirke, A. *et al*. 2014. Electric field-induced effects on yeast cell wall permeabilization. *Bioelectromagnetics* 35(2): 136–144.

Stroh, T. *et al*. 2010. Combined pulse electroporation--a novel strategy for highly efficient transfection of human and mouse cells. *PloS one* 5(3), ID: e9488.

Sun, P. *et al*. 2011. Influence of Pulsed Power Equipment's Driving Manners on Launching Process of the Electromagnetic Coil. *Advanced Materials Research* 383–390: 4895–4900.

Sundararajan, R. *et al*. 2004. Performance of Solid-State High-Voltage Pulsers for Biological Applications: A Preliminary Study. *IEEE Transactions on Plasma Science* 32(5): 2017–2025.

Suzuki, D.O.H. *et al*. 2011. Theoretical and Experimental Analysis of Electroporated Membrane Conductance in Cell Suspension. *IEEE Transactions on Biomedical Engineering* 58(12): 3310–3318.

Tang, T. *et al*. 2005. Nanosecond Pulse Generator Using Diode Opening Switch for Cell Electroperturbation Studies. *Pulsed Power Conference, 2005 IEEE*; 13-17 June 2005. 1258–1261.

Tao, S. *et al*. 2014. A Cascaded Microsecond-Pulse Generator for Discharge Applications. *Plasma Science, IEEE Transactions on* 42(6): 1721–1728.

Temple, V. 2004. "Super" GTO's push the limits of thyristor physics. *Power Electronics Specialists Conference, 2004 PESC 04 2004 IEEE 35th Annual*; 20–25 June 2004. 604–610.

Turner, S. 2014. Optimally testing numerical multi-function generator protection elements. *2014 67th Annual Conference for Protective Relay Engineers,* March 31 2014 – April 3 2014. 564–580.

Wallace, M. *et al*. 2009. Tolerability of Two Sequential Electroporation Treatments Using MedPulser DNA Delivery System (DDS) in Healthy Adults. *Molecular Therapy* 17(5): 922–928.

Wang, J. *et al*. 2012. Synergistic effects of nanosecond pulsed electric fields combined with low concentration of gemcitabine on human oral squamous cell carcinoma in vitro. *PloS one* 7(8): e43213.

Washizu, M.; Techaumnat, B. 2008. Polarisation and membrane voltage of ellipsoidal particle with a constant membrane thickness: a series expansion approach. *IET nanobiotechnology / IET* 2(3): 62–71.

Watanabe, M. *et al*. 1990. A 115-mm φ 6-kV 2500-A light-triggered thyristor. *Electron Devices, IEEE Transactions on* 37(1): 285–289.

Weaver, J.C. *et al*. 2012. A brief overview of electroporation pulse strength–duration space: A region where additional intracellular effects are expected. *Bioelectrochemistry* 87: 236–243.

Weihua, J. *et al*. 2004. Compact solid-State switched pulsed power and its applications. *Proceedings of the IEEE* 92(7): 1180–1196.

Wolfus, Y. *et al*. 2014. Double storey three phase saturated cores fault current limiter. *Journal of Physics: Conference Series* 507(3): 032058.

Xinjing, C. *et al*. 2008. 10 kV square wave generator. *High Power Particle Beams (BEAMS), 2008 17th International Conference on*; 6–11 July 2008. 1–3.

Yao, C. 2012. FPGA-Controlled All-Solid-State Nanosecond Pulse Generator for Biological Applications. *IEEE Transactions on Plasma Science* 40(10): 2366–2372.

Yi, L. *et al*. 2013. Trigger characteristics of two-electrode graphite spark gap switches in pulsed power conditioning system. *Plasma Science (ICOPS), 2013 Abstracts IEEE International Conference on*; 16–21 June 2013. 1–1.

Zeng, Q. *et al*. 2012. IPP5, a novel inhibitor of protein phosphatase 1, suppresses tumor growth and progression of cervical carcinoma cells by inducing G2/M arrest. *Cancer genetics* 205(9): 442–452.

Zhihao, Z. *et al*. 2014. A cost-effective circuit for three-level flying-capacitor buck converter combining the soft-start, flying capacitor pre-charging and snubber functions. *Energy Conversion Congress and Exposition (ECCE), 2014 IEEE*; 14–18 Sept. 2014. 3658–3663.

Zorec, B. *et al*. 2013. Skin electroporation for transdermal drug delivery: The influence of the order of different square wave electric pulses. *International journal of pharmaceutics* 457(1): 214–223.

Zorngiebel, V. *et al.* 2011. Modular 50-kV IGBT switch for pulsed-power applications. *Plasma Science, IEEE Transactions on* 39(1): 364–367.

Zutta, B.R. *et al.* 2011. Low- and High-Temperature Tolerance and Acclimation for Chlorenchyma versus Meristem of the Cultivated Cacti Nopalea cochenillifera, Opuntia robusta, and Selenicereus megalanthus. *Journal of Botany* ID347168: 1–6.

The List of Scientific Publications by the Author on the Subject of the Dissertation

In the reviewed scientific periodical publications

Novickij, V.; Grainys, A.; Švedienė, J.; Markovskaja, S.; Paškevičius, A.; Novickij, J. 2015a. Irreversible electro-permeabilization of the human pathogen Candida albicans: an in vitro experimental study, *European Biophysics Journal*, 44(1): 9–16. (ISI Web of Science)

Novickij, V.; Grainys, A.; Markovskaja, S.; Novickij, J; Tolvaišienė, S. 2014a. Compact electro-permeabilization system for controlled treatment of biological cells and cell medium conductivity change measurement, *Measurement Science Review,* 14(5): 279–284. (ISI Web of Science)

Novickij, V.; Tabašnikov, A.; Smith, S.; Grainys, A.; Novickij, J. 2015b. Analysis of planar circular interdigitated electrodes for electroporation, *IETE Technical Review*, Published Online 28 January: 1–8. (ISI Web of Science)

In other papers

Stankevič, V.; Novickij, V.; Balevičius, S.; Žurauskienė, N.; Baškys, A.; Dervinis, A.; Bleizgys, V. 2013. Electroporation system generating wide range square-wave pulses for biological applications. *IEEE Biomedical Circuits and Systems Conference - BioCAS 2013 Proceedings*: Oct. 31 – Nov. 2, 2013. 33–36.

Novickij, V.; Stankevič, V.; Balevičius, S.; Žurauskienė, N.; Dervinis, A.; Bleizgys, V. Stirkė, A. 2014b. Nanosecond square-wave pulse generator for pulsed electric field treatment of biological objects, *5th Euro-Asian Pulsed Power Conference – EAPPC 2014 Proceedings*, Sep. 8–12, 2014. ID: P1–43.

Summary in Lithuanian

Įvadas

Problemos formulavimas

Biologinių ląstelių membranos pralaidumo įvairioms medžiagoms reguliavimas yra aktuali biomedicinos mokslų problema, sulaukianti įvairių sričių mokslininkų dėmesio. Vienas iš biologinių ląstelių poveikio būdų yra impulsinių elektrinių laukų taikymas ląstelių membranos pralaidumo didinimui arba elektroporacijai.

Šiuo metu vienas iš pagrindinių elektroporacijos apribojimų yra ribotos elektroporatorių impulsų formavimo galimybės submikrosekundiniame ir mikrosekundiniame ruože. Todėl norint išplėsti elektroporacijos tyrimų galimybes atsiranda poreikis kurti didelės galios elektroporatorius su plačiu generuojamų impulsų trukmių ir amplitudžių ruožu bei stačiais impulsų frontais. Tokių parametrų grandinėse dėl reaktyvaus pobūdžio apkrovos atsiranda pereinamieji vyksmai. Pereinamųjų vyksmų metu, tekant didelėms srovėms, dėl parazitinių grandinės elementų generuojami viršįtampiai ir viršsroviai, iškraipantys išėjimo impulso formą, todėl didėja komutuojančio rakto gedimo rizika. Siekiant užtikrinti stačiakampę impulso formą, bei operatoriaus ir prietaiso saugumą reikalingas apsaugos ir kompensavimo grandinių projektavimas, bei jų tyrimas. Didelės galios impulsų generavimui plačiame trukmių

ruože turi būti tinkamai parinkta energijos kaupiklio talpa, maitinimo šaltinio galia ir kiti parametrai.

Elektroporatorių apkrova yra kintamo impedanso elektrolitas su biologinėmis ląstelėmis, kurios yra jautrios aplinkos sąlygoms. Daugumoje elektroporacijos srities darbų naudojamos mikrolitrinio tūrio kiuvetes *in vitro* eksperimentams. Tokių kiuvečių panaudojimas neleidžia stebėti elektroporacijos proceso realiuoju laiku, didėja rezultatų neapibrėžtis dėl ląstelių terpės užteršimo ir reikalingų papildomų manipuliacijų su ląstelėmis. Tačiau planarių mikroelektrodų panaudojimas leidžia sumažinti šių neigiamų veiksnių įtaką, atsiranda galimybė stebėti elektroporacijos procesą realiuoju laiku naudojant mikroskopiją. Tačiau kuriant planarias elektrodų struktūras elektroporacijos tyrimams reikia atsižvelgti į generuojamo elektrinio lauko pasiskirstymą bei įšilimo efektų įtaką tyrimų rezultatams.

Disertacijoje sprendžiama mokslinė problema – didelės galios plataus submikrosekundinio ir mikrosekundinio ruožo stačiakampių elektrinių impulsų generavimas, didelės galios elektroporatorių kūrimas ir taikymas ląstelių elektroporacijos tyrimuose.

Darbo aktualumas

Impulsiniai elektriniai laukai turi plačias taikymo galimybes biologijos moksluose, tačiau elektrinio lauko parametrai stipriai įtakoja biologinio poveikio tipą bei efektyvumą. Dėl šios priežasties eksperimentinė įranga, kuri yra naudojama šioje srityje yra siauro pritaikymo, neleidžianti atlikti kompleksinių elektroporacijos tyrimų. Atsirado poreikis kurti naujas didelės galios universalias sistemas, kurios tinka plačiam tyrimų ruožui, užtikrinančias elektrinių impulsų generavimą plačiame impulsų trukmių ir amplitudžių ruože.

Tokių sistemų sudėtingumas didėja dėl išplėstų reikalavimų impulsų formavimo galimybėms, kaupiamos energijos kiekiui, saugumui bei galutiniam elektroporatoriaus dydžiui. Dėl šių priežasčių kompaktiškų didelės galios elektroporatorių kūrimas reikalauja naujų elektronikos ir elektros inžinerijos sprendimų ir taikomųjų tyrimų.

Dėl neišvengiamos parazitinių grandinės induktyvumo ir talpos įtakos generuojamo impulso formai, reikia kurti generatorių imitacinius modelius bei tirti pereinamuosius vyksmus tam, kad galima būtų sukurti impulso formavimo, apsaugos ir kompensavimo grandines naujos kartos elektroporatoriams. Tokių elektroporatorių sukūrimas leis ištirti elektroporacijos proceso biofiziką plačiame impulsų trukmių ir amplitudžių ruože.

Tyrimų objektas

Pagrindiniai tyrimo objektai yra didelės galios elektroporatoriai, grandynų pereinamieji vyksmai, elektrodų formos įtaka elektrinio lauko pasiskirstymui.

Darbo tikslas

Sukurti ir ištirti didelės galios elektroporatorius, ištirti grandynų pereinamuosius vyksmus ir generuojamo elektrinio lauko pasiskirstymą.

Darbo uždaviniai

Toliau išvardinti uždaviniai darbo tikslui pasiekti:

1. Sukurti stačiakampių impulsų formos elektroporatorių imitacinius modelius, ištirti grandynų pereinamuosius vyksmus ir galimybes kompensuoti parazitinių parametrų įtaką generuojamo impulso formai.
2. Sukurti didelės galios stačiakampių impulsų formos elektroporatorių prototipus ir ištirti jų pritaikomumą ląstelių permeabilizacijos ir absorbcijos tyrimuose.
3. Sukurti elektroporacijos elektrodus ir ištirti generuojamo elektrinio lauko pasiskirstymą ir ląstelių terpės įšilimo dinamiką, nustatyti elektrodų formos įtaką elektrinio lauko homogeniškumui.

Tyrimų metodika

Darbe buvo taikomi skaitiniai ir eksperimentiniai metodai. Panaudojant PSPICE programinį paketą, buvo tirti pereinamieji vyksmai elektroporatorių grandinėse. Naudojant COMSOL programinį paketą, baigtinių elementų metodu atlikta planarių elektroporacijos mikroelektrodų analizė. Sukurti elektroporatoriai buvo ištirti eksperimentiškai elektroporacijos tyrimuose.

Darbo mokslinis naujumas

Atliekant darbe aprašytus tyrimus buvo gauti šie elektros ir elektronikos inžinerijos mokslui nauji rezultatai:

1. Pasiūlytas modelis, tinkamas analizuoti pereinamuosius vyksmus elektroporatorių grandinėse.
2. Pasiūlyta viršįtampių ir viršsrovių kompensavimo schema, susidedanti iš RC grandinės, diodų ir trumpiklių grandinės yra tinkama pereinamųjų procesų kompensavimui generatorių grandinėse submikrosekundiniame ir mikrosekundiniame impulsų trukmių ruožuose.
3. Sukurti planarūs elektroporacijos mikroelektrodai ląstelių permeabilizacijos tyrimams elektriniuose laukuose iki 2 kV/cm, su 5 °C ląstelių terpės įšilimo apribojimu.

Darbo rezultatų praktinė reikšmė

Sukurti naujos kartos didelės galios kontroliuojamų impulsų parametrų iki 4 kV, 5 μs – 10 ms ir iki 8 kV, 200 ns – 5 μs elektroporatoriai, taikytini kompleksiniuose elektroporacijos tyrimuose.

Sukurti elektroporatorių prototipai buvo pritaikyti „Mokslo, inovacijų ir technologijų agentūros“ (MITA) finansuojamame aukštųjų technologijų plėtros programos projekte „Gyvųjų ląstelių nanoelektroporatorius (BIOnanopore)“ Nr. 31V33. Taip pat sukurti elektroporatoriai buvo sėkmingai pritaikyti tarpdisciplinuose tyrimuose kartu su Valstybinio mokslinių tyrimų instituto Fizinių ir technologijos mokslų centro,

Gamtos tyrimų centro mokslininkais, tiriant elektrinio lauko poveikį biologiniams objektams. Sukurtas planarių elektroporacijos elektrodų lustas gali būti naudojamas tiriant elektroporacijos proceso biofiziką.

Ginamieji teiginiai

1. Sukurtų elektroporatorių imitacinių modelių rezultatai atitinka sukurtų generatorių eksperimentiškai nustatytus parametrus ir leidžia modeliuoti generuojamų elektrinių impulsų parametrus su neapibrėžtimis neviršijančiomis ±5 % milisekundinių ir ±10 % submikrosekundinių impulsų diapazonuose.
2. Sukurtas didelės galios elektroporatoriaus prototipas, sudarytas iš kintamos talpos elektros energijos kaupiklio, izoliuotos užtūros dvipolio tranzistorinio rakto ir kiuvetės, užtikrina stačiakampių iki 4 kV impulsų su priekiniu 550 ns ir galiniu 1.5 μs frontais generavimą plačiame 5 μs – 10 ms diapazone.
3. Sukurtas didelės galios elektroporatoriaus prototipas, susidedantis iš energijos kaupiklio, MOSFET tranzistorinio rakto ir kiuvetės užtikrina stačiakampių iki 8 kV impulsų su priekiniu 40 ns ir galiniu 145 ns frontais generavimą plačiame 200 ns – 5 μs diapazone.
4. Sukurtos planarios mikroelektrodų struktūros užtikrina elektrinio lauko stiprį iki 2 kV/cm, neviršijant 5 °C ląstelių terpės įšilimo ribos 5–500 μs impulsų ruože.

Darbo rezultatų aprobavimas

Disertacijos tema paskelbti 5 moksliniai straipsniai: 3 – Thomson Reuters ISI Web of Science duomenų bazėje referuojamuose mokslo žurnaluose su citavimo indeksu, 2 – kituose recenzuojamuose mokslo leidiniuose. Disertacijos rezultatai buvo pristatyti 4 tarptautinėse mokslinėse konferencijose:

1. Tarptautinėje mokslinėje konferencijoje „*IEEE Biomedical Systems and Circuits Conference – BIOCAS 2013“*. 2013. Rotterdamas, Olandija.
2. Tarptautinėje mokslinėje konferencijoje „*5th Euro-Asian Pulsed Power Conference – EAPPC 2014“*. 2014. Kumamoto, Japonija.
3. Tarptautinėje mokslinėje konferencijoje „*IEEE International Magnetics Conference – INTERMAG 2014“*. 2014. Dresdenas, Vokietija.
4. Tarptautinėje mokslinėje konferencijoje „*Electronics 2014“*. 2014. Palanga, Lietuva.

Disertacijos struktūra

Diseraciją sudaro įvadas, 3 skyriai, bendrosios išvados, šaltinių ir literatūros sąrašas, autoriaus mokslinių publikacijų disertacijos tema sąrašas ir santrauka lietuvių kalba. Disertacijos apimtis – 112 puslapių be priedų. Disertacijoje yra 57 paveikslai, 11 lentelių ir 6 numeruotos formulės, disertacijoje panaudoti 104 literatūros šaltiniai.

1. Elektrinių laukų generavimo ir taikymo apžvalga

Per paskutinius du dešimtmečius impulsinių elektrinių laukų taikymas biomedicinoje pastebimai išaugo. Veikiant biologines ląsteles impulsiniu elektriniu lauku, ląstelių membranose įvyksta grįžtami ir negrįžtami pokyčiai, padidėja membranos pralaidumas didelėms molekulėms. Šis fenomenas buvo pavadintas elektroporacija.

Skyriuje apžvelgiama elektroporacijos poveikio priklausomybė nuo impulsų parametrų. Nustatyta, kad stačiakampių impulsų generatoriai yra tinkamiausi ląstelių elektroporacijos tyrimams, bet vienas iš pagrindinių šiuolaikinių elektroporatorių trūkumų yra ribotos generuojamų impulsų trukmių ir amplitudžių valdymo galimybės. Tam, kad galima būtų ištirti elektroporacijos proceso biofiziką reikia kurti naujos kartos didelės galios plataus impulsų ruožo elektroporacijas sistemas. Kuriant tokias sistemas būtina spręsti pereinamųjų vyksmų elektrinėse grandinėse kompensavimo problemas, analizuoti įšilimo efektus ir elektrinio lauko pasiskirstymą elektroporacijos kiuvetėse, tirti ir projektuoti impulsų formavimo grandines.

Taip pat skyriuje apžvelgiami įtaisai, kurie yra taikomi impulso formavimo grandinėse, analizuojami jų trūkumai ir pritaikomumas elektroporacijos srityje. Atlikus literatūros analizę buvo nustatyta, kad IGBT ir MOSFET raktai yra tinkamiausi impulso formavimui didelės galios elektroporatoriuose.

Įvertinant dabartinę elektroporacijos srities būklę ir reikalavimus impulsinėms sistemoms, buvo nustatyta, kad turi būti sukurti naujos kartos stačiakampių impulsų elektroporatoriai iki 8 kV submikrosekundiniame ir iki 4 kV mikrosekundiniame ruožuose.

2. Didelės galios plataus diapazono stačiakampių impulsų elektroporatorių kūrimas ir tyrimas

Šiame skyriuje pristatomas, sukurtas pagal imitacinio PSPICE modelio rezultatus, iki 4 kV stačiakampių mikro-milisekundinio diapazono impulsų elektroporatorius. Imitacinio modelio schema pavaizduota S1 paveiksle. Elektroporatoriaus modelį sudaro IGBT rakto modelis, maitinimo šaltinis DCV, apkrova R_{LOAD} ir pereinamųjų procesų kompensavimo grandinė, susidedanti iš virsrovių ir viršįtampių ribojančios RCD grandinės R_{S1}, C_{S1}, D_{S1}, D_{S2} bei atgalinę srovę kompensuojančios trumpiklių grandinės D_{C1}, D_{C2}. Parazitinių elementų įtaka aproksimuota kaip L_{GS}, L_{LINE} ir C_{LOAD}.

Buvo išrirti pereinamieji vyksmai didelės galios elektrinių impulsų generatoriaus grandinėse. Naudojant sukurtą imitacinį modelį buvo nustatyta, kad pereinamųjų vyksmų metu grandinėje dėl parazitinių induktyvumo ir talpos elementų įtakos atsiranda viršįtampiai ir viršsrovės, didėja rakto gedimo rizika, bei iškraipoma įšėjimo impulso forma. Pasiūlyta viršsrovius ir viršįtampius ribojanti RCD grandinė R_{S1}, C_{S1}, D_{S1}, D_{S2} bei atgalinę srovę kompensuojanti trumpiklių grandinė D_{C1}, D_{C2} leidžia kompensuoti

parazitinių elementų įtaką bei užtikrinti stačiakampę impulso formą mikro-milisekundiniame diapazone.

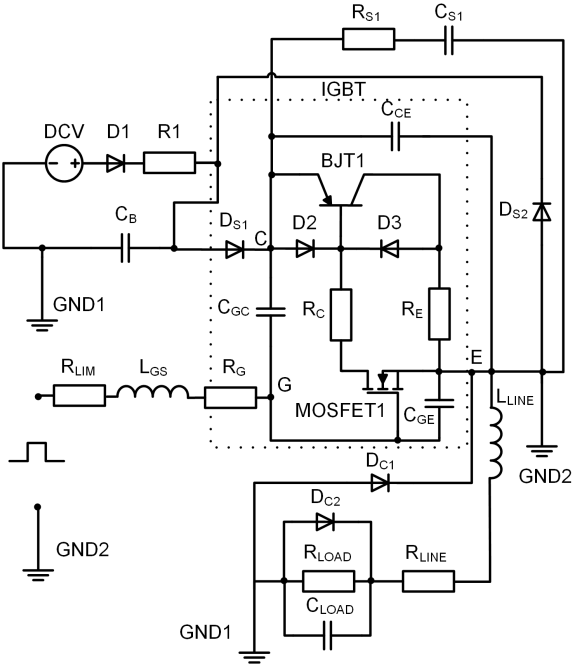

S1 pav. PSPICE imitacinio modelio iki 4 kV elektroporatoriaus schema

Pagal sukurto imitacinio modelio rezultatus buvo parinkta generatoriaus elementinė bazė, sukurtos valdymo, apsaugos, impulso formavimo ir kompensavimo grandinės.

Supaprastinta iki 4 kV, 5 μs – 10 ms stačiakampių impulsų elektroporatoriaus schema pavaizduota S2 paveiksle.

Sukurtas elektroporatorius sudarytas iš maitinimo šaltinio, kintamos talpos kondensatorių baterijos, IGBT rakto, valdymo grandinės bei impulsų registravimo grandinės. Maksimali elektroporatoriaus komutuojama impulsinė srovė – 100 A.

Visas elektroporacijos tyrimams skirtas mikro-milisekundinių impulsų diapazonas buvo padalintas į keturias dalis: impulsai iki 100 μs, iki 300 μs, iki 3 ms ir iki 10 ms. Kiekvienam impulsų ilgių rėžiui buvo priskirtos maksimalios leidžiamos pakrovimo įtampos, atsižvelgiant į energijos kiekį. Naudojant tokį impulsinio generatoriaus projektavimo metodą pasiektas ekonomiškai sėkmingas sprendimas – naudojami skirtingų talpų ir įtampų kondesatoriai, kurie yra komutuojami elektromechaniškai.

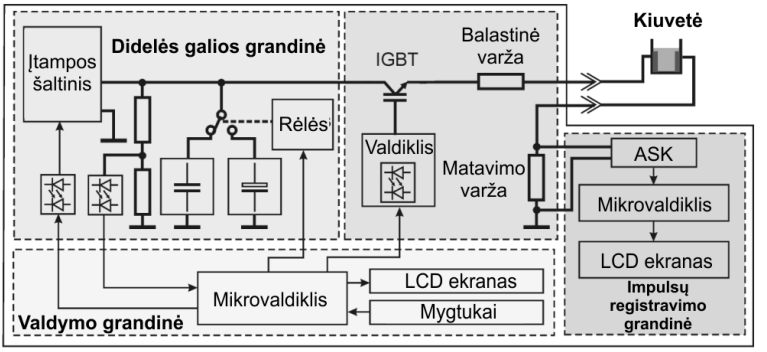

S2 pav. Iki 4 kV elektroporatoriaus schema

Sukurto elektroporatoriaus prototipas pavaizduotas S3 paveiksle. Prietaiso matmenys: 45 x 37 x 20 cm^3.

Eksperimentiškai nustatyta, kad sukurtas naujos kartos didelės galios elektroporatoriaus prototipas, sudarytas iš kintamos talpos energijos kaupiklio, IGBT tranzistorinio rakto IXEL40N400, apsaugos ir kompensavimo grandinės bei kiuvetės, užtikrina stačiakampių iki 4 kV impulsų su priekiniu 550 ns ir galiniu 1.5 µs frontais generavimą plačiame 5 µs – 10 ms diapazone.

Tam, kad galima būtų įvertinti sukurto mikro-milisekundinio stačiakampių elektrinių impulsų generatoriaus PSPICE imitacinio modelio rezultatų atitiktį eksperimentiniams rezultatams, modelio rezultatai buvo palyginti su eksperimentiškai nustatytais stačiakampio impulso parametrais.

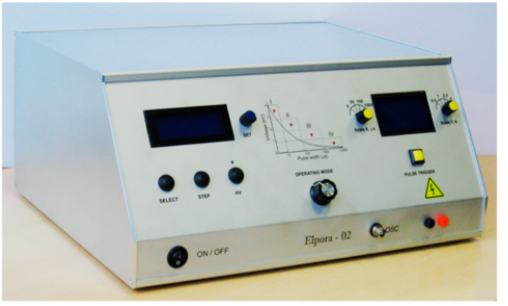

S3 pav. Iki 4 kV elektroporatoriaus prototipo nuotrauka

Sukurto iki 4 kV, 5 μs – 10 ms stačiakampių impulsų elektroporatoriaus išėjimo impulso forma pavaizduota paveiksle S4.

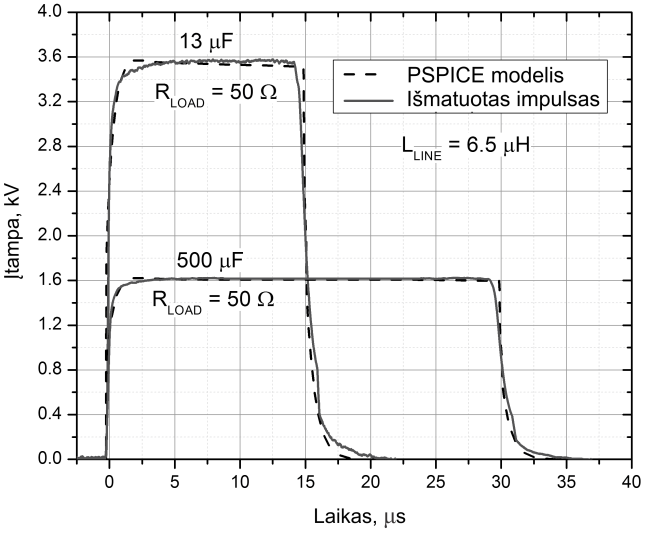

S4 pav. Sukurto iki 4 kV, 5 μs – 10 ms elektroporatoriaus išėjimo impulsas

Pasiūlyto elektroporatoriaus imitacinio modelio rezultatai atitinka eksperimentiškai nustatytus rezultatus ir leidžia modeliuoti generuojamų elektrinių impulsų parametrus su neapibrėžtimis neviršijančiomis ±5 %.

Taip pat šiame skyriuje pristatomas, sukurtas pagal imitacinio PSPICE modelio rezultatus, iki 8 kV stačiakampių nano-mikrosekundinio diapazono impulsų elektroporatorius. Imitacinio modelio schema pavaizduota S5 paveiksle. Generatoriaus modelį sudaro MOSFET rakto modelis ir, analogiškai iki 4 kV elektroporatoriaus modeliui, maitinimo šaltinis DCV, generatoriaus apkrova R_{LOAD} ir pereinamųjų procesų kompensavimo grandinė, susidedanti iš viršįtampius ir viršsrovius ribojančios RCD grandinės R_S, C_S, D_{S1}, D_{S2} bei atgalinę srovę kompensuojančios trumpiklių grandinės D_{C1}, D_{C2}. Analogiškai mikrosekundinių impulsų generatoriui, parazitinių elementų įtaka aproksimuota kaip L_{GS}, L_{LINE} ir C_{LOAD}.

Pagal sukurto imitacinio modelio rezultatus buvo parinkta iki 8 kV impulsų generatoriaus elementinė bazė, sukurtos valdymo, apsaugos, impulso formavimo ir kompensavimo grandinės. Tyrimų metų buvo nustatyta, kad parazitinių elementų įtaka nano-mikrosekundinio ruožo impulsų generatoriaus generuojamo impulso formai yra didesnė negu mikro-milisekundiniame ruože.

Pasiūlytos pereinamųjų vuksmų kompensavimo grandinės yra efektyvios kompensuojant parazitinio induktyvumo įtaką.

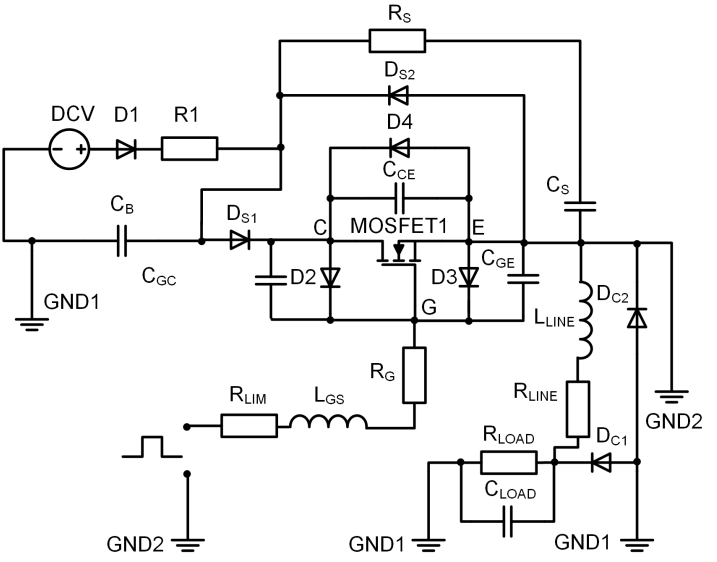

S5 pav. PSPICE imitacinio modelio iki 8 kV elektroporatoriaus schema

Tuo tarpu parazityviosios talpos kompensavimui galima naudoti nuosekliai apkrovai pajungtą balastinę varžą arba papildomą induktyvumą. Abu sprendimai nėra tikslingi dėl impulso frontų iškraipymų, kurie atsiranda kaip pasekmė, mažėjant generatoriaus apkrovai arba didėjant bendram grandinės induktyvumui.

Supaprastinta iki 8 kV, 200 ns – 5 μs stačiakampių impulsų elektroporatoriaus schema pavaizduota S6 paveiksle.

Impulsiniame generatoriuje yra aštuoni kondensatoriai po 70 μF, 1200 V, kurie yra sujungti nuosekliai (bendra talpa ir įtampa atitinkamai 8,75 μF, 9,6 kV). Apkrova susideda iš balastinės varžos ir kiuvetės. Impulsų generavimui, parametrų įvedimui ir įtampos matavimui buvo sukurta valdymo programa. Analogiškai mikro-milisekundiniam impulsiniam generatoriui impulso parametrų atvaizdavimui naudojamas 4x20 LCD ekranas.

Eksperimentiškai buvo nustatyta, kad sukurtas naujos kartos didelės galios nano-mikrosekundinių impulsų elektroporatoriaus prototipas, susidedantis iš kondensatorių, MOSFET tranzistorinio rakto HTS-91-12, apsaugos ir kompensavimo grandinės bei kiuvetės, užtikrina stačiakampių iki 8 kV impulsų su priekiniu 40 ns ir galiniu 145 ns frontais generavimą plačiame 200 ns – 5 μs diapazone.

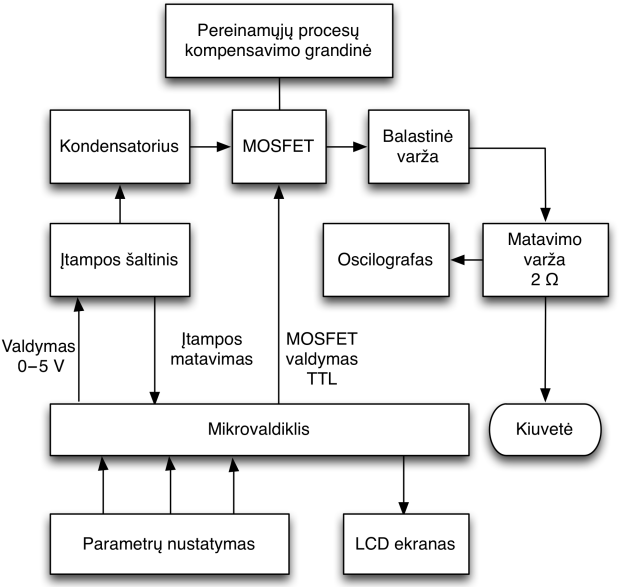

S6 pav. Sukurto iki 8 kV, 200 ns – 5 µs stačiakampių impulsų elektroporatoriaus schema

Sukurto elektroporatoriaus prototipas pavaizduotas S7 paveiksle. Prietaiso matmenys: 43 x 35 x 25 cm^3. PSPICE imitacinio modelio adekvatumas buvo patikrintas, lyginant modelio rezultatus su eksperimentiškai nustatytais stačiakampio impulso parametrais.

S7 pav. Sukurto iki 8 kV, 200 ns – 5 µs stačiakampių impulsų elektroporatoriaus prototipas

Įšėjimo impulso forma pavaizduota paveiksle S8.

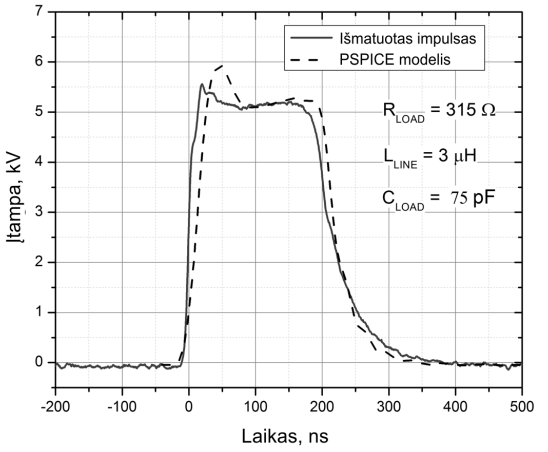

S8 pav. Sukurto iki 8 kV, 200 ns – 5 µs elektroporatoriaus išėjimo impulso forma

Pasiūlytas elektroporatoriaus imitacinis modelis yra adekvatus sukurto generatoriaus eksperimentiškai nustatytiems rezultatams ir leidžia modeliuoti generuojamų elektrinių impulsų parametrus su neapibrėžtimis neviršijančiomis ±10 %.

Taip pat šiame skyriuje nagrinėta planarių mikroelektrodų struktūra elektroporacijos tyrimams naudojant baigtinių elementų metodą. Įtampos potencialų pasisikirstymas parodytas S9 paveiksle.

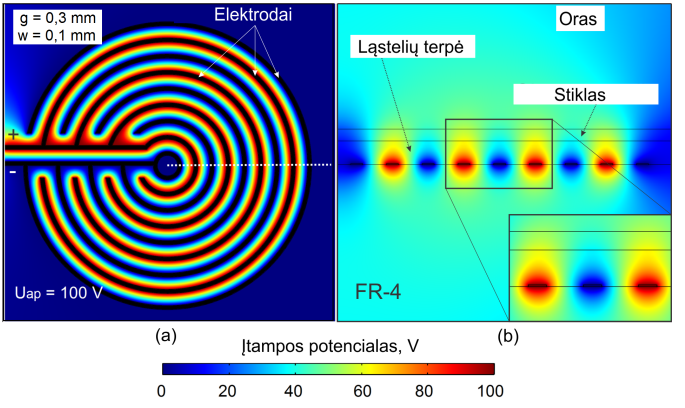

S9 pav. Įtampos potencialų pasisikirstymas, kur (a) x0y pjūvis; (b) y0z pjūvis

Keičiant elektrodų parametrus buvo tiriamas elektrinio lauko pasiskirstymas. Buvo nustatyta, kad optimali elektrodų struktūra yra kai tarpas tarp atskirų elektrodų yra 0,3 mm. Elektrinio lauko pasiskirstymas parodytas S10 paveiksle.

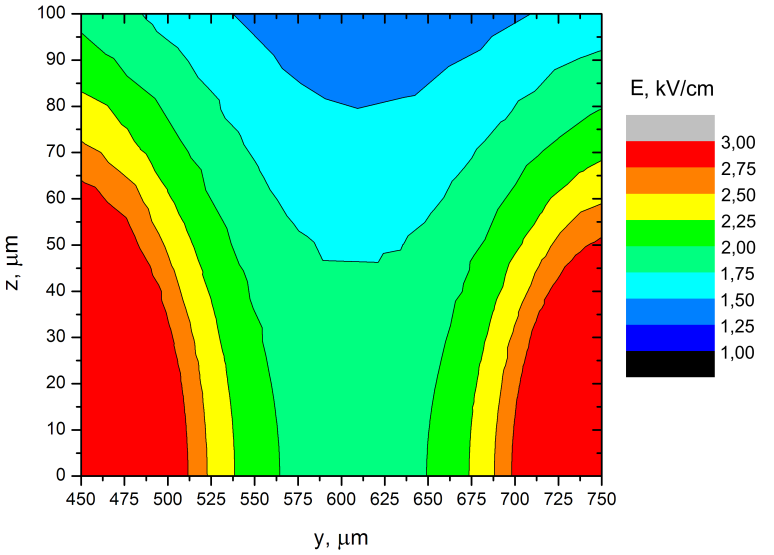

S10 pav. Elektrinio lauko pasiskirstymas, kai tarpas tarp elektrodų yra 0,3 mm, U_{AP} = 100 V

Didinant tarpą tarp elektrodų didėja homogeninio lauko segmentas. Šiuo atveju 557–650 µm segmente užtikrintas 2 kV/cm 85 % homogeninis elektrinis laukas. Tuo tarpu 570–640 µm segmente buvo užtikrintas 95 % homogeninis elektrinis laukas. Elektrinio lauko stiprio vertė ir pasiskirstymas tenkina elektroporacijos tyrimams keliamus reikalavimus.

Kadangi kaip apkrova naudojama elektrolitinė terpė su ląstelėmis, darbe buvo vertinami įšilimo efektai elektroporacijos metu. Terpės įšilimas gali neigiamai įtakoti eksperimentinius rezultatus, kadangi ląstelės yra jautrios temperatūrai. Terpės įšilimo dinamika pagal baigtinių elementų metodu pagrįstą imitacinį modelį pavaizduota paveiksle S11.

Iš paveikslo S11 matyti, kad terpės įšilimas neviršija 5 °C ribos. Toks šiluminis poveikis neturi įtakos elektroporacijos eksperimentams.

Įvertinant kompiuterinio modeliavimo rezultatus buvo sukurtas elektrodų lūsto prototipas. Elektrodų lustas buvo pagamintas Edinburgo universitete doktoranto stažuotės metu, naudojant universiteto infrastruktūrą (lazerinis ėsdinimas). Elektrodų lustas pavaizduotas S12 paveiksle.

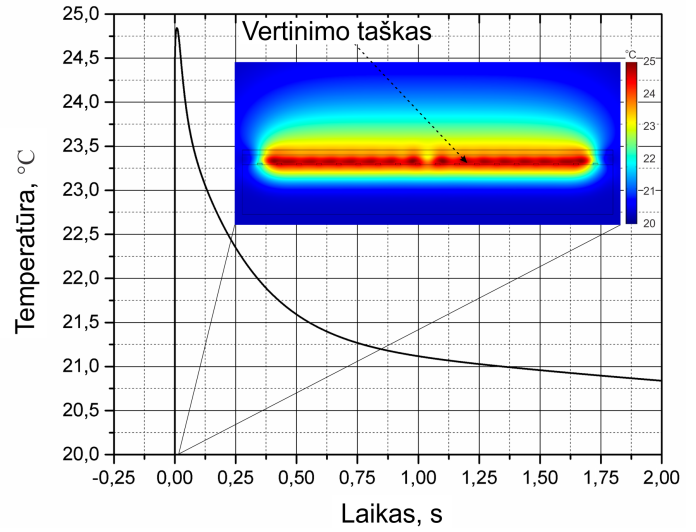

S11 pav. Ląstelių terpės įšilimo dinamika, kai U_{AP} = 100 V, 500 µs

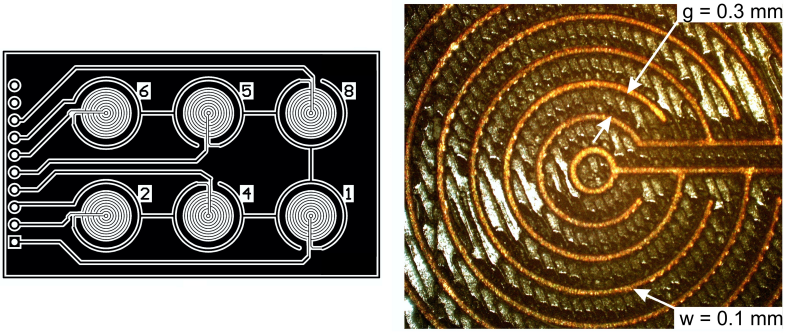

S12 pav. Sukurta elektrodų struktūra: (a) lustas; (b) elektrodų nuotrauka

Vario sluoksnio storis yra 7 µm. Sukurto elektrodų lusto matmenys yra 5,5 cm x 3,3 cm. Eksperimentiškai ištirtas šiluminis poveikis atitiko simuliacijos rezultatus – terpės įšilimas neviršija 3±1 °C. Elektrodai yra tinkami elektroporacijos tyrimams.

3. Stačiakampių impulsų elektroporatorių taikymas

Sukurti nano-mikrosekundinio ir mikro-milisekundinio diapazono elektroporatoriai buvo pritaikyti elektroporacijos tyrimuose.

Mikro-milisekundinio diapazono elektroporatorius buvo naudojamas negrįžtamos *Saprolegnia parasitica* ląstelių permeabilizacijos eksperimentuose. Ląstelės buvo veikiamos 1 ms įvairaus intensyvumo elektriniu lauku ir vertinama membranos morfologija. *Saproleginia parasitica* nuotraukos po elektroporacijos parodytos S13 paveiksle.

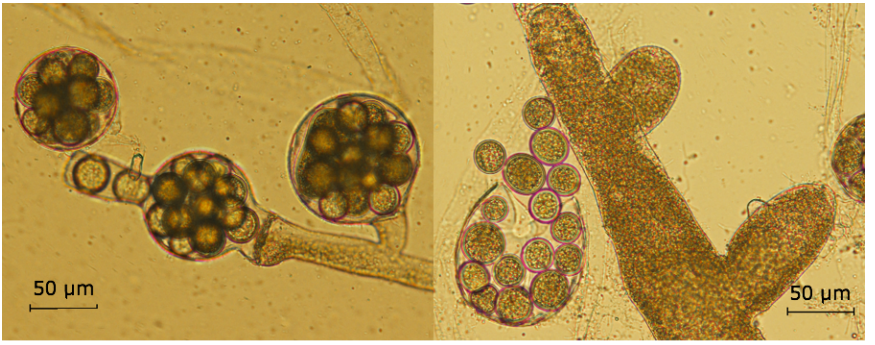

S13 pav. *Saproleginia parasitica* nuotraukos po elektroporacijos (a) 4 kV/cm, 20 x 1 ms impulsų; (b) 7 kV/cm, 20 x 1 ms impulsų

Tyrimų metu buvo nustatyta, kad 4 kV/cm elektrinis laukas neindukuoja pakankamo slenkstinio transmembraninio potencialo *Saprolegnia parasitica* rūšies ląstelėse. Tuo tarpu 7 kV/cm elektrinis laukas yra pakankamas sukurti negrįžtamą poveikį ląstelių membranose.

Taip pat mikro-milisekundinio diapazono elektroporatorius buvo pritaikytas tyrimuose su vaistais. Nustatyta, kad veikiant patogeninias *Candida albicans* grybų ląsteles impulsiniu elektriniu lauku kartu su antigrybiniais preparatais, galima pasiekti iki 35 % geresnį poveikio efektyvumą, negu naudojant tik vaistus arba elektrinį lauką atskirai.

Nano-mikrosekundinio diapazono stačiakampių elektrinių impulsų elektroporatorius buvo pritaikytas TPP+ absorbcijos tyrimuose.

Tyrimų metu buvo naudojamos *Saccharomyces cerevisiae* ląstelės ir priklausomai nuo impulsų ilgio ir kiekio vertinama TPP+ kationo absorbcijos vertė. Eksperimentiškai buvo nustatyta, kad didėjant impulsų ilgiui ir kiekiui, didėja TPP+ absorbcija. TPP+ absorbcijos dinamika priklausomai nuo poveikio intensyvumo parodyta paveiksle S14.

Abi sukurtos impulsinės sistemos atitinka disertacijos darbe keliamus reikalavimus.

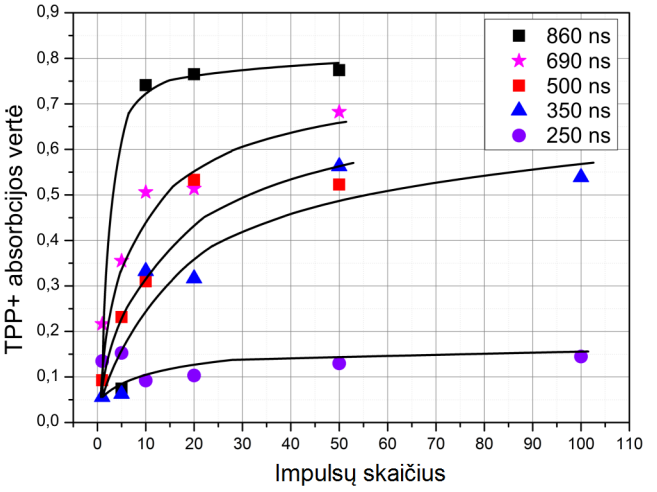

S14 pav. TPP+ absorbcijos dinamika priklausomai nuo poveikio intensyvumo, E = 13 kV/cm

Eksperimentiškai nustatyta, kad sukurti nano-mikrosekundinio ir mikro-milisekundinio diapazono stačiakampių impulsų elektroporatoriai yra taikytini kompleksiniuose elektroporacijos tyrimuose.

Bendrosios išvados

1. Sukurto iki 4 kV elektroporatoriaus imitacinio modelio rezultatai atitinka eksperimentinius rezultatus. Skaičiavimo ir matavimo rezultatų neapibrėžtis neviršija ±5 %. Pasiūlytas kompiuterinis modelis yra tinkamas vertinti ir kompensuoti pereinamuosius vyksmus mikro-milisekundinio diapazono didelės galios generatoriuose.
2. Sukurto iki 8 kV elektroporatoriaus imitacinio modelio rezultatai atitinka eksperimentinius rezultatus. Skaičiavimo ir matavimo rezultatų neapibrėžtis neviršija ±10 %. Pasiūlytas kompiuterinis modelis yra tinkamas vertinti ir kompensuoti pereinamuosius vyksmus submikrosekundinio diapazono didelės galios generatoriuose.

3. Pasiūlyta viršįtampių ir viršsrovių kompensavimo schema, sudaryta iš RC grandinės, diodų ir trumpiklių grandinės yra tinkama pereinamųjų procesų kompensavimui generatorių grandinėse formuojant 200 ns – 10 ms impulsus.
4. Sukurtas didelės galios iki 4 kV, 100 A elektroporatorius užtikrina stačiakampių su priekiniu 550 ns bei galiniu 1,5 μs frontais impulsų generavimą plačiame 5 μs – 10 ms ruože ir yra tinkamas ląstelių permeabilizacijos tyrimams.
5. Sukurtas didelės galios iki 8 kV, 100 A elektroporatorius užtikrina stačiakampių su priekiniu 40 ns bei galiniu 145 ns frontais impulsų generavimą plačiame 200 ns – 5 μs ruože ir yra tinkamas ląstelių TPP+ absorbcijos tyrimams.
6. Sukurti planarūs mikroelektrodai užtikrina elektrinio lauko stiprį iki 2 kV/cm, neviršijant 5 °C ląstelių terpės įšilimo ribos visame 5–500 μs impulsų ruože. Elektrodai yra tinkami elektroporacijai mikrosekundiniame diapazone, bet yra riboto pritaikymo fluorescencijos tyrimuose. Pasiūlytai elektrodų struktūrai reikia tiesioginio šviesos šaltinio fluorescencijos sužadinimui.

Annexes[1]

Annex A. The co-authors agreement to present publications material in the dissertation.
Annex B. Copies of scientific publications by the author on the topic of the dissertation.

[1] Annexes are available in the CD attached to the dissertation.

Vitalij NOVICKIJ

DEVELOPMENT OF HIGH POWER SQUARE WAVE ELECTROPORATORS

Doctoral Dissertation
Technological Sciences,
Electrical and Electronic Engineering (01T)

DIDELĖS GALIOS STAČIAKAMPIŲ IMPULSŲ ELEKTROPORATORIŲ KŪRIMAS

Daktaro disertacija
Technologijos mokslai,
elektros ir elektronikos inžinerija (01T)

2015 04 13. 10,25 sp. l. Tiražas 20 egz.
Vilniaus Gedimino technikos universiteto
leidykla „Technika“,
Saulėtekio al. 11, 10223 Vilnius,
http://leidykla.vgtu.lt
Spausdino BĮ UAB „Baltijos kopija“
Kareivių g. 13B, 09109 Vilnius